

BEN-GURION UNIVERSITY OF THE NEGEV  
FACULTY OF ENGINEERING SCIENCES  
DEPARTMENT OF INDUSTRIAL ENGINEERING AND MANAGEMENT

# Deterministic and stochastic models for light attenuation and controlling algorithm for microalgal growth

THESIS SUBMITTED IN PARTIAL FULFILLMENT OF THE REQUIREMENTS FOR THE M.Sc DEGREE

By: Elad Dan

October 2017

BEN-GURION UNIVERSITY OF THE NEGEV  
FACULTY OF ENGINEERING SCIENCES  
DEPARTMENT OF INDUSTRIAL ENGINEERING AND MANAGEMENT

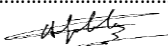
# Deterministic and stochastic models for light attenuation and controlling algorithm for microalgal growth

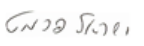
THESIS SUBMITTED IN PARTIAL FULFILLMENT OF THE REQUIREMENTS FOR THE M.Sc DEGREE


By: Elad Dan

Supervised by: Dr. Claude Aflalo, Prof. Yisrael Parmet, Prof. Yael Edan

Author:  Date: 26/10/17

Supervisor:  Date: 25/10/17

Supervisor:  Date: 26/10/17

Supervisor:  Date: 26/10/17

Chairman of Graduate Studies Committee:  Date: 26/10/17

October 2017

# Acknowledgments

This research was partially supported by the Paul Ivanier Center for Production Management, Ben-Gurion University of the Negev.

Foremost, I would like to express my deepest gratitude to my advisor Dr. Claude Aflalo for the continuous help and guidance in my M.Sc. research, for his patience, persistent, enthusiasm, and immense knowledge.

I wish to express my sincere gratitude to my academic advisors, Prof. Israel Parmet and Prof. Yael Edan, who were much helpful, and without their insights, support, guidance and assistance, this thesis would not have been fulfilled.

My sincere thanks also goes to Dr. Yoav Kerner for the much help in developing the stochastic model for light transfer.

Finally, I must express my profound gratitude to my friends, Tal Ze'evi and Elie Zemmour, for providing me with unfailing support and continuous encouragement throughout my study and through the process of researching and writing this thesis.

Thank you all.

# Abstract

Formatted: Space After: 0 pt

In recent years, the recognition of various high value substances produced by micro-algae when put under environmental stress stimulated this research field. Today, different species of micro-algae are cultivated for that purpose. This research aims to produce a dedicated control system that will serve for assessment and execution of microalgal growth by controlling environmental conditions adjustable by the user. The system reporting environmental and growth data, also controls physical factors to optimize growth. The highly flexible system is useful in physiological research of different micro-algal species, being able to store growth data, as well as environmental parameters as stress indicators. Moreover, two models have been developed: a deterministic model for predicting the biomass concentration inside the photo-bioreactor, that has been extended by statistical methods, and a stochastic model for describing the light transfer inside the photo-bioreactor in a single dimension.

The specific developments of the thesis include [development of:](#)

1. Control system software [and its implementation on an Arduino controller.](#)
2. Calibration procedure for transforming sensors readings to light intensity in terms of photosynthetically-active radiation (PAR).
3. Controlling algorithm for microalgae growth inside illuminated photo-bioreactor.
4. Deterministic model for predicting the concentration inside the photo-bioreactor.
5. Stochastic model describing the light transfer inside photo-bioreactors in a single dimension.

The system consists of a growth vessel illuminated by a LEDs array with two distinct colors. It is monitored and controlled by an Arduino Mega 2560 microprocessor, connected to the following input devices: two light sensors for incident and exiting light intensities, temperature sensor and a pH electrode. The Arduino board additionally controls LEDs light intensities as well as CO<sub>2</sub> supply valve to regulate the pH. The microprocessor was programmed using the native Arduino software, while using Megunolink Pro for data presentation and control. The system also enables data acquisition. The data gathered by the system was analyzed using R (RStudio), Matlab and Excel.

The algorithmic flow can be conceptually separated into two fundamental parts. The first is responsible for estimating the algal biomass content based on the measured light intensities before and after the photo-bioreactor. This updated estimate serves for determining the amount of each colored light that should in turn be supplied to the algae, to reach a constant light per biomass ratio. The second part consists of continuous measurement of pH and temperature. The pH of the suspension spontaneously increases with CO<sub>2</sub> consumption. Since the latter increases during active photosynthesis, CO<sub>2</sub> must be supplemented accordingly to keep a constant supply. An instantaneous target value for the pH is determined, considering the current light intensity and biomass concentration. The controlling algorithm was validated and the results were examined to be consistent and logic.

Analyses of collected data were conducted at different parts of the research: (i) validation of the research assumptions; (ii) formulating calibration procedure for transforming the local sensors readings to global light intensity in terms of photosynthetically-active radiation (PAR), in addition to estimation of the absorbance of the photo bioreactor in the absence of algae; (iii) the formulated deterministic model was fitted to observations collected by the system and actually measured in the lab.

**Keywords:** Microalgae, control system, monitoring system, controlling algorithm, statistical methods, Markov Chain, Arduino, light absorption, light transmission, light scattering.



## Table of Contents

<b>1. INTRODUCTION .....</b>	<b>1</b>
1.1. PROBLEM DESCRIPTION .....	1
1.2. OBJECTIVES .....	1
1.3. CONTRIBUTIONS.....	2
<b>2. LITERATURE REVIEW .....</b>	<b>3</b>
2.1. MICROALGAE.....	3
2.2. LIGHT .....	4
2.3. INTERACTION BETWEEN LIGHT AND AN OBJECT .....	5
2.4. MICROALGAL OPTICAL PROPERTIES .....	5
<b>3. RESEARCH METHODS.....</b>	<b>7</b>
3.1. OVERVIEW .....	7
3.2. SYSTEM COMPONENTS .....	7
3.3. ASSUMPTIONS .....	8
3.4. WORKING HYPOTHESIS .....	8
3.5. CALIBRATION .....	9
3.6. SYSTEM FLOW.....	10
3.7. DATA ACQUISITION AND PROCESSING .....	10
3.8. GROWTH PARAMETERS .....	11
3.9. CONTROLLING GROWTH CONDITIONS .....	12
3.10. PREDICTIVE MODELS .....	13
3.11. PERFORMANCE MEASUREMENT.....	14
3.12. ALGORITHM SIMULATION .....	14
3.13. STATISTICAL ANALYSIS .....	14
<b>4. CALIBRATION, MODELS AND ALGORITHM DEVELOPMENT .....</b>	<b><del>16</del>15</b>
4.1. CALIBRATION .....	<del>16</del> 15
4.2. EMPIRICAL MODELS .....	<del>17</del> 16
4.3. ALGORITHM FOR CONTROLLING GROWTH CONDITIONS .....	<del>25</del> 24
4.4. SIMULATION OF EXPONENTIAL GROWTH .....	<del>31</del> 30
<b>5. RESULTS &amp; DISCUSSION.....</b>	<b><del>33</del>32</b>
5.1. VALIDATION OF THE ASSUMPTIONS .....	<del>33</del> 32
5.2. CALIBRATION .....	<del>34</del> 33
5.3. DETERMINISTIC MODEL .....	<del>43</del> 42
5.4. STOCHASTIC MODEL.....	<del>47</del> 46
5.5. BEHAVIOR OF THE SYSTEM .....	<del>51</del> 50
5.6. VALIDATION OF THE CALCULATIONS IN THE ALGORITHM.....	<del>52</del> 51
<b>6. CONCLUSIONS &amp; RECOMMENDATIONS .....</b>	<b><del>59</del>58</b>
<b>7. REFERENCES .....</b>	<b><del>60</del>59</b>
<b>8. APPENDICES .....</b>	<b><del>63</del>62</b>
8.1. APPENDIX A – DECOMPOSITION OF LIGHT ATTENUATION.....	<del>63</del> 62
8.2. APPENDIX B – SYSTEM HARDWARE SPECIFICATION.....	<del>65</del> 64
8.3. APPENDIX C – CALCULATED INCIDENT LIGHT AT THE SURFACE OF THE PBR .....	<del>66</del> 65
8.4. APPENDIX D – ANALYSIS OF THE HETEROGENEOUS DATASET .....	<del>68</del> 67

## List of ~~tables~~Tables

Table 1 - Parameters formulated to control the culture's enviromental conditions .....	12
Table 2 - Possible states for a photon.....	<del>21</del> <a href="#">20</a>
Table 3 - Transition probabilities to go from state k to state l. ....	<del>21</del> <a href="#">20</a>
Table 4 - Definition of $\eta$ , the probability for a moving photon to get trapped in element j.....	<del>24</del> <a href="#">23</a>
Table 5 - Repetitions of light intensity measurements .....	<del>33</del> <a href="#">32</a>
Table 6 - Repetitions of lab measurements for pigments concentrations. ....	<del>33</del> <a href="#">32</a>
Table 7 - Representative measurements from lights sensors .....	<del>34</del> <a href="#">33</a>
Table 8 - Summary of the prediction models for lights in Hz .....	<del>38</del> <a href="#">37</a>
Table 9 - Local sensor readings and global PAR .....	<del>40</del> <a href="#">39</a>
Table 10 - Summary of the prediction model for normalized lights in PAR. ....	<del>42</del> <a href="#">41</a>
Table 11 - Conversion factors from local light intensity in Hz to global in PAR .....	<del>43</del> <a href="#">42</a>
Table 12 - Range of the concentrations and pigments in the culture .....	<del>43</del> <a href="#">42</a>
Table 13 - Results for fitting parameters in the models.....	<del>47</del> <a href="#">46</a>
Table 14 - Observations gathered within one year.....	<del>68</del> <a href="#">67</a>
Table 15 - Values for conversion factors from local Hz to global PAR and reference values.....	<del>68</del> <a href="#">67</a>
Table 16 - Values for the definition of $A_2$ .....	<del>69</del> <a href="#">68</a>
Table 17 - Results for fitting the parameters in the deterministic model .....	<del>72</del> <a href="#">71</a>

## List of Figures

Figure 1 - Qualitative behavior of growth rate caused by photoinhibition. ....	4
Figure 2 - Absorption spectrum of Chlorophyll a for (i) extracted cells in solution and (ii) packed cells in suspension.....	6
Figure 3 - Left panel: Side view for light behavior inside the photo-bioreactor. Right panel: $\langle L \rangle$ (i.e., the area under the curve) .....	8
Figure 4 - Conceptual flow chart for the Arduino sketch (code) driving the algal culture in the photo-bioreactor. ....	11
Figure 5 - The algorithm flow.....	13
Figure 6 - Schematic modelling of lighten suspension.....	<a href="#">1918</a>
Figure 7 - The Markov Chain for sub-model 1. ....	<a href="#">2221</a>
Figure 8 - Schema for the transition probabilities matrix $T$ . ....	<a href="#">2221</a>
Figure 9 - Dependence of light intensity on concentration according to equation 46.....	<a href="#">2928</a>
Figure 10 - Incident and exiting light sensors measurements (in Hz) for red and blue lights at increasing voltage .....	<a href="#">3534</a>
Figure 11 - Light out/Light in ratio for red and blue lights.....	<a href="#">3635</a>
Figure 12 - Calculated normalized measurements of incident and exiting light sensors.....	<a href="#">3736</a>
Figure 13 - Predictions and real values of the averaged normalized sensors measurements in Hz as function of PWM.....	<a href="#">3837</a>
Figure 14 - Calibration measurements of incident (Right) and outgoing (Left) red light intensities (PAR) by external sensor showing the average of the 12 LED combos .....	<a href="#">3938</a>
Figure 15 - Same as Figure 14, with blue LEDs.....	<a href="#">3938</a>
Figure 16 - Transmittance for red and blue lights in PAR .....	<a href="#">4039</a>
Figure 17 - Normalized PAR measurements of incident and exiting light for red (left) and blue (right) lights .....	<a href="#">4140</a>
Figure 18 - Prediction models for the averaged normalized sensors measurements in PAR. ....	<a href="#">4241</a>
Figure 19 - Calibration measurements of chlorophyll a and matching absorbance .....	<a href="#">4443</a>
Figure 20 - Chlorophyll a: real observations vs. predictions as function of red absorption. ....	<a href="#">4544</a>
Figure 21 - Chlorophyll a: measured vs. predicted values. ....	<a href="#">4544</a>
Figure 22 - Chlorophyll a: real observations vs. predictions as function of red absorption .....	<a href="#">4645</a>
Figure 23 - Same as in Figure 21. Predictions made by fitting equation A8.....	<a href="#">4645</a>
Figure 24 - Total transmission vs. $N$ .....	<a href="#">4847</a>
Figure 25 - Reflection, absorption and transmission at steady state. ....	<a href="#">4847</a>
Figure 26 - Results for reflection (left) and transmission (right) over the range of the elementary probabilities.....	<a href="#">4948</a>
Figure 27 - Same as Figure 26. $N=25$ . ....	<a href="#">4948</a>
Figure 28 - Comparison of the total transmission received by sub-models 1 and 2. ....	<a href="#">5049</a>
Figure 29 - Explore wide range of $N_{\max}$ effects of the total transmission. ....	<a href="#">5049</a>
Figure 30 - Biomass of pigments along growth period of seven days. ....	<a href="#">5251</a>
Figure 31 - Red and blue transmission as function of chlorophyll a concentration.....	<a href="#">5352</a>
Figure 32 - Light intensity in PAR [ $\mu\text{mol}/\text{m}^2/\text{s}$ ] vs. growth period of seven days.....	<a href="#">5453</a>
Figure 33 - Same as in Figure 32, for constant light-dark illumination mode. ....	<a href="#">5453</a>
Figure 34 - Same as Figure 32, for sinusoid daylight illumination mode.....	<a href="#">5554</a>
Figure 35 - Light available for absorbance .....	<a href="#">5655</a>
Figure 36 - Same as in Figure 35, for constant dark-light illumination mode. ....	<a href="#">5655</a>
Figure 37 - Same as in Figure 36, for sinusoid daylight illumination mode. ....	<a href="#">5756</a>



Figure 38 - Same as in Figure 37, for $FrR=0.3$ . .....	<a href="#">5756</a>
Figure 39 - electrical circuits at the LEDs panel. ....	<a href="#">6665</a>
Figure 40 - Total red incident light at the face of the PBR. ....	<a href="#">6766</a>
Figure 41 - Total blue incident light at the face of the PBR. ....	<a href="#">6766</a>
Figure 42 - Chlorophyll a: real observations vs. predictions as function of red PAR transmission.	

## 1. Introduction

### 1.1. Problem description

Microalgae are unicellular organisms able to use light energy to fix carbon dioxide and transform it into complex biomolecules (e.g., sugars, lipids, proteins) needed for their proliferation (Cronquist, 1960). The cellular process, known as photosynthesis, depends not only on the number and energy of photons absorbed per cell, but also on the frequency at which they are absorbed (proper light:dark exposure). The latter is determined by three major variables (Zarmi *et al.*, 2013): (i) incident light intensity and spectral quality, (ii) cells density (light absorption), and (iii) rate and mode of mixing (transfer between zones of high and low light intensities in the culture vessel).

Microalgal growth can be increased by optimal conditions (Borowitzka, 1999). Algal biomass of fixed composition accumulates at a maximal rate to generate daughter cells after division of mother cells. Under sub-optimal conditions, the organisms are under physiological stress, the growth rate is slower, and some microalgae overproduce compounds that assist them to overcome the stress (Borowitzka, 1999). The latter may represent compounds of high commercial value, such as protective pigments (antioxidants), and/or high nutritive value lipids (omega 3 and 6 poly-unsaturated fatty acids), or just excess oil, which can be extracted and processed to make biodiesel, an energy source that represents a renewable substitute to fossil fuel (petroleum-based). Sustainable production of high added-value compounds and/or alternative energies represents a major field for research and development of the future (Boussiba & Aflalo, 2005; Chisti, 2007; Li *et al.*, 2008).

In order to ensure a maximum yield, a prediction model for the growth rate is essential (Mata *et al.*, 2010). A few models have been proposed (Evers, 1991; Meireles *et al.*, 2008; Bernard & Remond, 2012; Tastan *et al.*, 2013; Zarmi *et al.*, 2013), but they address each of the environmental factors separately and often do not apply multivariate analysis or consider mutual relations.

Today, different tools and methods are available to support the growth process and evaluate the effect of various factors on production. **This research aims to produce a dedicated control system that will serve for assessment and execution of microalgal growth by controlling the environmental conditions. Moreover, two models have been developed; a deterministic model that has been extended by statistical methods for predicting the biomass concentration inside the photo-bioreactor and a stochastic model for describing the light transfer inside the photo-bioreactor in a single dimension.**

The (semi) automated control system, developed in this thesis, enables data acquisition, monitoring and controlling culture conditions (light intensity, light quality, temperature, pH, and CO<sub>2</sub> supply) in a photo-bioreactor containing a disposable culture vessel (20 L) illuminated by a panel of blue and red LEDs, and mixed by bubbling air (with or without CO<sub>2</sub>) over an appropriate growth period (7-14 days). Controlling, monitoring and real-time calculations is executed using the Arduino Mega 2560, an open-source microcontroller board containing a USB port for serial communication with a server, as well as several digital and analog I/O ports. A powerful package (MegunoLink Pro) functions as a visual interface with the microprocessor has been used, enabling both monitoring and user control of the system.

### 1.2. Objectives

The aim of this research is to develop a control system in support of microalgal growth. An algorithm for monitoring the growth and controlling the environmental conditions is developed.

A prediction model of the biomass concentration in the culture, using the light transmission measured by the light sensors has been proposed and developed. A stochastic model for the estimation of the

attenuated light in photo-bioreactors has been developed, considering the physical interaction between light and the algal cells (reflection, absorption and transmission).

The data monitored and processed by the system can assist in determining the conditions yielding maximum growth by performing a multivariate analysis.

The specific objectives are to develop:

1. Calibration procedures for light measurements. This enables estimation of the true light absorption by the microalgae.
2. An adequate estimation of the microalgal concentration in the bioreactor, based on the calibration procedures and statistical modeling of the correlation between light attenuation and the culture density.
3. A real-time algorithm to support microalgal growth in a semi-automated intelligent control system.
4. A model for describing the light transfer in the photo-bioreactor, for improved estimation of the attenuated light.

### 1.3. Contributions

- A deterministic model ~~The Beer-Lambert equation has been extended~~ was developed to enable (1) estimation of several pigments' concentrations and (2) consider the attenuated light owing to the scattering effect by extending the Beer-Lambert equation to account for scattering.
- A stochastic model ~~was developed~~ to consider the physical interactions of the photons and algae cells. The cells in suspension are modeled in a single dimension, which enables implementation in illuminated photo-bioreactors.
- Statistical techniques were used to apply real-time transformation of the voltage sent to the LEDs panel and the local sensors reading in Hz to the global light intensity in PAR units (flux) estimated on the incident and outgoing faces of the PBR (calibrated using an external independent quantum sensor).
- An automated control system was developed in C/C++, included ~3000 lines of code, and deployed in and implemented in Arduino.

## 2. Literature review

### 2.1. Microalgae

Microalgae are photosynthetic microorganisms that can grow rapidly and live under harsh conditions due to their unicellular structure (Li *et al.*, 2008). Similar to aerial plants, microalgae transform solar energy, water and CO<sub>2</sub> into chemical energy and biomass (Cronquist, 1960), mostly composed of carbohydrate (sugars), protein and oil (Richmond, 2004).

The number of microalgal species is estimated to be around 50,000, but only 30,000 have been identified (Cronquist, 1960; Richmond, 2004; Guiry, 2012). Some species naturally produce high value compounds (Meireles *et al.*, 2008), such as vitamins and pigments, and are extensively cultivated and studied around the world for various applications in the fields of pharmaceuticals, feed, energy and others (Boussiba & Aflalo, 2005; Mata *et al.*, 2010).

There are several factors influencing algal growth (Mata *et al.*, 2010): physical factors such as light intensity, light quality, temperature, CO<sub>2</sub>, pH, nutrient concentration, O<sub>2</sub>, salinity, and toxic chemicals; biotic factors such as bacteria, fungi, viruses and competition with other algae; operational factors such as stress produced by inappropriate mixing, dilution rate or harvest frequency.

Increasing energy demand, fossil fuels shortage, and environmental concerns have motivated the search for alternative and cleaner energy sources (Kirrolia *et al.* 2009). Microalgal species provide diverse sustainable solutions to human needs; they are widely produced for use of cosmetics, pharmaceutical, nutraceutical, and food industries (Richmond, 2004; Boussiba & Aflalo, 2005; Doughman *et al.*, 2007).

Microalgae have attracted considerable interest as a potential feedstock for biofuel production, as sugars and fats are the raw materials for bioethanol and biodiesel transport fuels (Carlsson *et al.*, 2007). Microalgae also produce proteins, a validated source for domestic animals feeding. After extracting some substances from the microalgae, the residue may serve as organic fertilizer (Richmond, 2004; Li *et al.*, 2008).

Production at industrial scale is usually performed in open ponds or raceways (Meireles *et al.*, 2008) and is preferred over agricultural crops due to the low water consumption and efficient use of CO<sub>2</sub> (Li *et al.*, 2008). Despite this, microalgal cultures are often characterized by low biomass productivity and are restricted to only a few species (Borowitzka, 1996; Boussiba & Aflalo, 2005). Several closed systems, usually of the tubular or flat-panel types, have been developed (Miron *et al.*, 1999); however, they present difficulties for effective control, require a large area of land, are expensive to operate and show high frequency of contamination by organisms competing on the microalgae (Meireles *et al.*, 2007). Therefore, new design of compact and clean photo-bioreactors is persistently pursued (Ogbonna, 1999).

Closed photo-bioreactors offer better control of culture conditions, such as CO<sub>2</sub> supply, water supply, optimal temperatures, and efficient exposure to light, culture density, pH levels, and mixing rates. For a large-scale production of biomass, efficient photo-bioreactors are required (Gupta *et al.*, 2015).

One of the major factors that affect microalgal growth is light (Borowitzka, 1996; Loera-Quezada *et al.*, 2011), needed as a primary energy source to drive carbon fixation; however, excess light can cause photoinhibition, promoting cell death (Evers, 1991). Hence, a light control system is desirable for closed photo-bioreactors to adjust light intensity to microalgal density. Assessment of the light available for photosynthesis, lowered by self-shading at high densities (Bricaud & Morel, 1986), is important in order to accomplish accurate and continuous control of light intensity (Evers, 1991; Zarmi *et al.*, 2013; Meireles *et al.*, 2008).

At saturating light intensities, CO<sub>2</sub> availability may limit algal photosynthesis (CO<sub>2</sub> fixation). pH is also an important factor for algal growth as in addition to its inference on CO<sub>2</sub> solubility, it can affect the activity of different enzymes. In general, microalgae have variable ranges for tolerance to pH (Ying *et al.*, 2014).

During photosynthesis, microalgae consume CO<sub>2</sub> (Cronquist, 1960) and the pH level correspondingly increases. In addition, evaporation of the former is taking place. Therefore, CO<sub>2</sub> must be supplied during the day.

CO<sub>2</sub> is not consumed during night (no light), since photosynthesis does not occur. The microalgae consume its energy by cellular respiration (Rich, 2003), a set of metabolic reactions which include the following processes: (i) digesting of inner materials (*e.g.*, glucose) combined with oxygen consumption. This process creates CO<sub>2</sub> and tends to lower the pH level in the culture. (ii) Intracellular organic acids consumption, tends to increase the pH level. Overall, the pH level in the culture is increasing in the dark and eventually stabilizes; therefore, CO<sub>2</sub> should not be supplied during night.

Temperature is the most important growth-influencing factor after light intensity (Huesemann *et al.*, 2016). The optimal temperature range is approximately 20 – 26°C. Many species can easily tolerate temperatures up to 15°C lower than their optimal, but exceeding the optimum temperature by only 2 – 4°C may result in substantial decrease of growth rate (Moheimani, 2005; Bernard & Remond, 2012).

## 2.2. Light

Photosynthetic active radiation (PAR) is the spectral range (wavelength) of solar radiation (visible light) between 400-700 nm (Thomas, 1994). Photosynthetic organisms uses those wavelengths while transforming it into chemical energy uses for growth. The growth rate is determined by both light intensity (Barber & Andersson, 1992), commonly described as PAR (in  $\mu\text{mol photons/m}^2/\text{s}$ ), and light quality (*i.e.*, wavelength) (Antoine D & Morel, 1996). The dependence of growth at light intensity is known as photoinhibition and shown in Figure 1; increase of growth rate at low light intensity, and decrease after reaching a maximum at high intensity (Kok, 1956).

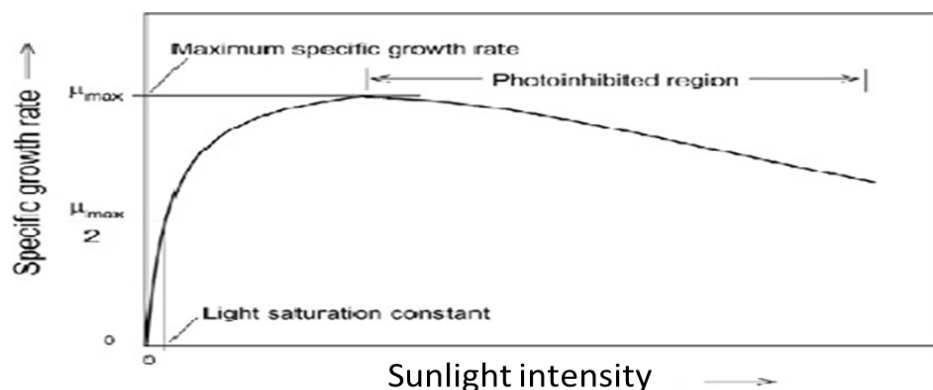


Figure 1 - Qualitative behavior of growth rate caused by photoinhibition. Above certain value of light intensity, a further increase in light level reduces the biomass growth rate (Kok, 1956).

The optimal light intensity should change in corresponding to the microalgae density in the suspension (Yuki *et al.*, 2014) since as the density increases, mutual shading occurs (between the cells) and as a result, the interaction of light with part of the cells is low (Chen *et al.*, 2011).

Photosynthetic organisms have unique preferences regarding the range of wavelength causing high growth rate (Lee, 1999). Wavelengths higher than 700 nm do not contain enough energy to initiate the photosynthetic process. On the other hand, wavelength lower than 400 nm may harm the cellular systems (protein/DNA) (Strid *et al.*, 1994).

### 2.3. Interaction between light and an object

Photon flux is defined as the number of photons striking a unit area per time as follows (Van der Meer, 2004):

$$I = \frac{\mu\text{mol photons}}{\text{m}^2 \cdot \text{second}} \quad (1)$$

When an object is irradiated by light, the incident photon flux is split due to the interaction of light with the object: (i) part of the radiation is reflected, (ii) the object absorbs some of the radiation, and (iii) the rest is transmitted through the object. The amount of the absorbed radiation is what affects the photosynthesis process. The radiation flux upholds the conservation of energy rule, as follows.

$$I_{in} = I_R + I_A + I_{out} \quad (2)$$

Where  $I_{in}$  is the total flux hits the object,  $I_R$  is the flux reflected by the object,  $I_A$  is the flux absorbed by the object and  $I_{out}$  is the flux transmitted through the object.

Since photon flux does not include information on their energy, the wavelength ( $\lambda$ ) of the photons (determining their energy) must be specified.

#### 2.3.1. Absorption

Absorption radiation is the radiation that stays in the object. The absorption radiation is usually transformed to another kind of energy, usually heat. Each substance is responsible for absorption at a different wavelength.

#### 2.3.2. Reflection

Reflection is defined as the ratio between the intensities of incident radiation ( $I_{in}$ ) and the reflected radiation ( $I_R$ ), as follows:

$$R_\lambda = \frac{I_R}{I_{in}} \quad (3)$$

The chemical characteristics and the micro topographical surface of the object influence that ratio, as well as the incident angle of the light source.

#### 2.3.3. Transmission

Transmission is defined as the amount of light radiation that goes through an object. The transmittance of an object is determined by its physical and chemical characteristics.

### 2.4. Microalgal optical properties

The optical properties of algae in suspension are derived from the pigmented cells, which are minute absorbing and scattering bodies (Bricaud & Morel, 1986). The absorption and scattering properties depend on the wavelength of a beam crossing a layer of suspension. The attenuation is defined as the sum of absorption and scattering. An additional but negligible property of the medium is the backscattering, which reflects the light scattered back to the light source direction (Bricaud & Morel, 1986).

The particular structure (shape, depth and width) in which absorbing species is contained and the chemical structure of its material effects the amount of energy absorbed by the body (Pottier *et al.*,

2005). Thus, absorption features can be directly related to the chemistry and structure of the cell. The absorption depth is an indicator for the amount of the material causing the absorption in a sample. Furthermore, the absorption depth is related to the particle's size. A larger cell has a greater internal path where photons may be absorbed according to Beer's Law (Beer, 1852). In smaller cells there are proportionally more surface reflections compared to the internal photon path lengths.

Chlorophyll is the main photosynthetic pigment in green algae and it is often used to quantify the microalgal biomass in a suspension (Bricaud & Morel, 1986). The specific absorbance of the pure pigments (*e.g.*, chlorophyll a, chlorophyll b & carotenoid) is determined using a spectrophotometer, by transmitting light at different wavelengths through the solution, which absorbed differently by the pigments (Harold, 1942). Despite this, the spectrum of the light absorbed by the specific pigments does not completely describe the actual light absorption in a suspension, due to the protein-binding within the cells (Bidigare *et al.*, 1990). Since the pigments are packed inside the cell (the "packing effect"), enhanced mutual shading of the pigment molecules accrues, which alters the absorption spectra as follows: (a) the peaks of the pigments are wavelength-shifted (Bidigare *et al.*, 1989) and (b) the spectrum is flattened and lower, comparing to that obtained from extracted cells in solution (see Figure 2). The overall efficiency of light absorption is lowered since the layout of the packed pigments inside the cells decrease the probability that the light passes through the suspension would strike a cell (Duysens, 1956).

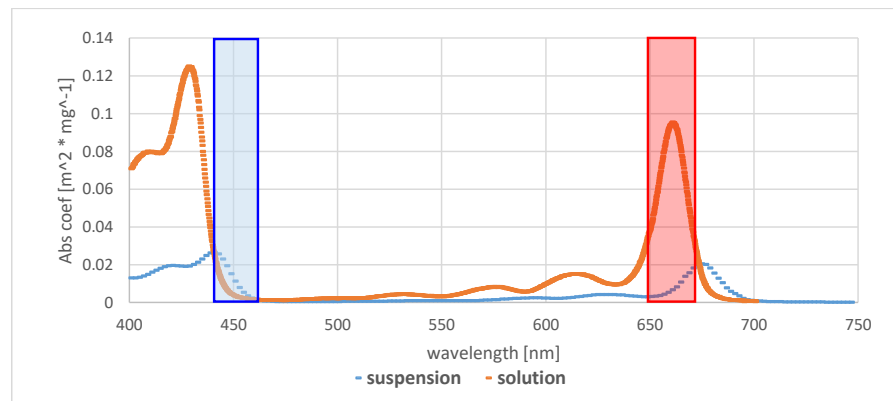


Figure 2 – Absorption spectrum of Chlorophyll a for (i) extracted cells in solution and (ii) packed cells in suspension. The latter was calculated by Bidigare *et al.*, 1990, according to Duysens' principles (Duysens, 1956); similar calculations were done for chlorophyll b and carotenoid (Bidigare *et al.*, 1990). Red (646-670 nm) and blue (440-464 nm) columns specify the ranges of wavelength supplied by the LEDs panel in our system.

## 3. Research methods

### 3.1. Overview

The main components of the system are presented in section [3.23-2](#), the assumptions are presented in section [3.33-3](#), the consensus methods, which serves as a basis for present development, are presented section [3.43-4](#), the calibration methodology in section [3.53-5](#), the system flow in section [3.63-6](#) and the acquisition and processing methods in section [3.73-7](#). The growth parameters are introduced in and used by the controlling algorithm described in section [3.93-9](#). Methods for statistical and stochastic models are described in section [3.103-10](#). The performance measures for the algorithm and models are presented in section [3.113-11](#).

### 3.2. System components

A custom-made photo-bioreactor was coupled to an acquisition and control system (see Appendix B – System hardware specification) and setup to illuminate an algal culture, controlling light quality and intensity, temperature and pH in a 20.0 L experimental culture vessel.

#### 3.2.1. Arduino

The system is monitored and controlled by an Arduino Mega 2560 microprocessor, an open-source microcontroller board containing [54](#) digital [I/O pins](#) and [16](#) analog [I/O ports/inputs](#).

#### 3.2.2. LEDs

Light is supplied by a LEDs array composed of 72 Red ( $\lambda = 665$  nm) and 12 blue ( $\lambda = 452$  nm) LEDs. The colored lights are controlled by separate dimmable constant current power supplies using voltage supplied by the Arduino board in a range of 0-255 Pulse Width Modulation (PWM) equivalent to DIM voltage of 0-5 V. In order to supply adequate light intensity to the microalgae culture, the light intensity received on the PBR surface has to be modeled as a function of PWM.

#### 3.2.3. Sensors: Light

The light sensors have different sensitivity to light color and were installed with different number of neutral density filters (to protect from excess light). Therefore, the measured light in Hz has to be properly processed. Moreover, since the light sensors reports light intensity in Hz (while the standard units are expressed in  $\mu\text{mol photons/m}^2/\text{s}$ ), units' conversion must be applied online.

#### 3.2.4. Sensor: pH

The pH level in the culture is monitored and continuously balanced by supplying  $\text{CO}_2$ . A valve, controlled by the Arduino, allows opening and closing of the  $\text{CO}_2$  supply in real time.

#### 3.2.5. Sensor: Temperature

The temperature is continuously monitored and uses for calibrating the pH sensor. The temperature is controlled by an external air conditioner set to 25°C.

#### 3.2.6. Biological materials

- Algae  
A sweet water green alga (Chlorophyta) *Chromochloris* (or *Chlorella*) *zofingiensis* was used, which has been reported to turn orange or red upon stress.
- Growth conditions (medium components and environmental conditions)  
The growth medium is composed of (mM):  $\text{NaNO}_3$ , 5.0;  $\text{KH}_2\text{PO}_4$ , 0.7;  $\text{K}_2\text{HPO}_4 \cdot 3\text{H}_2\text{O}$ , 0.7;  $\text{Na}_2\text{CO}_3$ , 0.19;  $\text{MgSO}_4 \cdot 7\text{H}_2\text{O}$ , 0.27;  $\text{CaCl}_2 \cdot 2\text{H}_2\text{O}$ , 0.24;  $\text{FeSO}_4 \cdot 7\text{H}_2\text{O}$ , 0.036;  $\text{Na}_2\text{-EDTA} \cdot 2\text{H}_2\text{O}$ , 0.047;  $\text{H}_3\text{BO}_3$ , 0.0463;  $\text{MnCl}_2 \cdot 4\text{H}_2\text{O}$ , 0.00915;  $\text{ZnSO}_4 \cdot 7\text{H}_2\text{O}$ , 0.00077;  $\text{Na}_2\text{MoO}_4 \cdot 2\text{H}_2\text{O}$ , 0.00161;  $\text{CuSO}_4 \cdot 5\text{H}_2\text{O}$ , 0.00032;  $\text{Co}(\text{NO}_3)_2 \cdot 6 \text{H}_2\text{O}$ , 0.00017.



Temperature around 25 °C, pH around neutral, mix of blue and red lights from LEDs with adjustable balance and specific intensities (per biomass). The culture in the 20.0 L experimental culture vessel (4 cm width) was mixed by bubbling air (with or without CO<sub>2</sub>) at rate of 0.3 vol gas/vol culture/minute.

### 3.3. Assumptions

- The total intensity for the incident or exiting light composed of multiple colors is the arithmetic sum of its components, as reflected by the sensors measurements.
- The fraction of the absorbed light is independent of the incident light intensity.
- The algal pigments absorb each light color differently.
- Light attenuated by the culture is the combination of the sum of absorbance by packed pigments and scattering by cells.
- The calibration procedure provide results independent of the variation of the LEDs intensity through time.
- Biomass of particles other than algae are neglected.

### 3.4. Working Hypothesis

The Beer-Lambert law was used to estimate the microalgal concentration based on the light intensity (LI) measured before (incident) and after (exiting) the photo-bioreactor (PBR), see illustration in [Figure 3](#). As a global working hypothesis for modeling purposes, the assumption is that the sensors represent the sum of intensities of red and blue lights. Moreover, the postulate that light absorption is independent of the incident light intensity has been verified; while this is valid at any given wavelength, this is not completely valid for a combination of colors.

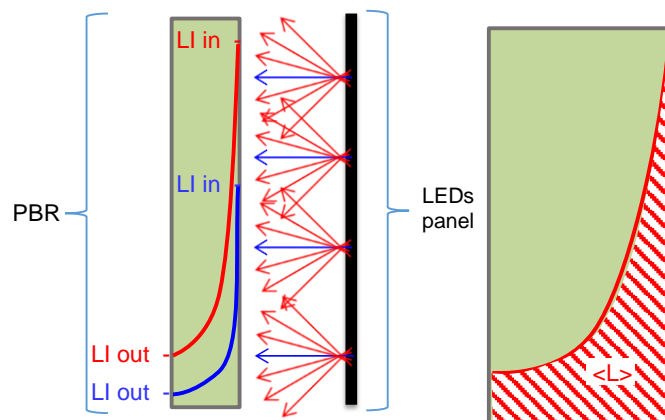


Figure 3 - Left panel: Side view for light behavior inside the photo-bioreactor. LI: Light intensity. The red and blue curves indicate local LI as a function of the position in the PBR. Right panel:  $\langle L \rangle$  (i.e., the area under the curve) represents the light intensity available to the suspension integrated over the PBR width.

Similarly, light attenuation in the culture will be modelled as the combination of the sum of absorbance by packed pigments and scattering by cells, for each color (see Appendix A – Decomposition of light attenuation). The treatment for each color is required since the pigments absorb the corresponding photons differently.

Finally, photosynthetic activity is determined by the rate of photons absorption. A well-known feature of the photosynthetic system is that after a photon has been absorbed, the resultant photosynthetic activity, directly dependent on the number of photons absorbed, is largely independent of the absorbed photon's energy, *i.e.*, wavelength.

Light transmission *in solution* is defined as (Marcuse, 1972):

$$Transmission = \frac{PAR_{out}(\lambda)}{PAR_{in}(\lambda)} \quad (4)$$

where  $PAR_{in}(\lambda)$  and  $PAR_{out}(\lambda)$  are the light intensities (as photons flux, expressed in  $\mu\text{mol photons/m}^2/\text{s}$ ) incident and exiting the containing vessel, respectively. In other words,  $PAR_{in}(\lambda)$  considered as the incident light intensity on the vessel surface and  $PAR_{out}(\lambda)$  as the light intensity after it passes through the solution.

Light absorbance at any wavelength  $\lambda$ , is defined as (Beer, 1852):

$$Abs(\lambda) = -\log_{10}(Transmission) = -\log\left(\frac{PAR_{out}(\lambda)}{PAR_{in}(\lambda)}\right) \quad (5)$$

Beer-Lambert law showing the relationship between absorbance and concentration of an absorbing species in solution (Beer, 1852):

$$-\log_{10}\left(\frac{PAR_{out}(\lambda)}{PAR_{in}(\lambda)}\right) = \varepsilon(\lambda) \cdot Concentration \cdot width \quad (6)$$

$\varepsilon(\lambda)$  is defined as the wavelength-dependent effective absorption coefficient, determined empirically for a given absorbing molecular species; *width*, optical path length for light absorption (in solution), could simply refer to the width of the vessel; *Concentration*, the algal concentration estimate based on the light absorption by the microalgal packed pigments.

Alternatively,

$$\frac{PAR_{out}(\lambda)}{PAR_{in}(\lambda)} = 10^{-\varepsilon(\lambda) \cdot Concentration \cdot width} \quad (7)$$

Isolating *Concentration* (independent of  $\lambda$ ) results in

$$Concentration = \frac{-\log_{10}\left(\frac{PAR_{out}(\lambda)}{PAR_{in}(\lambda)}\right)}{\varepsilon(\lambda) \cdot width} \quad (8)$$

Since each light color is absorbed differently by the algae (and by the photo-bioreactor), both the light intensities ( $PAR_{out}(\lambda)$ ,  $PAR_{in}(\lambda)$ ) and the effective absorption coefficient ( $\varepsilon(\lambda)$ ) should be arithmetically disassembled into red and blue components according to their respective intensities.

### 3.5. Calibration

The photo-bioreactor itself (its plastic components and the bubbling liquid medium) also contributes to apparent light absorption. In the special case where no algae exist in the photo-bioreactor (blank), the incident and outgoing light intensities are defined as  $PAR_{in\_blank}(\lambda)$  and  $PAR_{out\_blank}(\lambda)$ , respectively.

The total light absorbed by the system is defined as follows

$$Abs_{Total}(\lambda) = Abs_{Algae}(\lambda) + Abs_{blank}(\lambda) = -\log_{10}\left(\frac{PAR_{out}(\lambda)}{PAR_{in}(\lambda)}\right) - \log_{10}\left(\frac{PAR_{out\_blank}(\lambda)}{PAR_{in\_blank}(\lambda)}\right) \quad (9)$$

where  $Abs_{total}(\lambda)$  is the absorption by both the algae and the PBR components (blank). We can define the term  $-\log_{10}\left(\frac{PAR_{out}(\lambda)}{PAR_{in}(\lambda)}\right)$  as  $PBR(\lambda)$ , a constant correction to apply to the measured  $Abs_{Total}(\lambda)$  to obtain

$$Abs_{Algae}(\lambda) = Abs_{Total}(\lambda) - PBR(\lambda) \quad (10)$$

Therefore, the numerator in Right hand side of equation (8) should be updated as follows:

$$Concentration = \frac{-\log_{10}\left(\frac{PAR_{out}(\lambda)}{PAR_{in}(\lambda)}\right)}{\epsilon(\lambda) \cdot width} = \frac{Abs_{Total}(\lambda) - PBR(\lambda)}{\epsilon(\lambda) \cdot width} \quad (11)$$

The constant  $PBR(\lambda)$  for each light color ( $\lambda$ ) is therefore estimated through a separate calibration process conducted in the absence of algae (bubbling medium only in the container).

In addition, the local light measured by the sensors is determined in Hz units. Since the convention unit for photosynthetically active radiation (PAR) is  $\mu\text{mol photons/m}^2/\text{s}$ , the calibration procedure is extended to formulate the transformation functions from local light intensity in Hz measured by the sensor, to average light intensity as PAR measured by an independent light sensor (LI-COR LI-190R Quantum Sensor).

### 3.6. System flow

In the developed system<sup>1</sup>, sensors readings go through online preliminary processing (e.g., temperature measurement to fine-tune that of the pH, unit conversion, counting light pulses over time and compute Hz). Error-handling routines were implemented to avoid collecting aberrant data such as nulls or negative numbers. Furthermore, raw measurements of (continuous) light intensity are constantly aggregated into sums and averaged over 5 feasible samples in order to reduce noise and prevent data overload. For the latter reason, each sensor is sampled at independent time intervals, which are stored as variables and can be adjusted by the user.

Having the sensors readings available in the program in real-time as variables enables further online processing of the data measured and gathered (as discussed in section 3.2.3.2.3).

The algorithm steps for controlling the growth conditions and the estimation of the microalgal concentration are made in real-time and serve as an automatic control feedback to the system (see Figure 4), adapting its outputs (light intensity, light color, and pH level) accordingly. For that, the developed equations for each step of the algorithm and the deterministic model (see section 3.9.3.9) validated, deployed on the system in C/C++ and used in real time.

### 3.7. Data acquisition and processing

The system collects raw data from the sensors (*Light in, Light out, temperature, pH*; See Appendix B – System hardware specification). The data are continuously gathered, processed and summarized as results report, presented to the user through the control panel, and saved to a text file.

<sup>1</sup> <https://github.com/EladDan/ControlSystem/blob/master/ControlSystemR28.ino>

#### 3.7.1. Acquired data

- Illumination mode ([function: Cmd\\_SetIllumination](#)).
- Date and time ([function: Cmd\\_SetTimeDate](#)).
- Voltage levels (red and blue) currently supplied to the LEDs panel ([function: PowerLEDs](#)).
- Sensors readings (in Hz) at the incident and exiting faces of the photo-bioreactor ([lines: 674-760](#)).
- Temperature inside the photo-bioreactor ([function: ReadTemp](#)).
- pH level in the extra-cellular culture medium ([function: ReadPH](#)).

#### 3.7.2. Data processing

- Conversion of sensors readings (in Hz) into PAR (in  $\mu\text{mol photons/m}^2/\text{s}$ ) ([lines: 514-515, 2830-2831](#)).
- Red and blue light as PAR available for absorption to the algal cells in the culture ([function: L\\_availCalc](#)).
- Estimated concentration based on independent measurement of red and blue light absorption at moderate intensity, at fixed periods ([function: ConCalc](#)).
- Calculated growth rate between consecutive periods ([lines: 920](#)).

#### 3.7.3. Report

- Periodically update the user interface panel (acquired and processed data) ([function: UpdateIndicatorsFunction](#)).
- Add comments annotating user's initiated interventions ([function: PrintCSV](#)).
- Save the above in a file for further offline processing ([function: PrintCSV](#)).

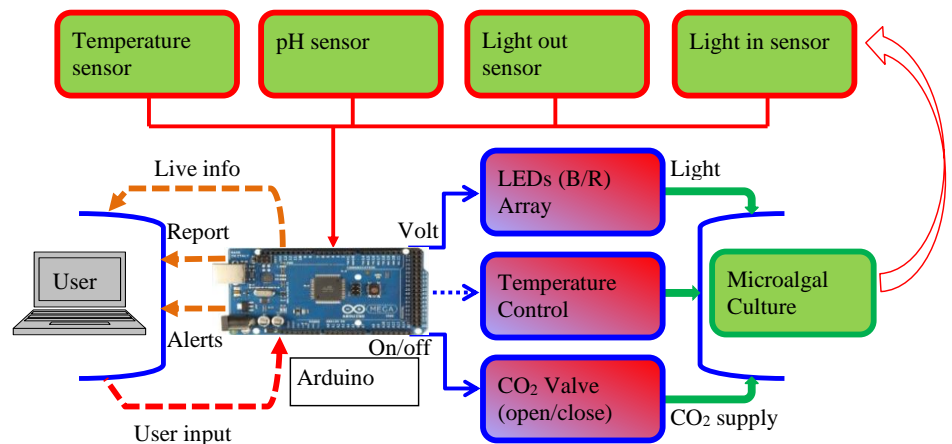


Figure 4 - Conceptual flow chart for the Arduino sketch (code) driving the algal culture in the photo-bioreactor.

#### 3.8. Growth parameters

The use of a control system over a closed photo-bioreactor enables monitoring the culture conditions. Culture parameters are acquired continuously to serve as inputs for possible multivariate analysis. Our modeling aim is to maximize the microalgal **growth rate**  $\mu$  ( $= \frac{\Delta \log_{10}(\text{Concentration})}{\Delta \text{time}}$ , assuming exponential growth).

The parameters presented in [Table 1](#) were chosen with the aim to assess and control the culture environmental conditions (see section [4.3.4](#)). Given the systems inputs and outputs, those parameters the potential to likely effect the growth rate; in simple words, they allow an adequate control of the light quality, diel light intensity and pH level as a proxy to CO<sub>2</sub> level.

*Table 1 - Parameters formulated to control the culture's enviromental conditions*

Parameter	General description	Details	Control
Fraction Red: Relative contribution of red light	Light quality	Independent power supply to red and blue LEDs	Auto
Ratio of ambient light per biomass	Light intensity	Ratio $\langle \text{PAR} \rangle^* / \text{Concentration}$ [ $\mu\text{mol photons} \cdot \text{L}/\text{m}^2/\text{s}/\text{mg}$ ]	Auto
Illumination mode	Distribution of light intensity during day	Standard illumination modes: 1. Continuous light 2. Constant light-dark 3. Sinusoid daylight	Auto
pH level (CO <sub>2</sub> supply)	Acidity level in the culture	Target for average pH	Auto

\* Total light available for absorption by the culture along the width of the photo-bioreactor

### 3.9. Controlling growth conditions

The algorithm flow (see Figure 5) was conceptually separated into two fundamental parts.

The first part is responsible mainly for measuring the lights intensities, estimating the algae concentration and determining the amount of each colored light that should be supplied to the algae, and finally supplying it, according to the illumination mode, by controlling the LEDs panel.

The second part consists of continuous measurement of pH and temperature. The pH of the suspension spontaneously decreases with CO<sub>2</sub> consumption. Since the latter increases during active photosynthesis, CO<sub>2</sub> must be supplied accordingly to balance the acidity level in the suspension. An instantaneous target value for the pH is determined, considering the current light intensity and biomass concentration (intense light and high biomass content necessitates increased CO<sub>2</sub> supply). Since the light intensity is already adjusted to the biomass concentration, the target pH value is determined solely according to light intensity.

The two parts are connected through the target pH level, which is determined based on the light supplied.

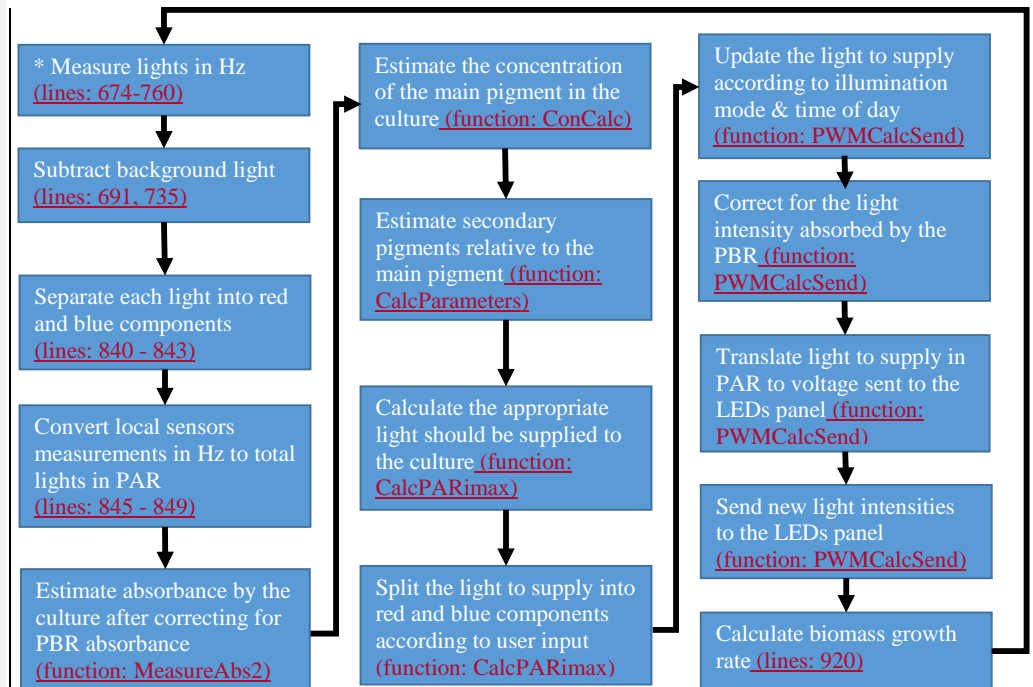


Figure 5 - The algorithm flow. \* represents a tentative start point.

### 3.10. Predictive models

Two models were developed:

1. **Deterministic model for concentration estimation (Section 4.2.14.2.4).** The Beer-Lambert law was extended to include the contribution of scattered light that modulates the optical path of light in the photo-bioreactor, thereby altering the odds for photon absorption, and thus microalgal growth. This deterministic approach differs from the currently used (e.g., Pottier *et al.*, 2005) assertion which models light scattering as an additional agent for light absorption. The formulated model aims to predict the concentration level of each of the light-absorbing pigments in the culture, using the light sensors measurements as inputs.
2. **Stochastic model for photon-cell interaction (Section 4.2.24.2.2).** The measured transmission is dependent on the concentration of the absorbing species (see equations {4, 8}). The transmission reflects also physical phenomena unrelated to absorption (e.g., scattering). In an effort to assess and correct the measured transmission, a stochastic model has been developed to predict the fate of light as it passes through a suspension. As a simplification, we considered a 1-dimensional problem, in which scattering (3-Dim) reduces to reflection (1-Dim). Thus, the model predicts the relative probabilities for absorption and reflection.

Two approaches for assessment and validation were explored:

1. **Linear and Non-Linear Regression Model.** Suitable transformations were applied as necessary to achieve Maximum Likelihood. For instance, log transform (Durbin *et al.*, 2002), and Box-Cox power transformation (Box & Cox, 1964) was applied.
2. **Markov Chain.** The Markov chain formalism was used to model the possible states of the incident light and its interactions with the culture cells along the photo-bioreactor.

### 3.11. Performance measurement

The performance of the models, algorithm, system (*i.e.*, sensors readings) and, lab results ~~and models~~ ~~are~~was assessed as follows:

- The deterministic model yields an equation predicting a value for biomass concentration (*chlorophyll a*). The latter is independently measured in the lab. The fit between predicted and measured values is evaluated using  $R$  squared indicator ( $R^2$ ).
- The stochastic model was evaluated using sensitivity analysis. The inputs of the model was explored and the results were tested to be rational and consistent.
- Validation of the algorithm was done using simulation. The deterministic model-based algorithm enables predicting a behavior for the culture (output) according to variable environmental conditions (inputs). Outputs are also simulated using an independent program (Matlab). The correctness of the output is evaluated for a range of inputs (sensors readings and user's target values).
- The repeatability of the light sensors measurements and the lab results for the assessed algae biomass (*i.e.*, *Chlorophyll a* concentration) is evaluated by five repetitions under similar conditions.

### 3.12. Algorithm simulation

A simulation<sup>2</sup> was programmed in Matlab in order to test the controlling algorithm correctness. The simulation imitates growth by a decrease of the light measured by the exiting sensor. In each iteration throughout the simulation, the algorithm calculates the environmental conditions (e.g., total PAR, red PAR, blue PAR, Fraction Red).

### 3.13. Statistical analysis

The formulated models are evaluated using  $R$  squared indicator ( $R^2$ ).  $R^2$  is commonly used as an indicator of how well observed outcomes fit the equation formulated in the model. Formally,  $R^2$  indicates the proportion of the explained variance (out of the total variance) of the dependent variable that is predictable from the independent variables and is defined as follows:

$$R^2 = 1 - \frac{SSE}{SST},$$

where  $SSE$  is the sum of squares error ( $error_i = Y_i - Y_{i,predicted}$ ) and is defined as:

$$SSE = \sum_{i=1}^n (Y_i - Y_{i,predicted})^2,$$

and  $SST$  is the total sum of squares, which is proportional to the variance of the dependent variable, and is defined as:

---

<sup>2</sup> <https://github.com/EladDan/AlgorithmSimulation>

$$SST = \sum_{i=1}^n (Y_i - \bar{Y})^2,$$

where  $n$  denotes the number of observations and  $\bar{Y} = \frac{\sum_{i=1}^n Y_i}{n}$ , is the average of observations.



## 4. Calibration, Models and Algorithm development

### 4.1. Calibration

The calibration procedure included: (a) a model for describing the local light intensity in Hz measured by the light sensors in the absence of algae (section [4.1.14.1.1](#)) and (b) a model for describing the global intensity as PAR (in  $\mu\text{mol photons/m}^2/\text{s}$ ) (section [4.1.24.1.2](#)).

Those procedures enable the prediction of both local Hz and global PAR measurements using the PWM.

#### 4.1.1. Calibration part 1

A calibration script<sup>3</sup> was programed to measure the local light intensities (in and out) at variable voltage. The voltage sent to the LEDs panel from the Arduino board as digital signal using Pulse Width Modulation (PWM) and ranges between 0 – 5 volt, is represented as 0 – 255 PWM.

In the calibration script, the voltage sent to the LEDs panel ranges from 30 (no light) to 245 PWM, in steps of 5. Each set of colored LEDs (72 red and 12 blue accordingly) was powered separately. The light sensors measured the light intensities at the incident and outcoming faces, respectively, in Hz units. The period for a single measurement was set to 10 seconds. For noise reduction, any light intensity, received at each step, was measured three times and the average intensity reported to a text file in comma separated values (CSV) format. Three sets of measurements were performed.

The following steps are done in order to model the local light intensities in Hz (measured by the light sensors) as function of PWM, with absence of algae.

1. In order to minimize the number of functions modeling the light intensity (in Hz), the measurements of the local light sensors in Hz are normalize to the light intensity at 140 PWM (moderate light used as reference, as discussed in section [4.3.14.3.1](#)). Therefore, the light of two colors and two sensors (four dependencies in total) is modeled as two functions (one per light color) and two scalars are used to distinguish the light sensor (in or out). It is assumed that the curves for the same light are similar up to a scalar (verified at section [5.2.15.2.1](#)).
2. The normalized light intensities are transformed using Box-Cox power transformation.
3. The transformed light intensities are modeled using linear regression.

#### 4.1.2. Calibration part 2

A second calibration was conducted in order to convert the local measurements in Hz received by the light sensors to global light intensity as PAR (in  $\mu\text{mol photons/m}^2/\text{s}$ ) at the incident and exiting surfaces of the PBR using an external and independent quantum sensor (LI-COR LI-190R Quantum Sensor). The measurements obtained from the latter represent PAR [ $\mu\text{mol photons/m}^2/\text{s}$ ], a photon-based flux light intensity.

The light intensities as PAR (in  $\mu\text{mol photons/m}^2/\text{s}$ ) were measured manually in front of each of the LEDs combos (12 measurements total). Since this calibration was done manually, the voltage sent to the LEDs panel ranges from 40 (apparent light) to 240 PWM, in steps of 50 (*i.e.*, 40, 90, 140, 190, 240). This procedure was done for each color (120 measurements total). Each measurement took about 10 seconds in order to achieve a statistically stable (noise-free) value.

---

<sup>3</sup> <https://github.com/EladDan/Calibration>

The following steps were conducted:

1. The measurements of all twelve LEDs combos were averaged.
2. Same as in section 4.1.14.1.1, the (averaged) measurements values were normalized to the light intensity in PAR at 140 PWM.
3. A model is built to predict the (averaged) normalized light intensities in PAR, using the normalized light intensities in Hz (see section 4.1.14.1.1).

## 4.2. Empirical Models

The Beer-Lambert equation is reformulated and extended in section 4.2.14.2.1, and its specific are estimated in section 5.35.3. Furthermore, a stochastic model (applying the Markov Chain formalism) considers the photons-cells interaction is developed in section 4.2.24.2.2.

### 4.2.1. Deterministic model for predicting the concentration

As explained in chapter 3.43.4, the concentration of absorbing pigments inside the photo-bioreactor is estimated using the formula in equation 11, resulting from the Beer-Lambert law.

However, although the calculated **concentration** must be **independent** on the light color considered, the product of  $\varepsilon(\lambda) \cdot \text{Concentration}$  in equation 6, reflecting the specific absorptivity of the pigment and its concentration, strongly depends on the wavelength absorbed. These considerations provide a powerful means to assess the relative pigments composition. The product  $\varepsilon(\lambda) \cdot \text{Concentration}$  is modeled as the sum of contributions of the different pigments:

$$\varepsilon(\lambda) \cdot \text{Concentration} = \sum_i (\varepsilon_i(\lambda) \cdot C_i), \quad (12)$$

where  $\varepsilon_i(\lambda)$  and  $C_i$  represent the specific absorptivity and the concentration of each pigment, respectively.

Three major pigments absorb light in the red and/or blue ranges: chlorophyll a, chlorophyll b, and carotenoids. The latter does not absorb red light. Therefore, the product  $\varepsilon(\lambda) \cdot \text{Concentration}$  is expressed as:

$$\sum_i (\varepsilon_i(\lambda) \cdot C_i) = \varepsilon_a(\lambda) \cdot C_a + \varepsilon_b(\lambda) \cdot C_b + \varepsilon_c(\lambda) \cdot C_c, \quad (13)$$

in which the indices  $a$ ,  $b$  and  $c$  stand for chlorophyll a, chlorophyll b and carotenoids, respectively.

Although the absorption properties of the pigments **in solution** are known, their existence in a packed state within cells **in suspension**, results in substantial deformation of their respective absorbance spectra (Duysens, 1956). Namely, since the pigments are packed inside the cell, the "packing effect" results in (i) flattening of pigments absorption spectra and (ii) wavelength red shift for their peaks. Thus,  $\varepsilon_i(\lambda)$  was estimated empirically according to Duysens principles (Bidigare *et al.*, 1990). Specifically, for each light color  $\lambda$  and pigment  $i$ ,  $\varepsilon_i(\lambda)$  is calculated as the average over the range of wavelengths of the red and blue LEDs used in our system, as given by equation 14.

$$\varepsilon_i(\lambda) = \frac{\sum_{\lambda=\lambda_{min}}^{\lambda_{max}} \varepsilon_i(\lambda)}{\lambda_{max} - \lambda_{min}}, \quad (14)$$

where  $\lambda_{min}$  and  $\lambda_{max}$  are the wavelengths around the peak enclosing 2/3 of each LED emission spectrum.

Moreover, the presence of particles in suspension (rather than solution) leads to scattering of light, which may result in considerably altering the effective optical path of the light in the photo-bioreactor, and hence the probability for light absorption. The latter phenomenon depends on the particles size, shape, and density (Duysens, 1956).

Thereby,  $OP$  is defined as the effective optical path length for light absorbance **in suspension**.  $OP$  is composed of the photo-bioreactor width and the effect of light scattering. We thereby postulate  $OP$  to be proportional to concentration. That is, the photo-bioreactor width is multiplied by a wavelength-dependent coefficient ( $K(\lambda)$ ) reflecting opto-geometrical properties of the particles and their density ( $C_d$ ) in a suspension.

$$OP = K(\lambda) \cdot C_d \cdot width, \quad (15)$$

in which  $C_d$ ,  $K(\lambda)$  and  $width$  stands for cell density, effective dependency of the optical path at the particles shape and size, and the actual photo-bioreactor width, respectively. The product  $K(\lambda) \cdot C_d$  represents the ratio between  $OP$ , the effective optical path in suspension (altered by scattering) to  $width$ , which is the optical path length in solution.

Equations 13 and 15 yields a more detailed form for attenuation than stated in equation 6, describing absorption by a pigment in solution:

$$-\log_{10} \left( \frac{PAR_{out}(\lambda)}{PAR_{in}(\lambda)} \right) = (\varepsilon_a(\lambda) \cdot C_a + \varepsilon_b(\lambda) \cdot C_b + \varepsilon_c(\lambda) \cdot C_c) \cdot K(\lambda) \cdot C_d \cdot width. \quad (16)$$

Alternatively, using relative concentrations to  $C_a$  ( $C_x^* = \frac{C_x}{C_a}$ ), namely  $C_b^*$ ,  $C_c^*$  and  $C_d^*$ , we get

$$-\log_{10} \left( \frac{PAR_{out}(\lambda)}{PAR_{in}(\lambda)} \right) = (\varepsilon_a(\lambda) + \varepsilon_b(\lambda) \cdot C_b^* + \varepsilon_c(\lambda) \cdot C_c^*) \cdot K(\lambda) \cdot C_d^* \cdot width \cdot C_a^2. \quad (17)$$

Note that equation 17 includes parameters independent of concentration ( $\varepsilon_a(\lambda) + \varepsilon_b(\lambda) \cdot C_b^* + \varepsilon_c(\lambda) \cdot C_c^*) \cdot K(\lambda) \cdot C_d^* \cdot width$ , and reveals a squared dependence on the concentration of the main pigment ( $C_a$ ), in which the cell density ( $C_d$ , or dry weight) is assumed to be proportional to the concentration of the main pigment ( $C_a$ ) in the suspension.

For simplification in the subsequent equations, a combined parameter reflecting a **specific attenuation coefficient** ( $SAC(\lambda)$ ) is introduced, including both absorbance and scattering on a chlorophyll  $a$  ( $C_a$ ) basis.

$$SAC(\lambda) = (\varepsilon_a(\lambda) + \varepsilon_b(\lambda) \cdot C_b^* + \varepsilon_c(\lambda) \cdot C_c^*) \cdot K(\lambda) \cdot C_d^*. \quad (18)$$

The concentrations  $C_i$  are independently measured in the laboratory after pigment extraction (Lichtenthaler & Buschmann, 2001). In the following development, these values will be regarded as **observations**. On the other hand, the corresponding values calculated in the Arduino sketch will be considered as **predictions**.

The specific absorption coefficients for **packed** pigments are used as previously assessed (Bidigare *et al.*, 1990) and further validated (Pottier *et al.*, 2005).

Finally, the parameter  $K(\lambda)$  could be calculated by resolving system of multiple equations {11, 13} obtained for each color, in which many variables are known (calculated in the Arduino sketch or measured in the lab), yielding also the pigments and cells density. Alternatively, it can be solved empirically using the respective observations measured at laboratory (Chlorophyll  $a$  concentration) and by the system (light transmission).

To conclude, the inputs for the model described in equation 19 (equation 11 updated by equation 18) are the parameters detailed above and the updated incident and exiting lights, estimated using the light sensors. The result (output) is the concentration (in mg/L) for the main pigment, *Chlorophyll a*. The concentration for the other pigments (*i.e.*, *Chlorophyll b* and *Carotenoid*) is achieved by multiplying each of their relative concentrations (*i.e.*,  $C_{xi}^*$ ) by the *Chlorophyll a* concentration.

$$C_a = \sqrt{\frac{-\log_{10}\left(\frac{PAR_{out}(\lambda)}{PAR_{in}(\lambda)} \frac{PAR_{inblank}(\lambda)}{PAR_{outblank}(\lambda)}\right)}{SAC(\lambda) \cdot width}} = \sqrt{\frac{Abs_{Total}(\lambda) - PBR(\lambda)}{SAC(\lambda) \cdot width}}. \quad (19)$$

#### 4.2.2. Stochastic model for photon-cell interaction

The concentration prediction model, developed in section 4.2.14.2.1, is based on measured  $PAR_{in}$ . However, the causality is that the transmission is partially determined by the concentration. Therefore, this chapter is dedicated to formulate a stochastic model that describes the transmission as function of the concentration.

The result of this model is the probability for an incident light to (a) reflect out of the PBR, (b) absorb inside the cells, or (c) exit the PBR (transmitted).

The suspension is modeled in a single dimension. Accordingly, cells are grouped into layers (which are reflecting and absorbing elements) that align in a 1D array along the width of the PBR (see Figure 6).

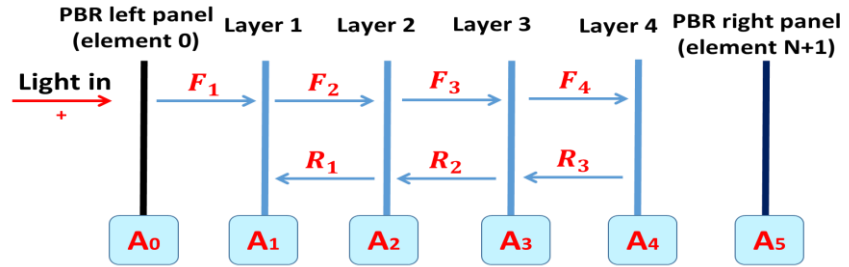


Figure 6 - Schematic modelling of light suspension: cells are modeled as  $N (=4)$  layers which interact with the incident light. Light states ( $F_i$ ,  $R_i$  and  $A_i$ ) are defined in Table 2.

Cells in suspension are modeled as cubes. Each cubic cell is projected upon the PBR area, such that they form  $N$  layers. The number of layers, which is proportional to the biomass concentration, is defined as follows:

$$N = \lceil \text{cell cross section} \cdot \text{width} \cdot \text{cell density} \rceil. \quad (20)$$

Incoming photons, traveling along the PBR width, encounter an algal element  $i$ . The incoming photons, represented by a flux  $I_{in}$ , may either

1. be reflected (scattered) with probability  $r$ , such that  $I_R = r I_{in}$ ;
2. be absorbed by the pigments in element  $i$ , with probability  $a$ , such that  $I_A = (1 - r) a I_{in}$ , or
3. pass through the element with probability  $t$ , such that  $I_{out} = (1 - r)(1 - a) I_{in} \implies (1 - r - a + ar) I_{in}$ .

The energy conservation relation  $I_{in} = I_R + I_A + I_{out}$  is thereby validated.

Thus, for element  $i$ , a fraction  $r$  of the incident light from a neighboring element ( $i-1$  or  $i+1$ ) will be reflected; a fraction  $(1 - r) a$  will be absorbed in element  $i$ , while the non-reflected and non-absorbed fraction  $(1 - r)(1 - a)$ , will pass through. Note that the process is bi-directional.

The inputs for the model are therefore the elementary probabilities for reflection ( $r$ ) and absorption ( $a$ ). The probability  $a$  depends on the inner cell properties and is defined based on Beer-Lambert law, assuming  $PAR_{in}$  is the light that was not reflected. The inner absorption by a cubic cell is defined as:

$$Abs = -\log_{10} \left( \frac{PAR_{out}}{PAR_{in}} \right) = (\varepsilon_a(red) + \varepsilon_b(red) \cdot C_b^* + \varepsilon_c(red) \cdot C_c^*) \cdot Chla_{in} \cdot cell\_dim\_cube, \quad (21)$$

where  $Chla_{in}$  is the intracellular Chlorophyll a concentration in  $mg/cm^3$  and  $cell\_dim\_cube$  is the dimension of cell width equivalent for a cube. Applying  $10^{-(x)}$  on the above equation yields:

$$\frac{PAR_{out}}{PAR_{in}} = 10^{-(\varepsilon_a(red) + \varepsilon_b(red) \cdot C_b^* + \varepsilon_c(red) \cdot C_c^*) \cdot Chla_{in} \cdot cell\_dim\_cube}, \quad (22)$$

which could be referred to as the probability for an entering beam,  $PAR_{in}$ , to go through the cell. Therefore, the (complementary) elementary probability for absorption by a "cubic" cell (corresponding also for layer of cells) is defined as:

$$a = 1 - \frac{PAR_{out}}{PAR_{in}} = 1 - 10^{-(\varepsilon_a(red) + \varepsilon_b(red) \cdot C_b^* + \varepsilon_c(\lambda) \cdot C_c^*) \cdot Chla_{in} \cdot cell\_dim\_cube} \quad (23)$$

Three formal states for photons are defined, in relation to each element  $i$ . The state space comprise three groups: (1)  $F_i$ : photons moving in the forward direction from element  $i-1$  to element  $i$ , (2)  $R_i$ : photons moving in the backward direction, from element  $i+1$  to element  $i$ , and (3)  $A_i$ : photons absorbed in element  $i$ .

Two **sub-models** for photon-cell interaction are examined:

1. The case of an integer number of  $N$  complete layers (sub-model 1).
2. An extended model in which the cells are distributed on a large number of layers ( $N_{max}$ ) containing holes (sub-model 2). In this case, the probability for photon-cell encounter is defined as:

$$p_{enc} = [cumulative\ cell\ cross\ section] / N_{max} \quad (24)$$

The number of elements in sub-model 1 is  $N+2$ . For modeling purposes, elements with index  $i = [1, ..., N]$  represent the layers, while indices  $i = 0$  and  $N+1$  represent the PBR borders in which incident light enter from the left side. For indexing purposes,  $N_{max}$  replaces  $N$  in sub-model 2.

We shall use the Markov Chain formalism to describe the possible transitions from one state to another. For that purpose, we build a 2D square matrix consisting of the probabilities of transition from an initial state  $k$  in rows, to a final state  $l$  in columns; these probabilities will be denoted as  $p_{kl}$ .

The process starts in one of these states and moves stepwise from one state to another. If the chain is currently in state  $k$ , then it moves to state  $l$  at the next step with a probability denoted by  $p_{kl}$ .

Table 2 shows the possible states for a photon, which may be dynamic (photon is in motion – group states  $F_i$  or  $R_i$ ) or static (photon is trapped – group state  $A_i$ ).

The transition probabilities to go from state  $k = [1, ..., 3N - 1]$  to state  $l = [1, ..., 3N - 1]$  are defined in Table 3.

Table 2 - Possible states for a photon

Group state	Size	Matrix element index	Description	State Type
$F_i$ - Moving Forward $i=[1,...,N]$	$N$	$k=[1,...,N]$	Beam is moving in positive direction from element $i-1$ to element $i$ .	Transient
$R_i$ - Moving Backward $i=[1,...,N-1]$	$N-1$	$k=[N+1,...,2N-1]$	Beam is moving in negative direction from element $i+1$ to element $i$ .	Transient
$A_i$ - Absorbed $i=[0,...,N+1]$	$N+2$	$k=[2N,...,3N+1]$	Beam is absorbed in element $i$ .	Absorbing

Table 3 – Transition probabilities to go from state  $k$  to state  $l$ ; the probabilities rely on the elementary probabilities defined above.

State	Matrix element index	Probabilities for sub-model 1	Probabilities for sub-model 2
$F_l$	$k = 1$	$p_{1,l} = \begin{cases} t, & \text{if } l = 2 \\ r, & \text{if } l = 2N \\ (1-r)a, & \text{if } l = 2N+1 \\ 0, & \text{otherwise} \end{cases}$	$p_{1,l} = \begin{cases} (1-p_{enc}) + p_{enc} \cdot t, & \text{if } l = 2 \\ p_{enc} \cdot r, & \text{if } l = 2N \\ p_{enc} \cdot (1-r)a, & \text{if } l = 2N+1 \\ 0, & \text{otherwise} \end{cases}$
$F_i$	$k = [2, ..., N-1]$	$p_{k,l} = \begin{cases} t, & \text{if } l = k+1 \\ r, & \text{if } l = k+N-1 \\ (1-r)a, & \text{if } l = k+2N \\ 0, & \text{otherwise} \end{cases}$	$p_{k,l} = \begin{cases} (1-p_{enc}) + p_{enc} \cdot t, & \text{if } l = k+1 \\ p_{enc} \cdot r, & \text{if } l = k+N-1 \\ p_{enc} \cdot (1-r)a, & \text{if } l = k+2N \\ 0, & \text{otherwise} \end{cases}$
$F_N$	$k = N$	$p_{N,l} = \begin{cases} r, & \text{if } l = 2N-1 \\ (1-r)a, & \text{if } l = 3N \\ t, & \text{if } l = 3N+1 \\ 0, & \text{otherwise} \end{cases}$	$p_{N,l} = \begin{cases} p_{enc} \cdot r, & \text{if } l = 2N-1 \\ p_{enc} \cdot (1-r)a, & \text{if } l = 3N \\ (1-p_{enc}) + p_{enc} \cdot t, & \text{if } l = 3N+1 \\ 0, & \text{otherwise} \end{cases}$
$R_l$	$k = N+1$	$p_{N+1,l} = \begin{cases} r, & \text{if } l = 2 \\ t, & \text{if } l = 2N \\ (1-r)a, & \text{if } l = 2N+1 \\ 0, & \text{otherwise} \end{cases}$	$p_{N+1,l} = \begin{cases} p_{enc} \cdot r, & \text{if } l = 2 \\ (1-p_{enc}) + p_{enc} \cdot t, & \text{if } l = 2N \\ p_{enc} \cdot (1-r)a, & \text{if } l = 2N+1 \\ 0, & \text{otherwise} \end{cases}$
$R_i$	$k = [N+2, ..., 2N-1]$	$p_{k,l} = \begin{cases} r, & \text{if } l = k-N+1 \\ t, & \text{if } l = k-1 \\ (1-r)a, & \text{if } l = k-N \\ 0, & \text{otherwise} \end{cases}$	$p_{k,l} = \begin{cases} p_{enc} \cdot r, & \text{if } l = k-N+1 \\ (1-p_{enc}) + p_{enc} \cdot t, & \text{if } l = k-1 \\ p_{enc} \cdot (1-r)a, & \text{if } l = k-N \\ 0, & \text{otherwise} \end{cases}$
$A_i$	$k = [2N, ..., 3N+1]$	$p_{k,l} = \begin{cases} 1, & \text{if } l = k \\ 0, & \text{otherwise} \end{cases}$	$p_{k,l} = \begin{cases} 1, & \text{if } l = k \\ 0, & \text{otherwise} \end{cases}$

The Markov Chain (see Figure 7) is defined based on Table 2 (states space) and Table 3 (transition probabilities).

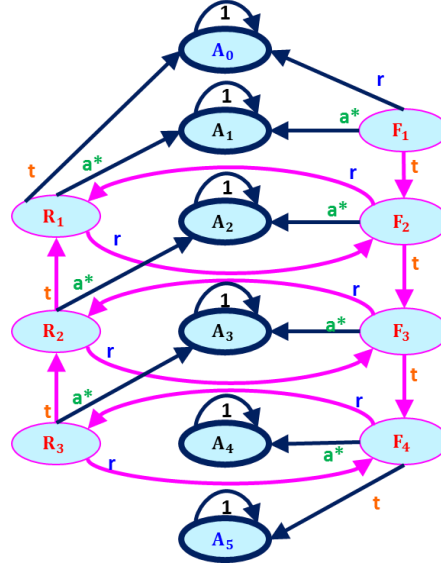


Figure 7 - The Markov Chain for sub-model 1.  
 $a^*$  denotes  $(1-r)a$ ; example for  $N=4$

The **transitions matrix  $T$**  (sized  $3N+1 \times 3N+1$ ) is built based on the transition probabilities in Table 3. Figure 8 shows the transitions matrix  $T$  for  $N$ , the number of full layers, equals five.

$k$	$l$	1	2	3	4	5	6	7	8	9	10	11	12	13	14	15	16
$k$	State	$F_1$	$F_2$	$F_3$	$F_4$	$F_5$	$R_1$	$R_2$	$R_3$	$R_4$	$A_0$	$A_1$	$A_2$	$A_3$	$A_4$	$A_5$	$A_6$
1	$F_1$	0	$t$	0	0	0	0	0	0	0	$r$	$(1-r)a$	0	0	0	0	0
2	$F_2$	0	0	$t$	0	0	$r$	0	0	0	0	0	$(1-r)a$	0	0	0	0
3	$F_3$	0	0	0	$t$	0	0	$r$	0	0	0	0	0	$(1-r)a$	0	0	0
4	$F_4$	0	0	0	0	$t$	0	0	$r$	0	0	0	0	0	$(1-r)a$	0	0
5	$F_5$	0	0	0	0	0	0	0	0	$r$	0	0	0	0	0	$(1-r)a$	$t$
6	$R_1$	0	$r$	0	0	0	0	0	0	0	$t$	$(1-r)a$	0	0	0	0	0
7	$R_2$	0	0	$r$	0	0	$t$	0	0	0	0	0	$(1-r)a$	0	0	0	0
8	$R_3$	0	0	0	$r$	0	0	$t$	0	0	0	0	0	$(1-r)a$	0	0	0
9	$R_4$	0	0	0	0	$r$	0	0	$t$	0	0	0	0	0	$(1-r)a$	0	0
10	$A_0$	0	0	0	0	0	0	0	0	0	1	0	0	0	0	0	0
11	$A_1$	0	0	0	0	0	0	0	0	0	0	1	0	0	0	0	0
12	$A_2$	0	0	0	0	0	0	0	0	0	0	0	1	0	0	0	0
13	$A_3$	0	0	0	0	0	0	0	0	0	0	0	0	1	0	0	0
14	$A_4$	0	0	0	0	0	0	0	0	0	0	0	0	0	1	0	0
15	$A_5$	0	0	0	0	0	0	0	0	0	0	0	0	0	0	1	0
16	$A_6$	0	0	0	0	0	0	0	0	0	0	0	0	0	0	0	1

Figure 8 - Schema for the transition probabilities matrix  $T$ . Example for  $T$  matrix when  $N = 5$ .

Each matrix element ( $T_{k,l}$ ) is the probability to transit from an initial state  $k$  (in rows) to reach a final state  $l$  (in columns), in a single step. Since we model the states of photons, which travel at the speed of light, a large number of such transits can be accomplished rapidly, eventually reaching a steady state. In

addition, the probabilities for transient states vanish after a high number of steps (Grinstead & Snell, 2012).

The transition probabilities matrix,  $\mathbf{T}$ , should stabilize (steady state probabilities) after a large number of iterations, where each iteration is the multiplication of the transition matrix by itself (raising the matrix to power 2).

Therefore,  $\pi$  is defined as the steady-state matrix (size  $3N+1 \times 3N+1$ ) where each element ( $\pi_{k,l}$ ) is the probability to eventually absorb in state  $l$ , given we started in state  $k$ . Since states  $k, l = [1, \dots, 2N-1]$  are transients, they should be zeroed, meaning  $\pi_{k,l} = 0$  for those states.

$\pi_k^{(A_i)}$  (sub matrix of  $\pi$ ) denotes the matrix probabilities (size  $2N-1 \times N+2$ ) to eventually absorb in state  $l$ , one of the **absorbing states** (group state  $A_i$ , or states  $l = [2N, \dots, 3N+1]$ ), given we started at state  $k$ , (group states  $F_i$  and  $R_i$  or states  $k = [1, \dots, 2N-1]$ ). Therefore  $\pi_k^{(A_i)}$  is the partial steady-state matrix which contains the elements of our interest (which are not expected to zero at steady state).

Since the incident beam is considered as the first state ( $k=1$ ), we care only about the first row of the partial steady-state matrix -  $\pi_{k=1}^{(A_i)}$ , which indicates the probabilities of the incident beam to absorb in each of the absorbing states ( $A_i$  states group).

As mentioned, one way to obtain  $\pi_k^{(A_i)}$  is by multiplying the transition matrix  $\mathbf{T}$  by itself. This way is less favorable since we deal with real time system, where high computation time could result in low performances (e.g., not closing/opening the CO<sub>2</sub> valve on time). A more elegant way to obtain  $\pi_k^{(A_i)}$  is by solving a system of equations as follows.

For a photon moving toward element  $i=[1, \dots, N]$ , meaning states  $k = [1, \dots, 2N-1]$ , the probability to eventually get locked in group state  $A_j$  is composed of the probabilities for all of the moving forward ( $F_i$  group) and backward ( $R_i$  group) photons to eventually absorb in one of the absorbing states ( $A_j$  group), and is defined as:

$$\pi_k^{(A_j)} = \pi_{Fi}^{(A_j)} + \pi_{Ri}^{(A_j)}, \quad (25)$$

where

$$\begin{aligned} \pi_{Fi}^{(A_j)} &= r \cdot \pi_{Ri-1}^{(A_j)} + t \cdot \pi_{Fi+1}^{(A_j)} + (1-r) a \cdot I_{\{i=j\}}, \\ \pi_{Ri}^{(A_j)} &= r \cdot \pi_{Fi+1}^{(A_j)} + t \cdot \pi_{Ri-1}^{(A_j)} + (1-r) a \cdot I_{\{i=j\}}. \end{aligned}$$

Where  $I_{\{i=j\}}$ , a column vector (size  $2N-1 \times 1$ ), holds "1" at rows (corresponding to the transition matrix  $\mathbf{T}$ ) in which moving photons (group states  $F_i$  and  $R_i$ ) get trapped (group states  $A_j$ ) in the next step, and "0" otherwise.

Note that in the generalized form of the above set of equations, the special cases where photons exit the PBR in either direction (reverse or forward, elements  $i=0$  and  $N+1$ , respectively) are considered as trapped (out of the PBR). The required modifications are applied later with the definition of  $\underline{\eta}^{(A_j)}$ .

More generally, for any  $i$ , and a specific absorbing state  $A_j$ , it could expressed as follows:

$$\underline{\pi}^{(A_j)} = \hat{\mathbf{P}} \cdot \underline{\pi}^{(A_j)} + \underline{\eta}^{(A_j)} \quad (26)$$

Where  $\hat{\mathbf{P}}$  is a partial transition matrix (size  $2N-1 \times 2N-1$ ) for only the transient states  $k, l = [1, \dots, 2N-1]$  and  $\underline{\eta}^{(A_j)}$  is a vector (size  $2N-1 \times 1$ ) that holds the probabilities for states  $k = [1, \dots, 2N-1]$  (a



moving photon; group states  $F_i$  or  $R_i$ ) to absorb in element  $l = [2N, \dots, 3N + 1]$  (trapped photon; group state  $A_j$ ) in the next step. In other words,  $\underline{\eta}^{(A_j)}$  holds the probabilities to move from states  $F_i$  and  $R_i$  to state  $A_j$ . Following is the formal definition for  $\underline{\eta}^{(A_j)}$ :

$$\underline{\eta}^{(A_j)} = p(\text{Photon trapped} - A_j | \text{moving Photon} - F_i \text{ or } R_i)$$

Table 4 shows the definition for  $\underline{\eta}^{(A_j)}$  (for each absorbing state  $j$ ).

Table 4 - Definition of  $\underline{\eta}^{(A_j)}$ , the probability for a moving photon to get trapped in element  $j$ .

Absorbing state	Value for $\underline{\eta}^{(A_j)}$
$j = 1$	$(\eta^{(A_j)})_k = \begin{cases} r, & k = j \\ t, & k = N + j \\ 0, & \text{otherwise} \end{cases}$
$1 < j < N + 2$	$(\eta^{(A_j)})_k = \begin{cases} a(1 - r), & k = j \text{ or } k = N + j \\ 0, & \text{otherwise} \end{cases}$
$j = N + 2$	$(\eta^{(A_j)})_k = \begin{cases} t, & k = N \\ 0, & \text{otherwise} \end{cases}$

Equation 26 could be solved by isolating  $\underline{\pi}^{(A_j)}$  as follows:

$$\underline{\pi}^{(A_j)} - \hat{\mathbf{P}} \cdot \underline{\pi}^{(A_j)} = \underline{\eta}^{(A_j)} \quad (27)$$

$$(\mathbf{I} - \hat{\mathbf{P}}) \cdot \underline{\pi}^{(A_j)} = \underline{\eta}^{(A_j)} \quad (28)$$

$$\underline{\pi}^{(A_j)} = (\mathbf{I} - \hat{\mathbf{P}})^{-1} \cdot \underline{\eta}^{(A_j)} \quad (29)$$

Where  $\underline{\pi}^{(A_j)}$  a vector (size  $2N-1 \times 1$ ), shows the probabilities for any moving beam to absorb in state  $A_j$  and  $\mathbf{I}$  is an identity matrix (size  $2N-1 \times 2N-1$ ) in which the elements on the main diagonal are equal to one and the other elements are equal to zero.

Thus, concatenating  $\underline{\pi}^{(A_j)}$  (by columns) for any absorbing state  $A_j$ , should produce the desired stabilized probabilities matrix  $\underline{\pi}^{(A_j)}$ . As mentioned, since our interest is the initiate beam probability to absorb in any element, we take only the first row of the stabilized probabilities matrix -  $\underline{\pi}_{k=1}^{(A_j)}$ .

After obtaining an analytical solution for  $\underline{\pi}_{k=1}^{(A_j)}$ , we propose another solution that evade matrix multiplication. This solutions should consider  $N$ , the number of grouped cells, as a parameter.

We saw that the expression for  $\underline{\pi}^{(A_j)}$  is composed of the multiplying of  $(\mathbf{I} - \hat{\mathbf{P}})^{-1}$  by  $\underline{\eta}^{(A_j)}$ .  $\underline{\eta}^{(A_j)}$  is known and was defined earlier. Finding an equation to express the elements of  $(\mathbf{I} - \hat{\mathbf{P}})^{-1}$ , or only it first row, will enable us to multiply that row by the relevant column vector  $\underline{\eta}^{(A_j)}$  for any  $j$ . This will yield  $\underline{\pi}_{k=1}^{(A_j)}$  for a specific  $A_j$ . The sum of probabilities for the initiate beam to eventually absorb in any state  $A_j$  equals 1. Therefore, one may calculate  $\underline{\pi}_{k=1}^{(A_j)}$  only for  $j = 0$  and  $j = N+1$  (the left and right sides of the PBR), and

reduce those values from 1 in order to obtain the probability for the initiate beam to absorb in any element  $j = 1..N$  (the suspension).

In order to find an expression for  $(I - \hat{P})^{-1}$ , we use the following rule:

$$(I - \hat{P})^{-1} \cdot (I - \hat{P}) = I. \quad (30)$$

We address the elements at the first row of  $(I - \hat{P})^{-1}$ ,  $Z_i$ , as variables:

$$(Z_1, Z_2, \dots, Z_{2N-1}) \cdot (I - \hat{P}) = I. \quad (31)$$

Alternatively, we address  $Z_i$  as two groups of variables as follows:

$$(X_0, X_1, \dots, X_{N-1}, Y_1, Y_2, \dots, Y_{N-1}) \cdot (I - \hat{P}) = I. \quad (32)$$

Where  $X_0 = Z_1 \dots X_{N-1} = Z_N$  and  $Y_1 = Z_{N+1} \dots Y_{N-1} = Z_{2N-1}$  (or shortly:  $Y_j = X_{N+j-1}$ ).

The following system of equations is expressing the equations formulating by the multiplication of  $Z_i$  at any row of  $(I - \hat{P})$  with the result of the corresponding column at the first row of  $I$  (1, 0, 0, ..., 0):

$i = [1, \dots, N]$  yields:

$$\begin{aligned} X_0 &= 1 \\ X_{j-1} \cdot (1 - a) \cdot (1 - r) + Y_{j-1} \cdot r &= X_j \end{aligned} \quad (33)$$

and  $i = [N+1, \dots, 2N-1]$  yields:

$$\begin{aligned} X_j \cdot r + Y_{j+1} \cdot (1 - a) \cdot (1 - r) &= Y_j \\ Y_{N-1} &= r \cdot X_{N-1} \end{aligned} \quad (34)$$

Where for  $i = [1, \dots, N]$  and  $i = [N+1, \dots, 2N-1]$  we consider  $Y_j$  and  $X_j$  as constants, respectively.

The above system of equations produces a 2-dimensional recursive equation (with two conditions). In order to find  $Z_i$  elements, the equations could be solved using Wolfram Mathematica. This produces equations dependent on  $N$ , the number of layers, and enabling to deploy and solve it in real-time while avoiding the built of  $P$  and  $(I - P)^{-1}$  matrices.

#### 4.3. Algorithm for controlling growth conditions

A summary for the algorithm steps described in this chapter is presented as follows.

1. Measure incident and exiting lights.
2. Background lights subtraction.
3. Separate the measured lights into it red and blue components based on the routinely measured reference light, as solution of system of equations.
4. Convert local measurements in Hz to PAR intensity on the PBR surfaces in  $\mu\text{mol photons/m}^2/\text{s}$ .
5. Estimate absorbance by the culture (after reducing the PBR absorbance) based on Beer-Lambert law.
6. Concentration estimation of *Chlorophyll a* pigment, based on the absorbed lights, using the deterministic model.
7. Estimate *Chlorophyll b*, *Carotenoid* and *Dry Weight* relative to the *Chlorophyll a* concentration.
8. Calculate the appropriate total light as PAR that should be supplied to the culture, according to the biomass concentration.

9. Split the total incident light to supplied into it red and blue components according to the user's input (target red fraction of available light for absorbance by the biomass' cells) and the effective absorption of the biomass' cells.
10. Update the incident light to be supplied according to (i) the illumination mode (users' input), (ii) the time of day (e.g., maximum light supplied at noon), as well as the reduction of light due to the photo-bioreactor absorption (i.e., independent of the algae). Translate calculated PAR intensity to be supplied into voltage values sent to the LEDs panel.
11. Update LEDs panel to supply the appropriate lights intensity.
12. Calculate the red fraction light available for absorbance.
13. Calculate the biomass growth rate.
14. Go to step one.

#### 4.3.1. Light intensity and quality

The incident ( $Light_{in}$ ) and outcoming ( $Light_{out}$ ) lights from the photo-bioreactor are measured continuously and independently by the respective sensors. In order to reduce the measurement error, low light intensities measured during a relatively long period. The period for measuring each light sensor is constrained between 0.2 to 2 seconds for  $Light_{in}$  and 7.5 to 10 seconds for  $Light_{out}$ .

The pulses from the light sensors are summed up throughout that period and used for calculating a time-averaged light intensity in Hz as follows:

$$Light = \frac{Pulses\ received}{Period} \quad (35)$$

The measured total light intensities are finally averaged over time (5 to 15 min).

As previously discussed, The light intensities are separated into it components (according to light color), and determine the contribution of each color to the light sensors,  $Light_{in}$  and  $Light_{out}$ .

In order to detect possible changes in the relative pigments composition occurring slowly during growth, we measured periodically (every 4h) the absorption of red and blue light separately at moderate (PWM=140) incident light intensities. The changes in absorbance reflect the changes in pigments composition. We shall use the notations  $Light_{out,ref}(red)$ ,  $Light_{in,ref}(red)$ ,  $Light_{out,ref}(blue)$  and  $Light_{in,ref}(blue)$  for the corresponding periodically updated reference intensities.

We first postulate that the light measured at the sensors is the arithmetic sum of its red and blue components:

$$Light_{out} = Light_{out}(red) + Light_{out}(blue) \quad (36)$$

$$Light_{in} = Light_{in}(red) + Light_{in}(blue) \quad (37)$$

where  $Light_{in}$  and  $Light_{out}$  are knowns and  $Light_{out}(red)$ ,  $Light_{in}(red)$ ,  $Light_{out}(blue)$ ,  $Light_{in}(blue)$  are unknowns.

In a second step, since the ratio  $\frac{Light_{out}(\lambda)}{Light_{in}(\lambda)}$  is independent of incident light intensity, we shall use the periodically updated reference value to generate two additional equations, as follows:

$$Light_{out}(red) = Light_{in}(red) \cdot \frac{Light_{out,ref}(red)}{Light_{in,ref}(red)} \quad (38)$$

$$Light_{out}(blue) = Light_{in}(blue) \cdot \frac{Light_{out,ref}(blue)}{Light_{in,ref}(blue)} \quad (39)$$

The resolution of the system of equations {36, 37, 38, 39} enables assessing the contribution of each light color to the total absorbance of composite light in the photo-bioreactor.

Those variables will serve as two sets of inputs (one set for each light color) for computing the ratio  $\frac{Light_{out}(\lambda)}{Light_{in}(\lambda)}$  which itself be used in the calculation of the algae concentration inside the photo-bioreactor.

Once the concentrations of the pigments in the photo-bioreactor are known using equation 19 in section 4.2.14.2.1, the incident light intensity supplied by the LEDs panel should be dynamically adjusted the new concentration. An increase of the concentration level should result in enhancement of the light intensity and *vice versa*.

In order to determine the appropriate light intensity for the new concentration estimated, we shall consider the ratio  $\frac{\langle PAR(\lambda) \rangle}{Concentration}$  as the amount of light available per biomass.  $\langle PAR(\lambda) \rangle$  represents the total amount of light available to the cells inside the photo-bioreactor (*i.e.*, the area under the curve in the graphs LI vs. width in Figure 3), and  $Concentration$  represents the amount of Chlorophyll a photo-bioreactor (estimated using equation 17). We consider that ratio as constant, enabling us to control the specific amount of light supplied per biomass.

For the definition of  $\langle PAR(\lambda) \rangle$ , we consider the light intensity,  $PAR(\lambda)$ , as a function of  $x$ , the local position along the width of the photo-bioreactor. Thus, in this section,  $PAR(\lambda, x)$  is considered as the light intensity at width  $x$  (in centimeters) of the photo-bioreactor. Correspondingly,  $PAR_{in}(\lambda)$  and  $PAR_{out}(\lambda)$  is the light intensities at width 0 and *width* of the photo-bioreactor and denoted as  $PAR(\lambda, 0)$  and  $PAR(\lambda, w)$ , correspondingly. Re-assigning those in equation 7 gives:

$$PAR(\lambda, x) = PAR(\lambda, 0) \cdot 10^{-\varepsilon(\lambda) \cdot Concentration \cdot x}, \quad (40)$$

or by applying equations {13, 15, 18},

$$PAR(\lambda, x) = PAR(\lambda, 0) \cdot 10^{-SAC(\lambda) \cdot C_a^2 \cdot x}. \quad (41)$$

Integrating equation 41 over  $x$  yields the total amount of light available for absorbance throughout the width of the photo-bioreactor:

$$\langle PAR(\lambda) \rangle = \int_0^{width} PAR(\lambda, x) \cdot dx = PAR(\lambda, 0) \cdot \frac{1 - e^{-2.303 \cdot SAC(\lambda) \cdot C_a^2 \cdot width}}{SAC(\lambda) \cdot C_a^2} \quad (42)$$

Where the constant 2.303 represents  $\ln(10)$ , needed for integration. Note that  $\langle PAR(\lambda) \rangle$  is inversely proportional to the **square** of Chlorophyll a concentration.

Once an expression for the total amount of light available for absorption by the cells inside the photo-bioreactor is obtained, the ratio  $\frac{\langle PAR \rangle}{C_a}$  is used for determining the light available for absorption **per biomass** of algae.

This ratio should remain constant thought-out the growth period as a condition (imposed requirement) for adequate light supply, keeping a **constant** specific light supply whose value is:

$$\frac{\langle PAR(\lambda) \rangle}{C_a} = \frac{PAR(\lambda, 0) \cdot (1 - e^{-2.303 \cdot SAC(\lambda) \cdot C_a^2 \cdot width})}{SAC(\lambda) \cdot C_a^3 \cdot width} \quad (43)$$

We note that this constant ratio is now inversely proportional to the **cube** of Chlorophyll a concentration.

As a mean for proper control, this constant ratio will serve to compute the new light intensity to be supplied after any change in Chlorophyll a concentration. Thus, the **available light intensity per biomass** (one of the main growth conditions) is kept constant over time, so that

$$\frac{PAR(\lambda,0) \cdot (1 - e^{-2.303 \cdot SAC(\lambda) \cdot C_a^2 \cdot width})}{SAC(\lambda) \cdot C_a^3 \cdot width} = \frac{PAR(\lambda,0)' \cdot (1 - e^{-2.303 \cdot SAC(\lambda) \cdot C_a'^2 \cdot width})}{SAC(\lambda) \cdot C_a'^3 \cdot width} \quad (44)$$

where  $PAR(\lambda,0)'$  and  $C_a'$  represent the new net incident light intensity that should be supplied and the new estimated concentration, respectively, while  $PAR(\lambda,0)$  and  $C_a$  represent the respective old values.

After simplification, the following constant ratio (denoted as *SpecificLightSupply*( $\lambda$ ), or shortly  $SLS(\lambda)$ ) is received:

$$SLS(\lambda) = \frac{PAR(\lambda,0) \cdot (1 - e^{-2.303 \cdot SAC(\lambda) \cdot C_a^2 \cdot width})}{C_a^3} = \frac{PAR(\lambda,0)' \cdot (1 - e^{-2.303 \cdot SAC(\lambda) \cdot C_a'^2 \cdot width})}{C_a'^3} \quad (45)$$

Similarly to  $\frac{\langle PAR(\lambda) \rangle}{C_a}$ ,  $SLS(\lambda)$  should also remain constant throughout the growth period, to insure an even growth condition.

Isolating the new light intensity to supply,  $PAR(\lambda,0)'$ , from equation 45, yields the following expression:

$$PAR(\lambda,0)' = SLS(\lambda) \cdot \frac{C_a'^3}{1 - e^{-2.303 \cdot SAC(\lambda) \cdot C_a'^2 \cdot width}} \quad (46)$$

Thus enables us to dynamically update the light intensity supplied by the LEDs panel according to changes of the concentration level, while ensuring that the light intensity per biomass remains constant.

Equation 46 also reveals that  $SLS$  accounts for the proportion between the new (measured) concentration and the adjusted new light to supply. This allows us to use it in the system as a tuning variable, which controls the integrated light intensity per biomass during the experiment, so the amount of light intensity available per unit biomass (expressed as *Chlorophyll a*) is constrained, predetermined and sustained throughout the growth period.

$SLS$  maximal value is limited for any  $\lambda$  by (a) the maximal incident light intensity in PAR that could be supplied by the LEDs panel and (b) the maximum biomass concentration ( $C_{a,max}$ ) we chose during the experiment. Thereby,  $SLS$  maximal value is calculated as follows:

$$SLS(\lambda)_{max} = \frac{PAR(\lambda,0)_{max} \cdot (1 - e^{-2.303 \cdot SAC(\lambda) \cdot C_{a,max}^2 \cdot width})}{C_{a,max}^3} \quad (47)$$

Figure 9 demonstrates the power relation between increasing concentration levels to the matching incident light intensity should be supplied. In addition, it shows that the light intensity per biomass ( $\frac{\langle PAR(\lambda) \rangle}{C_a}$  ratio) remains constant. In the figure,  $PAR$  was calculated using equation 46 and  $\frac{\langle PAR(\lambda) \rangle}{C_a}$  ratio using equation 43, see parameters in Figure 9 legend.

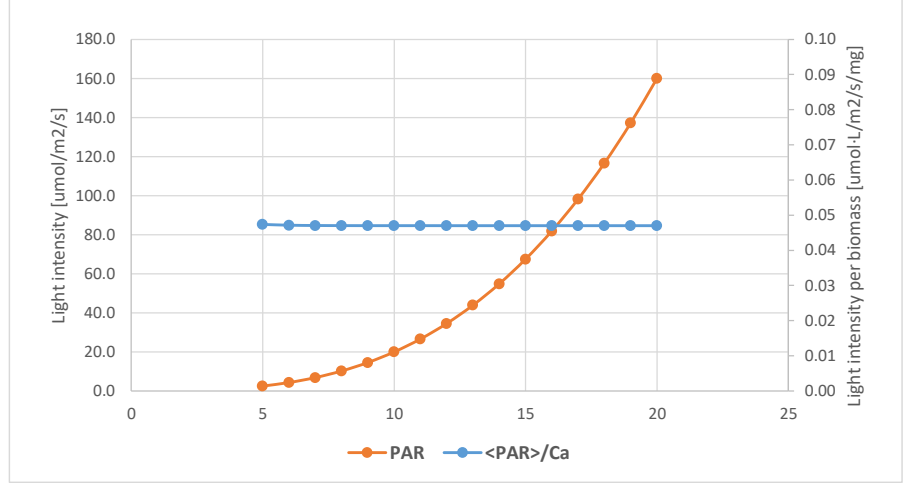


Figure 9 – Dependence of light intensity on concentration according to equation 46.  $\langle \text{PAR} \rangle / \text{Ca}$  ratio is calculated at any concentration level and remains constant. This illustrates the case for concentration level increasing linearly from 5 to 20.  $\text{SAC} = 0.106$ ,  $\text{SLS}(\lambda)_{\max} = 0.02$ ,  $\text{width} = 4$ .

After obtaining an expression for determining the incident light intensity to supply in PAR, one has to determine how should it be distributed between the red and blue lights, i.e., the contribution of light quality.

*FractionRed* ( $FrR$ ) is used as a tuning variable, accounts for the fraction of the red light available for absorption by the algae out of the total incident light available for absorption inside the photo-bioreactor, composed of red and blue lights. Therefore,  $FrR$  is defined as follows:

$$FrR = \frac{\frac{\langle \text{PAR} \rangle_{\text{Red}}}{C_a}}{\frac{\langle \text{PAR} \rangle_{\text{Red}}}{C_a} + \frac{\langle \text{PAR} \rangle_{\text{Blue}}}{C_a}} = \frac{\langle \text{PAR} \rangle_{\text{Red}}}{\langle \text{PAR} \rangle_{\text{Red}} + \langle \text{PAR} \rangle_{\text{Blue}}} \quad (48)$$

Using  $\langle \text{PAR} \rangle$  defined in equation 42, and reducing further yields:

$$FrR = \frac{\frac{\text{PAR}(\text{red}, 0) \cdot (1 - e^{-2.303 \cdot \text{SAC}(\text{red}) \cdot C_a^2 \cdot \text{width}})}{\text{SAC}(\text{red})}}{\frac{\text{PAR}(\text{red}, 0) \cdot (1 - e^{-2.303 \cdot \text{SAC}(\text{red}) \cdot C_a^2 \cdot \text{width}})}{\text{SAC}(\text{red})} + \frac{\text{PAR}(\text{blue}, 0) \cdot (1 - e^{-2.303 \cdot \text{SAC}(\text{blue}) \cdot C_a^2 \cdot \text{width}})}{\text{SAC}(\text{blue})}} \quad (49)$$

Isolating  $\text{PAR}(\text{blue}, 0)$  yields:

$$\text{PAR}(\text{blue}, 0) = \frac{1 - FrR}{FrR} \cdot \frac{\text{SAC}(\text{blue})}{\text{SAC}(\text{red})} \cdot \frac{1 - e^{-2.303 \cdot \text{SAC}(\text{red}) \cdot C_a^2 \cdot \text{width}}}{1 - e^{-2.303 \cdot \text{SAC}(\text{blue}) \cdot C_a^2 \cdot \text{width}}} \cdot \text{PAR}(\text{red}, 0) \quad (50)$$

Thus, expressions for  $\text{PAR}(\text{red}, 0)$  and  $\text{PAR}(\text{blue}, 0)$  are formulated, so the light intensity and **light quality per biomass is pre-determined** by the user and will remain constant through-out the growth period as follows:

$$\text{PAR}(\text{red}, 0) = \text{SLS}(\text{red})_{\max} \cdot \frac{C_a'^3}{1 - e^{-2.303 \cdot \text{SAC}(\text{red}) \cdot C_a'^2 \cdot \text{width}}} \quad (51)$$

$$\text{PAR}(\text{blue}, 0) = \frac{1 - FrR}{FrR} \cdot \frac{\text{SAC}(\text{blue})}{\text{SAC}(\text{red})} \cdot \frac{1 - e^{-2.303 \cdot \text{SAC}(\text{red}) \cdot C_a'^2 \cdot \text{width}}}{1 - e^{-2.303 \cdot \text{SAC}(\text{blue}) \cdot C_a'^2 \cdot \text{width}}} \cdot \text{PAR}(\text{red}, 0) \quad (52)$$

Since those equations do not consider  $SLS(blue)_{max}$ , one has to make sure that the obtained  $SLS(blue)$  ratio does not exceed  $SLS(blue)_{max}$ .

To conclude the last steps, the *Chlorophyll* concentration inside the photo-bioreactor was estimated using the measurements of the light sensors. According to the concentration level, the amount of incident light to supply the algae was determined, and the fraction each color should contribute to the light composition. Those yielded an expression for determining the incident light intensity in PAR that should supplied for each light color ( $PAR(\lambda, 0)$ ).

As discussed in section 3.8.3-8, the light intensity to supply to the algae is also varying according to the illumination mode (continuous light / constant light-dark / sinusoid daylight). The previously obtained expressions for  $PAR(red, 0)$  is considered as the maximal light to supply at noon and is denoted as  $PAR(\lambda, 0)_{max}$ . The expressions for determining the current light to supply (in each of the illuminations mode) keeps the total light intensity supplied during the day (24 hours) equal.

Thus, the current light to supply, considering the illumination mode (and the time), is determined according to the following formulas, ensuring similar amount of light supply during a full day:

1. Continuous light:

$$PAR(\lambda, 0) = PAR(\lambda, 0)_{max} * 0.5 * \frac{day\_length}{24} \quad (53)$$

2. Constant light-dark:

$$PAR(\lambda, 0) = \begin{cases} PAR(\lambda, 0)_{max} * 0.5, & is\_day \\ 0, & otherwise \end{cases} \quad (54)$$

3. Sinusoid daylight:

$$PAR(\lambda, 0) = \begin{cases} PAR(\lambda, 0)_{max} \cdot 0.5 \cdot \left(1 - \cos\left(\frac{2\pi \cdot (tod - day\_start)}{day\_length}\right)\right), & is\_day \\ 0, & otherwise \end{cases} \quad (55)$$

where  $day\_length$  is a parameter indicating the length of daylight in hours (e.g., 18 hours),  $day\_start$  is the hour for sunrise and is defined as  $\frac{24 - day\_length}{2}$  and  $is\_day$  is a Boolean variable indicating if it is daytime as follows:

$$is\_day(time) = \begin{cases} true, & day\_start < time < 24 - day\_length \\ false, & otherwise \end{cases} \quad (56)$$

At the next step, the current light intensity to supply is enhanced in order to reflect the light absorbance by the incident face of the PBR. In other words, the obtained net light intensity should be supplied ( $PAR(\lambda, 0)$ , denoted as  $PAR(\lambda, 0)_{net}$ ) is increased to gross light intensity to supply as follows:

$$PAR(\lambda, 0)_{gross} = \frac{PAR(\lambda, 0)_{net}}{PBRTrans(\lambda)} \quad (57)$$

Where  $PBRTrans$  is the estimated transmission (according to the calibration procedure) of the PBR plastic components and bubbling water (see methods, calibration) and is defined as:

$$PBRTrans(\lambda) = 10^{-0.333 \cdot \log_{10} \frac{PAR(\lambda, width)_{blank}}{PAR(\lambda, 0)_{blank}}} \quad (58)$$

Note that only  $\frac{1}{3}$  of the transmission is attributed to the incident face of the PBR.

The gross PAR (for each color) is then converted back to the voltage (in PWM) that should be sent to the LEDs array, for each light color. The transformation is done by reversing the calibration procedures described in section 4.14.1. That is, the desired gross light intensity in PAR is converted to the PWM to be sent to the LEDs array in order to produce that gross light intensity.

#### 4.3.2. Measured pH and CO<sub>2</sub> supply

During photosynthesis, the microalgae consumes CO<sub>2</sub> and protons, causing the pH level in the suspension to increase. The control of the pH level is done by opening and closing of a CO<sub>2</sub> valve; if the pH level is above or below upper and lower boundaries ( $pH_{high}$  and  $pH_{low}$  accordingly), the CO<sub>2</sub> valve is opened and closed, correspondingly. The range for the pH level is determined according to a target pH level ( $pH_{target}$ ) as follows:

$$pH_{high} = pH_{target} + 0.05$$

$$pH_{low} = pH_{target} - 0.05$$

As discussed in section 3.9.3, the target pH is determined by the supplied light intensity ( $Light$ ) to the structure of a logistic function as follows

$$pH_{target}(Light) = pH_{min} + \frac{pH_{range}}{1 + e^{-steepness \cdot (Light - Light_{middle})}}, \quad (59)$$

where  $pH_{min}$  is the minimum pH target level could be determined (i.e.,  $pH_{target}$  minimum value is  $pH_{min}$ ),  $pH_{range}$  is the pH level could be determined above  $pH_{min}$  (i.e.,  $pH_{min} < pH_{target} < pH_{min} + pH_{range}$ ),  $steepness$  is the slope  $\frac{dpH}{dLight}$  at the inflexion point and  $Light_{middle}$  is the value for  $Light$  at the inflexion point. The point is where the curve changes from being concave up to concave down.

#### 4.4. Simulation of exponential growth

Exponential growth rate is calculated as follows:

$$Concentration_t = Concentration_0 \cdot e^{\mu \cdot t} \quad (60)$$

where  $t$  is the time elapsed from time 0 ( $t=0$ ), at which the concentration equals  $Concentration_0$ .

The ratio between concentrations at two sequential time units ( $t$ ,  $t+\Delta t$ ) is therefore  $e^{\mu}$ , as follows:

$$\frac{Concentration_{t+\Delta t}}{Concentration_t} = \frac{Concentration_0 \cdot e^{\mu \cdot (t+\Delta t)}}{Concentration_0 \cdot e^{\mu \cdot t}} = e^{\mu} \quad (61)$$

The formula of the deterministic model (equation 19) is used to replace  $Concentration_i$ ; constant terms were gathered and denoted as  $A_1$  and  $A_2$  (as defined in [Appendix D – Analysis of the heterogeneous dataset](#), equations {D1, D2}). Using the definition

$$e^{\mu} = \frac{Concentration_{t+\Delta t}}{Concentration_t} = \frac{\left( \frac{-\log_{10}(Transmission_{t+\Delta t} \cdot A_1)}{A_2} \right)^{\beta_{pow}}}{\left( \frac{-\log_{10}(Transmission_t \cdot A_1)}{A_2} \right)^{\beta_{pow}}} = \left( \frac{\log_{10}(Transmission_{t+\Delta t} \cdot A_1)}{\log_{10}(Transmission_t \cdot A_1)} \right)^{\beta_{pow}} \quad (62)$$

$$e^{\frac{\mu}{\beta_{pow}}} = \frac{\log_{10}(Transmission_{t+\Delta t} \cdot A_1)}{\log_{10}(Transmission_t \cdot A_1)} \quad (63)$$

$$(Transmission_t \cdot A_1)^{e^{\frac{\mu}{\beta_{pow}}}} = Transmission_{t+\Delta t} \cdot A_1 \quad (64)$$

Combining equation 64 with the definition of transmission (equation 4), and assuming that  $PAR_{in,t+\Delta t}$  is effectively equal to  $PAR_{in,t}$  for small enough time increment,  $\Delta t$ , we get:



$$PARout_{t+\Delta t} = PARout_t e^{\frac{\mu}{\beta_{pow}}} \cdot \left( \frac{A_1}{PARin_t} \right)^{\frac{\mu}{\beta_{pow}} - \Delta t} \quad (65)$$

Thus, in order to simulate an exponential growth rate, the new exiting light,  $PARout_{t+\Delta t}$ , given in equation 65. The incident light ( $PARin$ ) at any time interval is taken as constant.

Note that for the purpose of simulation, the obvious dependence of  $\mu$  on available light intensity has been disregarded ( $\mu$  assumed to be constant).

## 5. Results & Discussion

### 5.1. Validation of the assumptions

The assumptions presented in section 3.3.3 are critically assessed as follows:

- The measurements obtained by the calibration procedure are independent of the LEDs intensity variation.

Repetitions of 5 measurements was conducted at 140 PWM, see Table 5.

Table 5 - Repetitions of light intensity measurements at 140 PWM for each light color and for both light sensors, taken by our system. Information regarding the pigments' concentrations is reported in Table 6 (Chlorophyll a is around 5.7).

Repetition #	Red in [Hz]	Red out [Hz]	Ratio out/in	Blue in [Hz]	Blue out [Hz]	Ratio out/in
1	17207	285.1	0.01657	9152	15.33	0.00168
2	17200	284.1	0.01652	9145.6	15.28	0.00167
3	17185	285.1	0.01659	9142	15.23	0.00167
4	17189	284.1	0.01653	9141	15.03	0.00164
5	16844	274.1	0.01627	8896	14.83	0.00167
Avg	17125	282.5	0.0165	9095.3	15.14	0.00166
Std	157.3	4.72	0.00013	111.5	0.21	0.000012
$\frac{Std}{Avg}$	0.919%	1.672%	0.775%	1.226%	1.370%	0.717%

It is shown that the standard deviation (relative to the averaged values) is low (~1.3%) for each light sensor and light color, and even lower for the apparent transmission (~0.7%). As shown, the ratio *out/in* (representing the uncorrected transmission) for blue light is one order of magnitude lower than that for red light, due to the higher absorbance of blue light for both the PBR and the microalgae.

- The lab results providing a fair approximation for the real biomass concentrations. Repetitions of 5 lab measurements (by spectroscopic analysis) was done for a given culture. The pigments concentrations are presented in Table 6.

Table 6 - Repetitions of lab measurements for the pigments concentrations.

Repetition #	Chlorophyll a [mg/L]	Chlorophyll b [mg/L]	Carotenoid [mg/L]
1	5.3239	1.9160	3.0495
2	5.5663	1.9930	3.2200
3	6.0195	2.1589	3.4547
4	5.8104	2.1061	3.3628
5	6.0343	2.1835	3.4859
Avg	5.7509	2.0715	3.3146
Std	0.3051	0.1137	0.1806
$\frac{Std}{Avg}$	5.31%	5.49%	5.45%

On the average, the standard deviation (relative to the average value) is of the order of 5%, a commonly accepted accuracy for this kind of measurements.

- The total intensity for the incident or exiting light, composed of multiple colors, is the arithmetic sum of its components.  
It is shown in Table 7 that the arithmetic sum of the colored light measured by the light sensors (in Hz) is similar to the measurements of both light colors projected together.

*Table 7 – Representative measurements from lights sensors; the arithmetic sum of separate colored lights at 140 PWM is about the same light intensity received by projecting 140 PWM by both lights simultaneously. Representative values for calibration, done in the absence of algae.*

	Red	Blue	Blue + Red	Blue & Red	Relative difference
Light In [Hz]	14573.1	7152.5	21725.6	21626.7	-0.46%
Light Out [Hz]	3166.7	708.7	3875.4	3878.6	0.08%

- The observed relative differences are substantially low and are conserved in the order of magnitude, but not the sign (randomly negative or positive).
- The fraction of the absorbed light, calculated in terms of PAR, is independent of the incident light intensity.  
This statement is shown to be valid in section [5.2.25-2-2](#).
- The algal pigments absorb each light color differently.  
Light measurements of the same culture result in a different transmission for each light color, and thereby different absorbance, see Table 5.
- Light attenuated by the culture is the combination of the sum of absorbance by packed pigments and scattering by cells.  
Based on literature review - spectra of solution (absorbance only) vs. suspension (absorbance + scattering).
- Biomass of particles other than algae are neglected.  
This assumption has not been assessed.

## 5.2. Calibration

As described in section 3.2., the ratio  $\frac{PAR_{inblank}(\lambda)}{PAR_{outblank}(\lambda)}$  represents the transmission for the photo-bioreactor and the bubbling water (absence of algae). The ratio is decomposed arithmetically ( $\frac{PAR_{inblank}(red)+PAR_{inblank}(blue)}{PAR_{outblank}(red)+PAR_{outblank}(blue)}$ ), enabling the estimation of each of its elements, as locally measured by the system. Moreover, the global light intensity at the face of the PBR is measured as PAR by an external quantum sensor (Li-COR 190R, USA) at increasing PWM.

Therefore, models for describing the local light intensity in Hz measured by the light sensors is formulated in Section [5.2.15-2-1](#), while in Section [5.2.25-2-2](#) the global light intensity (in PAR) at the incident face of the PBR is modeled as a function of the local light intensity in Hz given by the light

sensors. Note that the ensemble of both models results in the estimation of the global light intensity in PAR as function of PWM.

#### 5.2.1. Calibration part 1: LEDs and local light sensors [Hz]

Measurements of the light sensors at increasing PWM are presented at Figure 10.

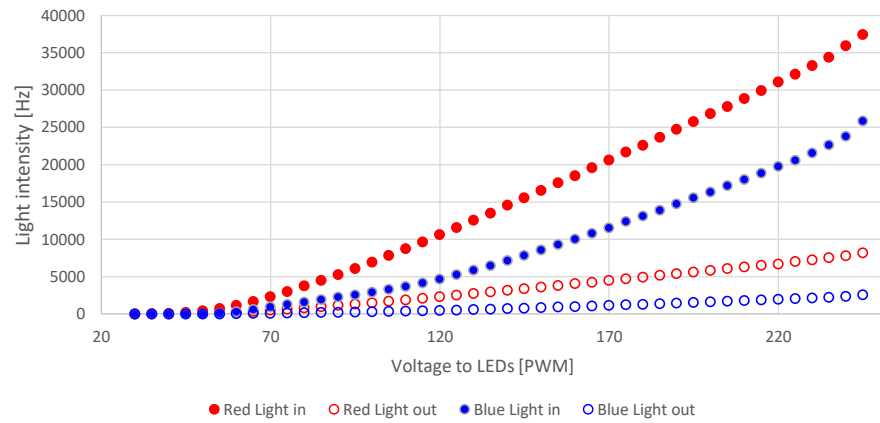


Figure 10 – Incident and exiting light sensors measurements (in Hz) for red and blue lights projected by the LEDs panel at increasing voltage (in steps of 5 PWM, see section 4.1.14.1.1). This figure shows measurements for a single repetition in the absence of algae.

The results reveal that the light intensities for the red light is higher than the blue light (Figure 10). The differences is due to the number of red and blue LEDs (for specifications of the LEDs panel, see Appendix B – System hardware specification). In addition, it is clear that the dependence of the light intensity on the PWM is not linear.

The ratio  $\frac{Light\ out_{blank}(\lambda)}{Light\ in_{blank}(\lambda)}$  (which is proportional to the transmission, but differ since it is not calculated in PAR and not includes the correction of filters and sensitivity of the light sensor) for each colored light, at any light intensity is presented in Figure 11.

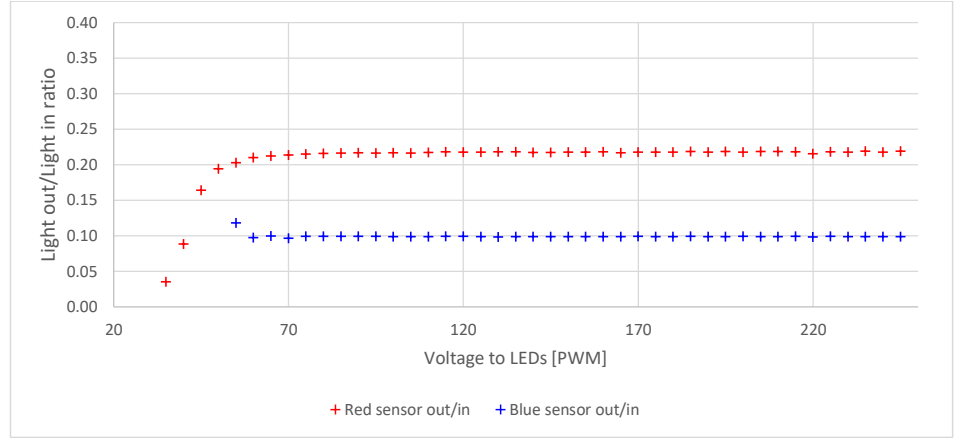


Figure 11 – Light out/Light in ratio (proportional to the transmission) for red and blue lights, calculated based on the light sensors local measurements in Hz.

It is shown that the ratio, as measured by the local sensors, is apparently dependent on the PWM; It is constant for PWMs higher than 65 and 60 for the red and blue lights, respectively, but varies strongly at lower PWMs (Figure 11). This phenomenon is due to imperfection in the LEDs panel circuit, which does not result in similar current supplied to the LEDs combos at the same low voltage input (PWM). Consequently, the light sensors, located in front of LEDs combos, report different values than expected (not a constant ratio at low light intensities).

In the following section ([Calibration part 2: local light sensor \[Hz\] and independent sensor](#)) another calibration procedure is performed in order to replace the **local** measurements in Hz by relevant **global** measurements in PAR, averaged over the PBR area.

In addition, Figure 11 shows that each light color has different  $\frac{Light\ out_{blank}(\lambda)}{Light\ in_{blank}(\lambda)}$  ratio, which means that (according to equations {4, 5}) the lights are absorbed differently by photo-bioreactor components (specifically, by the plastic bag and the bubbling water). This dictates the use of a different ratio  $\left(\frac{Light\ out_{blank}(\lambda)}{Light\ in_{blank}(\lambda)}\right)$  for each light color  $\lambda$ .

Figure 12 shows the light sensors measurements (average of three repetitions), **normalized** to the sensor measurement at 140 PWM (at corresponding colors) as a function of PWM. To evaluate the similarity between incident and exiting lights (of the same color), the difference between the normalized values for each sensor, relative to their average was calculated.

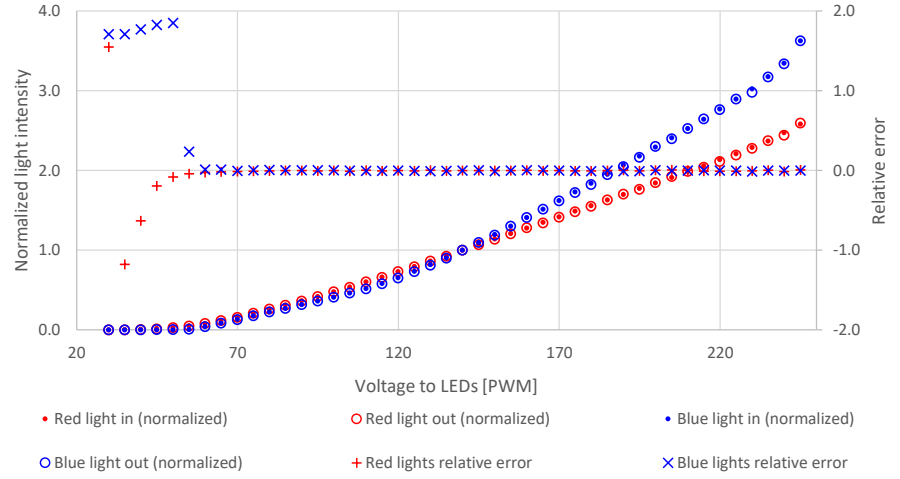


Figure 12 – Calculated normalized measurements of incident and exiting light sensors and their relative errors. The raw measurements were normalized to reference measurement at 140 PWM for each light color. The reported values are the average of three repetitions. The error bars for the standard deviations were omitted since they values are smaller than the symbols. A relative error was calculated according to the following equation:  $\frac{\text{Normalized } \langle \text{color} \rangle \text{ light in} - \text{Normalized } \langle \text{color} \rangle \text{ light out}}{\text{Average of normalized } \langle \text{color} \rangle \text{ light in and out}}$ . Relative error is non zero only for low PWM values, in which the LEDs panel electric current flow is not stable.

It is shown that measurements of the same light color yields similar curves, regardless to the light sensor (in or out) (Figure 12). The curves therefore differ only by a scale factor (that is used for normalizing those measurements). Thus, the normalized measurements as function of PWM could be modeled **by the same function**, while the scale factor is used to distinguish them. The scale factor for each light color and light sensor was determined as the measurements at 140 PWM (moderate light used as reference, as discussed in section 4.3.14.3.1), and are presented in the first and third columns of Table 9. The error bars is close to zero (for light measured at PWMs higher than 55 and 60 for the red and blue lights accordingly). This approves the claim that each colored light creates similar curves by both of light sensors, which is distinguish by a scale factor.

The light intensity in Hz, for each color, is therefore modeled as the average (of both light sensors) of the normalized lights (denoted as  $Y$ ).

Since the curves are non-linear, Box-Cox transformation (see equation 66) is applied to  $Y$ , and a linear regression model (see equation 67) is fitted to predict the transformed  $Y$  values based on the PWM (denoted as  $X$ ).

$$Y_{\text{transformed}} = \frac{Y^{\Lambda} - 1}{\Lambda} \quad (66)$$

$$Y_{\text{transformed\_predicted}} = \beta_0 + \beta_1 \cdot X \quad (67)$$

The model (see equation 68) is therefore composed of the Box-Cox transformation parameter,  $\Lambda$ , and the linear regression coefficients,  $\beta_0$  and  $\beta_1$ .

$$Y_{\text{predicted}} = (\Lambda \cdot (\beta_0 + \beta_1 \cdot X) + 1)^{1/\Lambda} \quad (68)$$

The parameters of the models and the indicators for the goodness of fit are summarized in Table 8.

Table 8 - Summary of the prediction models for lights in Hz

[Hz]	$\Delta$	$\beta_0$	$\beta_1$	SSE	SST	$R^2$
Red light	0.665	-1.823	0.0128	0.0730	29.038	0.997
Blue light	0.518	-2.353	0.0169	0.0615	30.709	0.998

Figure 13 shows, for each light color, the processed measurements (averaged and normalized) and the values fitted by the model in equation 67, using the fitted parameters in Table 8.

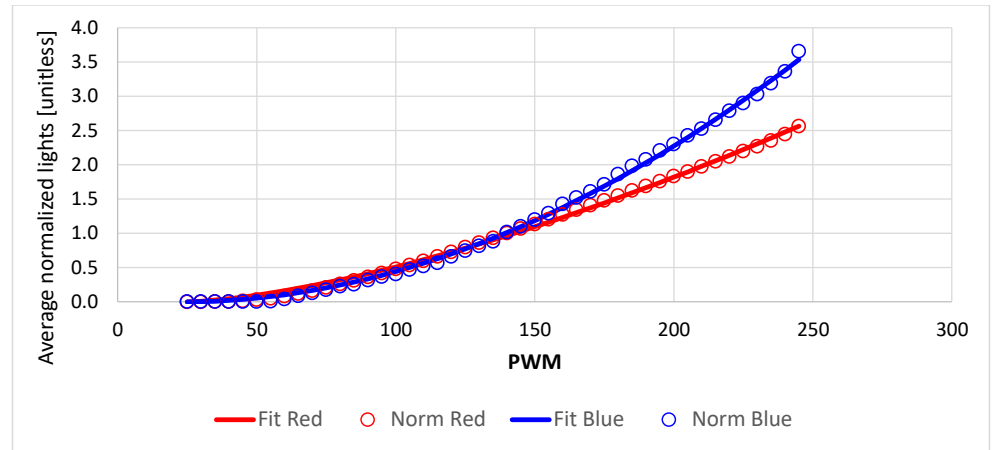


Figure 13 – Predictions and real values of the averaged normalized (to reference measurement at 140 PWM) sensors measurements in Hz as function of PWM. Predictions is done according to the model in equation 68, using the parameters in Table 8.

#### 5.2.2. Calibration part 2: local light sensor [Hz] and independent sensor [PAR]

Figure 14 and Figure 15 show the averaged raw measurements of the light intensity in PAR in front of each of the twelve LEDs combos and their standard deviation and range, for red and blue lights correspondingly. [Appendix C – Calculated incident light at the surface of the PBR](#) shows the respective local red and blue light intensities (as PAR) at the incident face of the PBR.

It is explicit that each of the twelve LEDs combos produces different light intensities (Figure 14 and Figure 15). This, again, illustrates the imperfection in the LEDs panel circuit, as previously discussed in section [5.2.15-2.1](#).

Figure 16 shows the transmission by the photo-bioreactor (in the absence of algae), calculated by the averages light intensities in PAR, and measured using the external sensor.

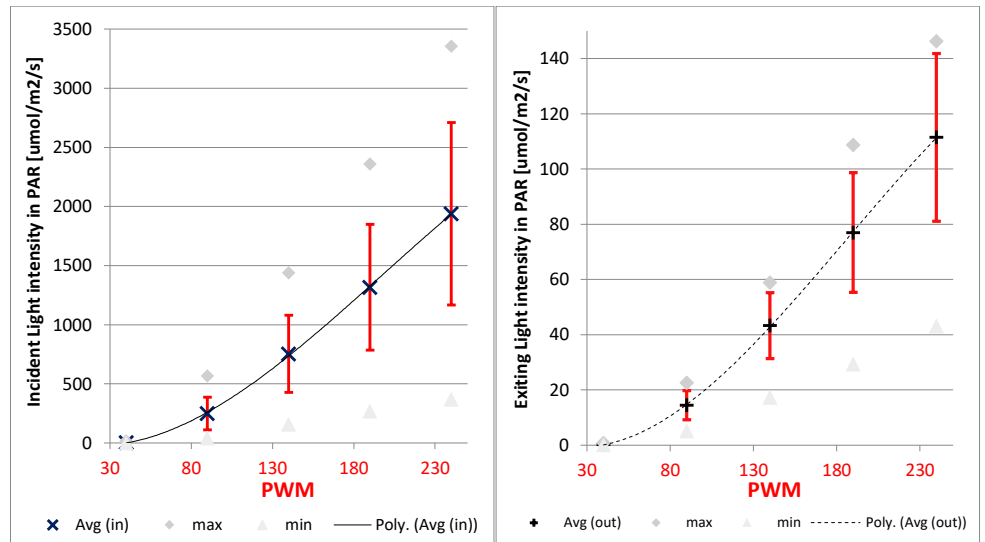


Figure 14 - Calibration measurements of incident (Right) and outgoing (Left) red light intensities (PAR) by external sensor showing the average of the 12 LED combos and their standard deviation (error bar), at 5 selected PWMs. The light sensor (LI-COR LI-190R Quantum Sensor) was placed in front each LEDs combo. Min and max light intensities illustrate the range for each PWM among the 12 LED combos.

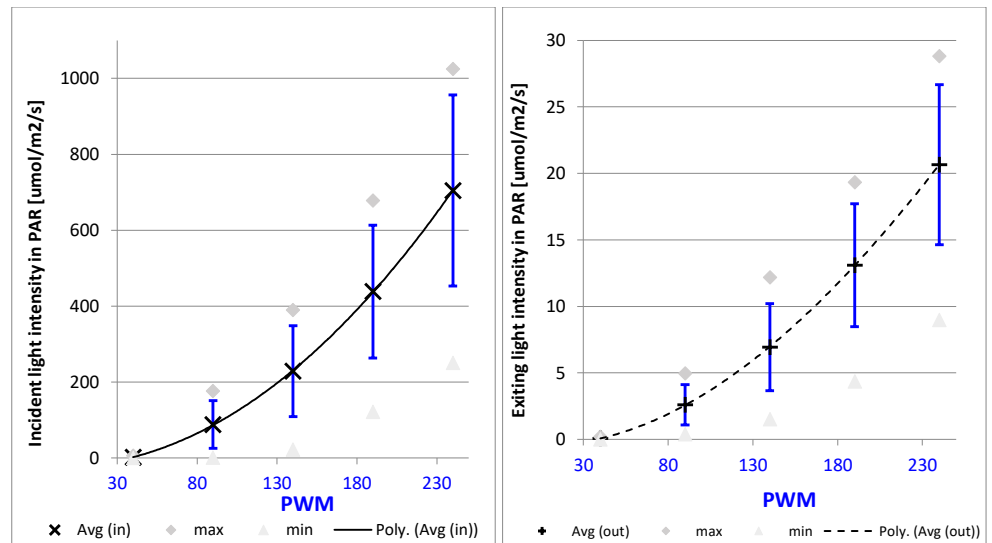


Figure 15 – Same as Figure 14, with blue LEDs.



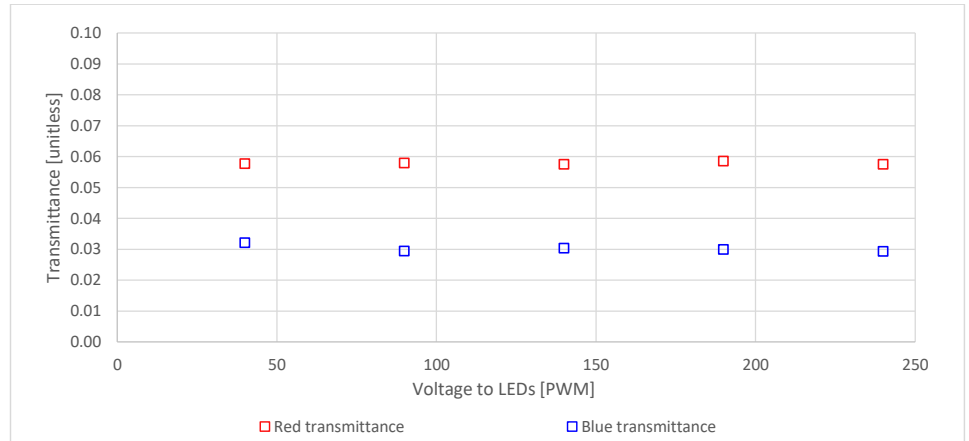


Figure 16 – Transmittance for red and blue lights in PAR, calculated based on external light sensor (LI-COR LI-190R Quantum Sensor).

It is shown in Figure 16 that once all twelve LEDs combos are considered (by using their average light intensity in PAR, as presented in Figure 14 and Figure 15), the transmission (and thereby the absorbance, see equation 5) is constant also at low light intensities (*e.g.*, 40 PWM). This illustrates the limited diagnostic value of the raw numbers provided by the light sensors (in Hz) since they represent local rather than total light intensity impinging on the PBR face. Therefore, **one must process the local measurements received in real time from the light sensors (in Hz) to yield the total-real light intensity (calculated as PAR)**.

As conducted in the previous section ([Calibration part 1: LEDs and local light sensors \[Hz\]](#)), light intensities as PAR are normalized to a reference light intensity at 140 PWM (see Table 9 for reference values).

Table 9 – Local sensor readings [Hz] and global PAR [ $\mu\text{mol photons/m}^2/\text{s}$ ] measured at 140 PWM (reference intensity) by the local sensors and quantum sensor, correspondingly, for each color and each face (in and out) of the PBR, in the absence of algae. The raw measurements were normalized to the reference values (by dividing each measurement by the corresponding reference intensity).

Reference intensities	Sensor: Red [Hz]	PAR: Red [ $\mu\text{mol photons/m}^2/\text{s}$ ]	Sensor: Blue [Hz]	PAR: Blue [ $\mu\text{mol photons/m}^2/\text{s}$ ]
in	14755.95	752.98	7462.33	228.77
out	3027.91	43.30	682.80	6.94

Figure 17 shows the normalized light intensities as PAR and the relative difference between normalized incident and exiting intensities for each color, as function of PWM.

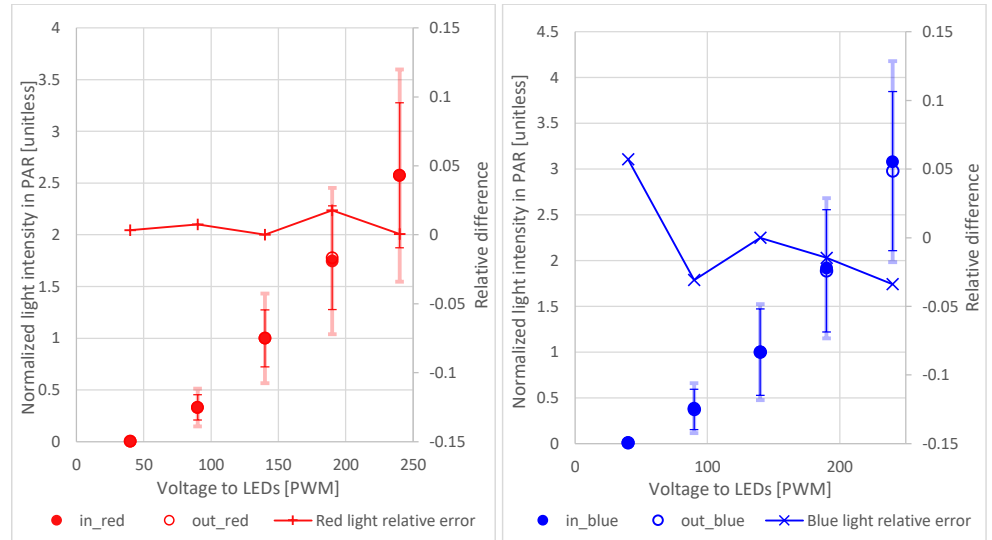


Figure 17 – Normalized PAR measurements of incident and exiting light for red (left) and blue (right) lights and their standard deviation (error bars). Data were processed as in Figure 12. The processed values are calculated from the averages reported in Figure 14 and Figure 15.

It is shown in Figure 17 that the normalized light intensities of same light color becomes relatively robust owing to the normalization processing, as shown by the low calculated relative differences between incident and exiting normalized intensities .

Since both parts of the calibration (sections [4.1.14.1.1](#) and [4.1.24.1.2](#)) were conducted at similar PWM light intensity in Hz could be converted to the matching light intensity as PAR.

For this purpose, a linear regression model,

$$Y = \beta_0 + \beta_1 \cdot X, \quad (69)$$

was build to predict the normalized PAR values (presented in Figure 17 and denoted as  $Y$ ) based on the normalized sensor measurements in Hz (denoted as  $X$ ). The intercept of the model ( $\beta_0$ ) was set to zero in order to reflect that "zero light" reported by the sensors should yield in "zero light" in PAR units.

Figure 18 shows the processed measurements (averaged and normalized) and the values fitted by the model, for each light color, is given in Table 10.

A regression model was formulated for each light color, using measurements at both sides of the PBR (in and out). The parameters of the models and the indicators for the goodness of fit are summarized in Table 10.

In order to estimate the real light intensity in PAR (based on the PWM level), one has to multiply the fitted normalized lights in PAR by the scale factor – the light intensity at 140 PWM (Table 10).

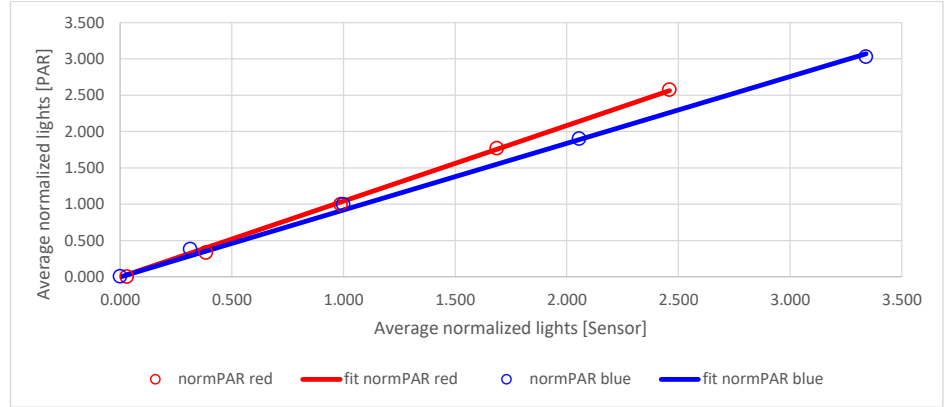


Figure 18 - Prediction models for the averaged normalized sensors measurements in PAR. See the parameters for the formulated equations in Table 10.

Table 10 - Summary of the prediction model for normalized lights in PAR.

[PAR]	$\beta_0$	$\beta_1$	SSE	SST	$R^2$
Red light	0	1.0408	0.0157	8.8342	0.998
Blue light	0	0.9192	0.0383	11.903	0.997

To conclude, the prediction of the real light intensity in PAR, according to the PWM sent to the LEDs array, is based on both calibrations. The steps are summarized as follows:

1. **Normalized\_Sensor( $\lambda$ ) = Calibration1(PWM( $\lambda$ )):**  
The PWM value is first processed to yield normalized sensor (local) values using the procedure conducted in section 5.2.15-2.1.
2. **Normalized\_PAR( $\lambda$ ) = Calibration2(Normalized\_Sensor( $\lambda$ )):**  
The normalized Hz values are processed to yield normalized PAR values based on the procedure conducted in this section.
3. **PAR( $\lambda$ ) = Normalized\_PAR( $\lambda$ ) · reference\_factor\_PAR( $\lambda$ )**  
Finally, the normalized light intensity in PAR is multiplied by the reference factor (light intensity in PAR received at 140 PWM, for the corresponding light color). The result is the average light intensity in PAR.

Due to the frequent need for transforming local measurements by the light sensor in Hz to global light intensity in PAR, transformation factors (see Table 11) has formulated according to the calibration procedures, for both red and blue lights. In which, the local measured light intensities are (a) divided by  $Hz_{blank,ref}^\lambda$  for normalizing by the light intensity at Hz, received at 140PWM, (b) multiplied by  $\beta_1^\lambda$ , the conversion factor previously obtained (see Table 9) for transforming the normalized Hz to normalized PAR intensities, and (c) multiplying by  $PAR_{blank,ref}^\lambda$  in order to unnormalise it to estimated light intensity at PAR.

Table 11 - Conversion factors from local light intensity in Hz measured by the sensors to global light intensity in PAR

Hz2PAR	Red	Blue
In	$\frac{PAR_{in,blank,ref}^{red} \cdot \beta_1^{red}}{Hz_{in,blank,ref}^{\lambda=665nm}} = 0.0531$	$\frac{PAR_{in,blank,ref}^{blue} \cdot \beta_1^{blue}}{Hz_{in,blank,ref}^{blue}} = 0.0281$
Out	$\frac{PAR_{out,blank,ref}^{red} \cdot \beta_1^{red}}{Hz_{out,blank,ref}^{red}} = 0.0148$	$\frac{PAR_{out,blank,ref}^{blue} \cdot \beta_1^{\lambda=452nmblue}}{Hz_{out,blank,ref}^{blue}} = 0.0093$

Where  $PAR_{blank,ref}^{\lambda}$  and  $PAR_{blank,ref}^{\lambda}$  are the averages light intensities in PAR received on the incident and exiting face of the PBR at 140 PWM, respectively;  $Hz_{blank,ref}^{\lambda}$  and  $Hz_{blank,ref}^{\lambda}$  are the locals light intensities measured by the light sensors at 140 PWM. And  $\beta_1^{\lambda}$  is the transformation coefficient from normalized (local) light intensity in Hz to normalized (global) light intensity in PAR.

### 5.3. Deterministic model

The aim of this section is to examine whether the model for predicting the Chlorophyll a concentration ( $C_a$ ) inside the PBR using the light transmission is valid.

The dataset available for analysis contains 15 observations measured at random times; each row contains measurements taken by the system (red and blue absorbance) and the matching pigments concentration measured at the lab (chlorophyll a, chlorophyll b, carotenoid and dry weight). However, those observations does not constitute a homogenous dataset since each row reflects an unique physiological state of the culture (*i.e.*, different pigments composition). The range of the pigments concentrations and the calculated relative concentrations observed in the system are presented in Table 12.

Table 12 - Range of the concentrations and relative concentrations (to chlorophyll a) of the pigments in the culture measured in the lab during a period of one year.

	chlorophyll a mg/L	chlorophyll b mg/L	Carotenoid mg/L	dry weight mg/L	$C_b^*$ --	$C_c^*$ --	$C_d^*$ --
Min	1.39	0.81	1.17	63.33	0.32	0.50	29.61
Max	18.44	6.60	15.12	760.0	0.78	1.41	89.11
Avg	7.67	3.12	5.44	365.3	0.43	0.72	47.68
Std	4.39	1.60	3.72	216.8	0.09	0.19	15.26
$\frac{Std}{Avg}$	57.2%	51.4%	68.3%	59.3%	20.3%	26.0%	32.0%

The high variation of the relative concentrations in Table 12 emphasizes the heterogeneous nature of the samples composing the dataset.

Therefore, in a formal matter, the observations in the dataset could not be related, or analyzed, as a homogeneous set of data. Nevertheless, we show, as expected, that **analysis of the dataset, including the use of speculative models, yields poor results**, see [Appendix D – Analysis of the heterogeneous dataset](#)~~Appendix D—Analysis of the heterogeneous dataset~~.

For assessment of the model developed in section [4.2.14.2.1](#), two sets of calibration measurements are used, taken after progressively adding dense algal culture to the photo-bioreactor. This ensures similar

pigments composition at each set of measurements, thus yielding two small but homogeneous datasets. The calibration measurements are presented in Figure 19.

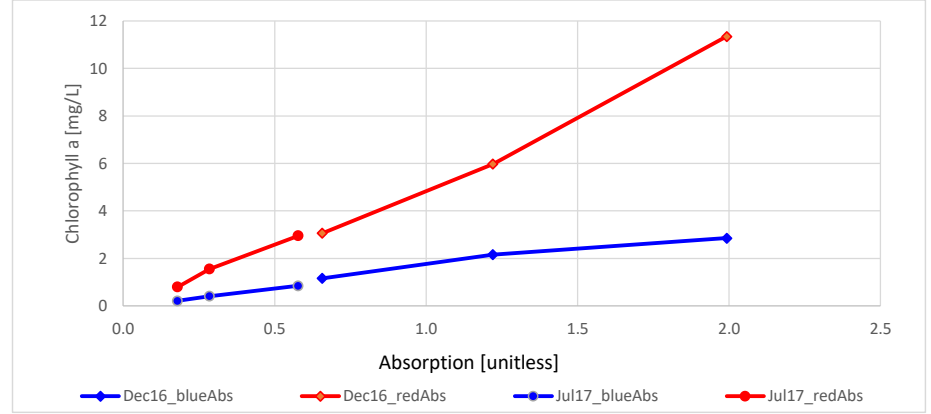


Figure 19 - Calibration measurements of chlorophyll a (measured at lab) and matching absorbance (calculated by the system). Dec16:  $C_b=0.48$ ,  $C_c=1.65$ ,  $C_d=52.51$ . Jul17:  $C_b=0.33$ ,  $C_c=1.21$ ,  $C_d=39.41$ .

The input variable of the model to be fitted is the red light absorption ( $Abs(red) = -\log_{10} \left( \frac{PAR_{out}(red)}{PAR_{in}(red)} \right)$ ) which is calculated by the system. The red absorption is preferred over the blue absorption since the former does not include the absorption by carotenoid (*i.e.*,  $\epsilon_{carotenoid}^{red} = 0$ ). In addition, chlorophyll, the main pigment in the culture, absorbs around the wavelength of red light.

The model described by equation 19 is fitted for each set of calibration measurements by changing the parameter  $K(\lambda)$  so the *SSE* is minimized; the results of the fitted models are presented in the first row of Table 13 and plotted in Figure 20.

It is shown that the predictions of the model do not yield curves similar to the real measurements (Figure 20), in addition to relatively low  $R^2$  (around 0.7) (Table 13). This indicates that the relation between the red absorption and the chlorophyll a concentration was not obtained by the model.

For further assessment of the fitted model, Figure 21 presents the measured vs. predicted values of chlorophyll a.

As expected, the curves in Figure 21 do not fall on the same line, and present slopes substantially lower than 1.0 and strongly positive intercepts, indicating that (i) the predictions of chlorophyll a are significantly lower than the corresponding measured values and (b) the model fails to "translate" the absence of absorbance as insignificant level of chlorophyll a concentration.

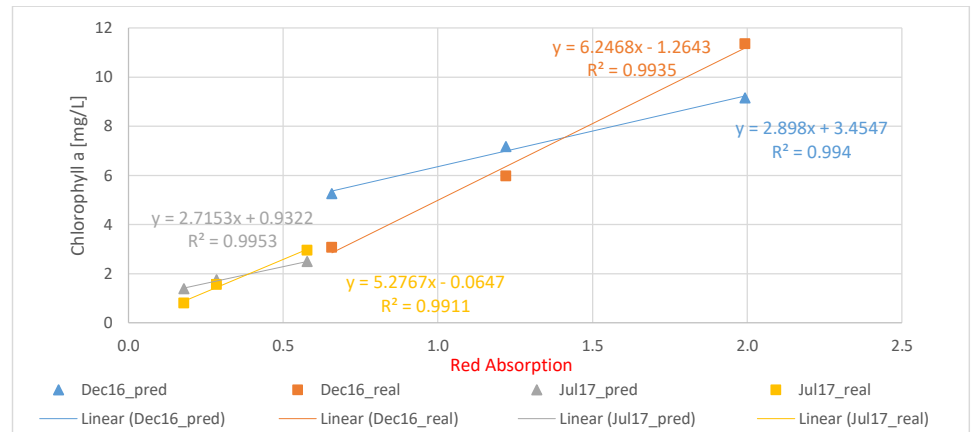


Figure 20 - Chlorophyll a: real observations vs. predictions as function of red absorption. Predictions made by fitting the parameter  $K(\lambda)$  in equation 19 to two sets of calibration measurements (Dec16 & Jul17).

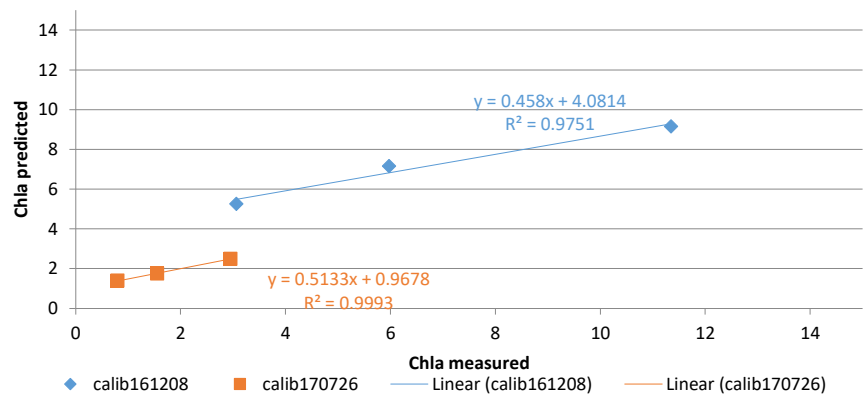


Figure 21 - Chlorophyll a: measured vs. predicted values. Predictions made by equation 19. Straight lines passing from the origin and with slope=1.0 indicate good fit.

Equation A8 in section 8.18-1 matches a simple form of the Beer-Lambert law, in which the effective absorption coefficient was extended with additive scattering coefficient. The model is fitted to the calibration measurements by changing the scattering coefficient so the  $SSE$  is minimized. The results of the fitted model are presented in the second row of Table 13 and plotted in Figure 22.

It is shown in Figure 22 that the curves of the measurements and the corresponding predictions have similar slopes in both set of calibrations, especially in calibration Dec16. Moreover, the  $R^2$  is relatively high (above 0.97) for both sets of calibrations. This indicates the powerful estimation of the relation between the red absorption and chlorophyll a concentration, in compare to the observed relation. In addition, the curves fall on almost the lines.

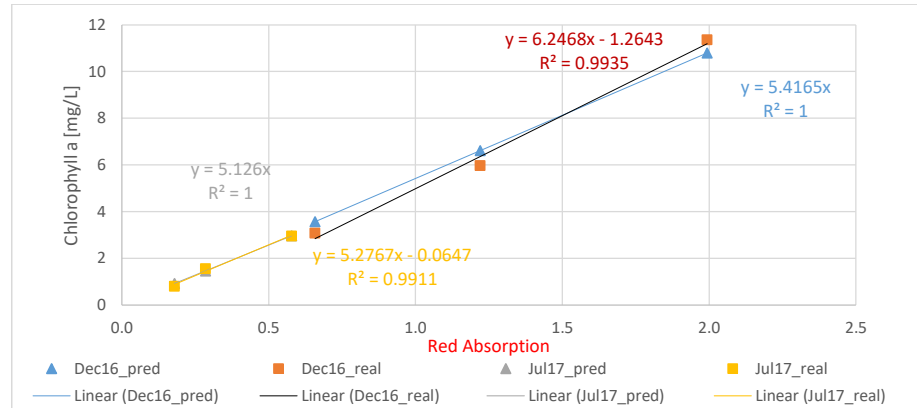


Figure 22 - Chlorophyll a: real observations vs. predictions as function of red absorption. Predictions made by fitting the parameter  $scat(\lambda)$  in equation A8 to two sets of calibration measurements (Dec16 & Jul17).

In addition, the estimated values of the scattering coefficients seems to be negative and equals (Figure 22). This indicates that (i) the specific absorption coefficients taken from Bidigare (Bidigare et al., 1990) may already include the scattering by the particles and (ii) this has generalization capabilities as it was able to fit two sets of calibration with the same scattering coefficient value.

The model is further assessed by plotting the measured vs. predicted values of chlorophyll a in Figure 23.

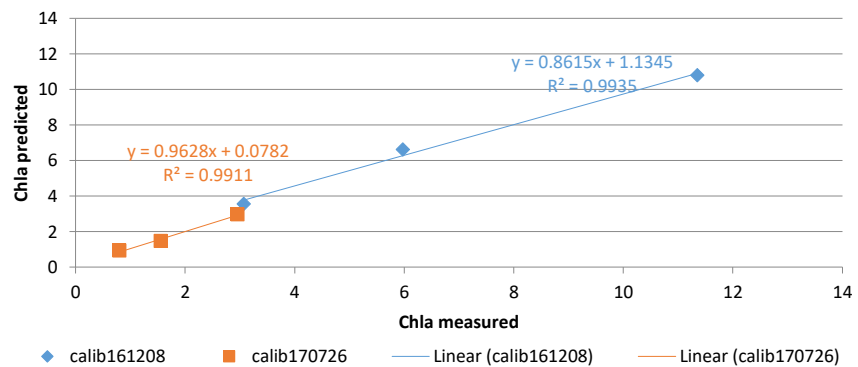


Figure 23 – Same as in Figure 21. Predictions made by fitting equation A8.

It is shown that the curves of the predictions in Figure 23 present slopes close to 1.0 (fall almost on the same line) and their intercepts is very low in compare to those formulate by our model in Figure 21. This indicates that the model in equation A8 succeed in predicting the chlorophyll a concentration.

In both models the relation between measurements and predictions creates straight lines (for each set of calibration), which indicates a fair relation between the absorption to the concentration.

In the simplified model in equation A8, the relation between the absorption and the chlorophyll a concentration is kept similar in the measured and predicted values at both sets of calibrations. This indicates a good proportion between the chlorophyll a concentration and the red absorption. However, this is qualitatively claims against the use of power of 0.5 in equation 19, since no correction of the curves (formulated by the simplified model) is needed.

*Table 13 - Results for fitting parameters in the models to raw experimental results presented in Figure 19. The first row shows the results for fitting equation 19 to the measurements by changing  $K(red)$ . The second row shows the results for fitting equation A8 to the same measurements by changing  $scat(red)$ .*

	Calibration set	$\beta_{K(red)}$	SSE	SST	$R^2$
Fit equation 19 to calibration measurements by changing $\beta_{K(red)}$	Dec16	0.0010	11.04	35.32	0.687
	Jul17	0.0059	0.602	2.396	0.749
	Calibration set	$scat(red)$	SSE	SST	$R^2$
Fit equation A8 to calibration measurements by changing $scat(red)$	Dec16	-0.0013	0.960	35.32	0.973
	Jul17	-0.0013	0.024	2.395	0.990

#### 5.4. Stochastic model

The results obtained by sub-model 1 ( $N$  complete layers) and sub-model 2 ( $N_{max}$  layers with holes) described in section 4.2.24-2-2, and implemented in Matlab<sup>4</sup>, are presented in this section. That is, reaching a convergent solution for steady-state, in which the final probabilities (represented by  $\pi_{k=1}^{(A_j)}$ ) for an incident flux (initial state  $F_I$ ) to be reflected out of the PBR ( $A_0$ ), absorbed in cells ( $\sum A_i$ ), or transmitted out of the PBR ( $A_{N+1}$ ).

Figure 24 present the total transmission for sub-model 1 and 2. The results were obtained, for each sub-model, by solving numerically (raising  $\mathbf{T}$  to high power) and by solving analytically (using equation 26).

Figure 24 shows that the results of both sub-models are similar and hence we conclude that the analytical solution for the study-state is valid.

The final probabilities for an incident flux to be absorbed by each of the elements in the model (PBR sides or layers of grouped cells), represented by  $\pi_{k=1}^{(A_j)}$ , is presented in Figure 25 (for sub-model 1).

<sup>4</sup> [https://github.com/EladDan/EladThesis\\_Model2](https://github.com/EladDan/EladThesis_Model2)



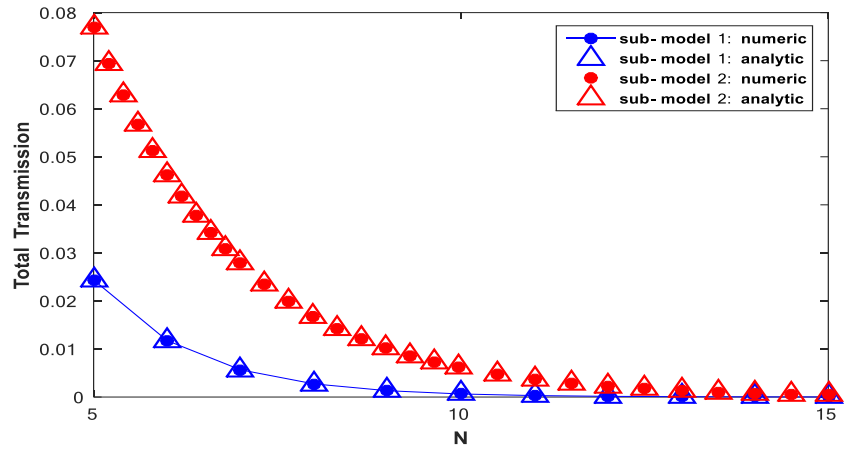


Figure 24 – Total transmission vs.  $N$  (number of layers), obtained by solving sub-models 1 and 2 numerically and analytically. The inputs for the models are:  $r=0.2$ ,  $a=0.43$ ; for sub-model 2:  $N_{max}=500$ .

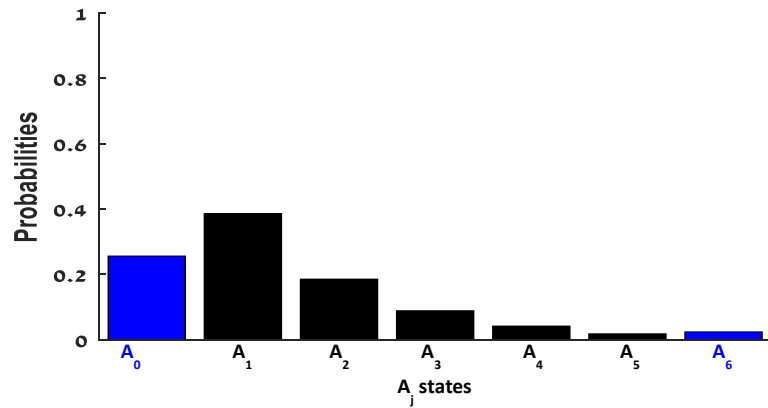


Figure 25 - Reflection, absorption and transmission at steady state. The inputs for the model are:  $N=5$ ,  $r=0.2$ ,  $a=0.43$  ( $cell\_in=5.2$  [mg/cm<sup>3</sup>],  $cell\_dim\_cube=4.8360e-04$  [cm], see equation 23 in [1]). The order of magnitude for the elementary probability  $r$  was set to yield a value for transmission similar to that calculated in our experimental system.

Figure 26 shows the total reflection and transmission of sub-model 1, for  $N=5$  and varying range of  $r$  and  $a$ . The probability for absorption is omitted since it can be calculated by subtracting the other probabilities from 1.0. Moreover, the probability for total absorption is defined based on beer lambert law (given the total transmission), what makes the definition for total absorption by this model redundant.

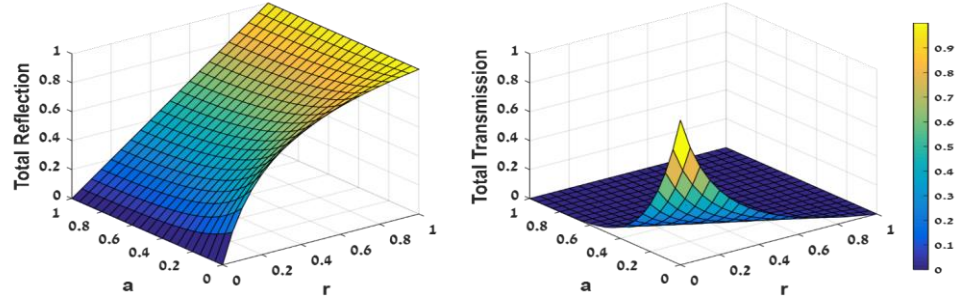


Figure 26 - Results for reflection (left) and transmission (right) over the range of the elementary probabilities  $a$  and  $r$ .  $N=5$ .

The results (Figure 26) reveal that, as expected, the total transmission increases for low values of  $a$  and  $r$ . It is also shown that the total reflection is increases for high values of  $r$  and for low values of  $a$ . An explanation for the behavior of the latter could be that as less photons are absorbed, they are more likely to be either **reflected** or transmitted.

The behavior for the total reflection and transmission is similar for various values of  $N$ , see Figure 27 for example in which  $N=25$ .

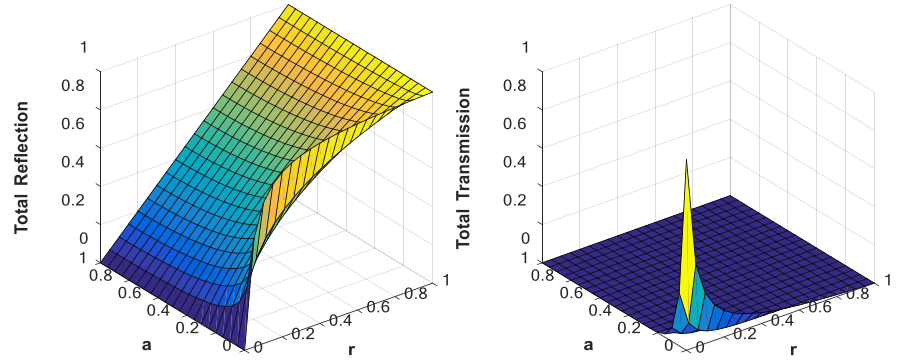


Figure 27 - Same as Figure 26.  $N=25$ .

The changes in both of the graphs in Figure 26 and Figure 27 is seen only for small values of  $a$ , probably since the photons is absorbed quickly by the layers and vanish from the system (do not reflect of transmitted). As one could expect, the graph for the total transmission is lower for higher values of  $N$ . However, **the graph for the total reflection is higher for higher values of  $N$** . This behavior is suited with the assumption made in the last section, in which the scattering effect is significant only for high levels of concentrations (*i.e.*, high  $N$ ).

Figure 28 explores the total transmission for different number of layers with holes ( $N_{max}$  in sub-model 2), compared to layers with no holes (sub-model 1).

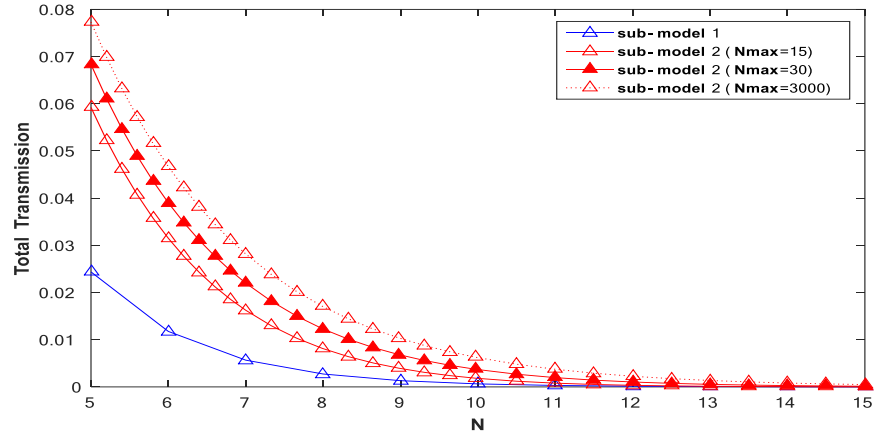


Figure 28 – Comparison of the total transmission received by sub-models 1 and 2. Sub-model 2 was examined for range of  $N_{max}$  ( $N_{max}=15,30,3000$ ). Results were calculated for  $a=0.43$  and  $r=0.2$ .

$N_{max}$  examined for a wider range Figure 29.

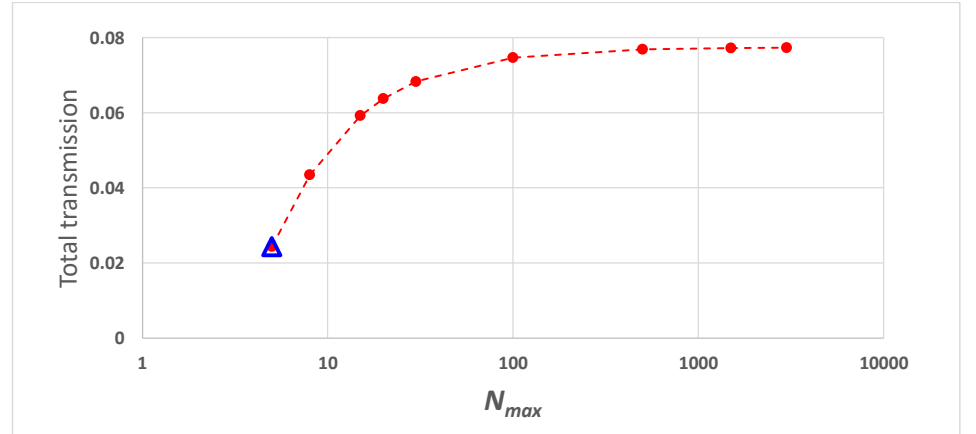


Figure 29 - Explore wide range of  $N_{max}$  effects of the total transmission. Results were calculated for  $N=5$ ,  $a=0.43$ ,  $r=0.2$ . X axis is logarithmic scaled.

As one can see in Figure 28 and Figure 29, for decreasing values of  $N_{max}$ , the behavior of sub-model 2 is getting similar to sub-model 1, as the total size of holes is lower (for low values of  $N_{max}$ ). Despite that, sub-model 2 with  $N_{max}=15$  is closer to other higher values in sub-model 2 than in sub-model 1 for low values of  $N$ . The gap is minimized with the increase of  $N$ , which reduces the size of holes. Note that the minimum value for  $N_{max}$  is limited by  $N$  (i.e.,  $N_{max} \geq N$ ). In addition, when  $N_{max}$  increases,  $p_{enc}$  decrease (see equation 24), which makes the probability for transmission higher since "there are more holes in the layers" and thereby it is more likely for a photon to be transmitted through a layer.

Figure 28 also show that, as expected, for higher values of  $N$ , the total transmission is lower. For a fixed value of  $N_{max}$ , the total transmission decreases with the increase of  $N$ .

Similarly to Figure 28, Figure 29 shows that the increase of  $N_{max}$  results in higher total transmission. However, the marginal addition for the total transmission is lower for high values of  $N_{max}$ .

In addition, as shown in Figure 29, for fixed values of  $N$ , increasing  $N_{max}$  increases the total transmission. That is, the volume is higher (increasing  $N_{max}$ ), but the number of cells is the same (fixed  $N$ ); therefore, as the density (or concentration) decreases the transmission increases, as expected.

### 5.5. Behavior of the system

When a newly inoculated culture (previously exponentially growing under fixed continuous white light conditions) was initiated in our system, we observed a failure of the culture to grow under the set of conditions chosen for routine function of the system ( $FrR=0.75, 0.95$ ;  $SLS(\text{red})=SLS_{max}(\text{red})=0.0959$ ;  $SLS(\text{blue})=SLS_{max}(\text{blue})=0.02806$ ;  $pH_{\text{target}}=8.5$ ;  $pH_{\text{min}}=6.5$ ;  $pH_{\text{range}}=2.0$ ;  $steepness=-0.00008$ ;  $Light_{\text{middle}}=2000$ ;  $Illumination\ mode=\text{Sinusoid daylight}$ ).

The failure may be attributed to one or more of the following reasons:

1. The light supply was not adequate (photo-inhibition for excess light, or photo-limitation otherwise).
2. The balance between red and blue light supply was improper.
3. The  $\text{CO}_2$  supply/acidity of the medium was inappropriate.
4. Mixing achieved by bubbling was inefficient.

Every one of the above reasons can be tested individually using the system we developed.

### 5.6. Validation of the calculations in the $\alpha$ Algorithm

The algorithm goal is to supply proper environmental conditions as detailed in section 3.93.9 (light intensity, light quality, illumination mode and pH). In this section, the environmental conditions owing to light (i.e., light intensity, light quality, illumination mode) are presented, as calculated by the algorithm over growth periods of seven days. The results are shown for different ranges of growth parameters (introduced in section 3.83.8). In this section, the part of the algorithm for controlling the (by CO<sub>2</sub> supply) was not validated, due to the simplicity of that process. The parameters in equation 59 (*steepness*, *pH<sub>range</sub>*, *Light<sub>middle</sub>*, etc.) need to be adjusted.

Figure 30 presents the concentration levels for each of the pigments, over a growth period of seven days. Initial conditions for light measurements were taken to indicate low *Chlorophyll a* concentration. The initial conditions and description of the simulation procedure is described in the legend.

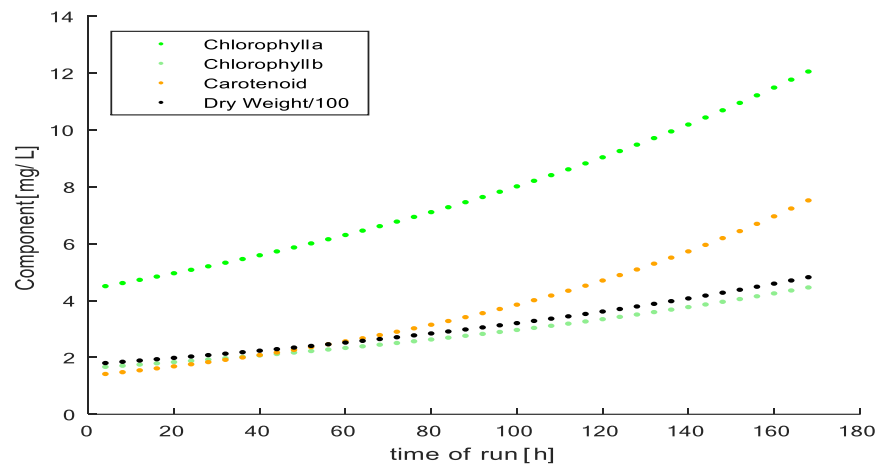


Figure 30 - Biomass of pigments along growth period of seven days. The biomass was calculated every 4 hours. Reference inputs for light sensors: red in=14,576[Hz], red out=999.1[Hz], blue in=7,461.9[Hz], blue out=170.7[Hz]. Inputs for growth rate:  $\mu(\text{red})=0.015$ ,  $\mu(\text{blue})=0.018$ . Initial conditions: Chlorophyll a=4.39[mg/L], Chlorophyll b=1.63[mg/L], Carotenoid=1.35[mg/L], DW=175.95[mg/L]. Time period between two iterations was simulated as 15 minutes (total of 672 iterations, plus setup iteration), in which the process described shortly in Figure 5 was executed and the relevant data was saved in a structure.

The results (Figure 30) reveal, as expected, that the concentrations of the pigments grow exponentially. In addition, the carotenoid increases faster than the chlorophyll since the growth rate parameter,  $\mu(\text{blue})$ , was set accordingly.

The measured transmission is presented in Figure 31.

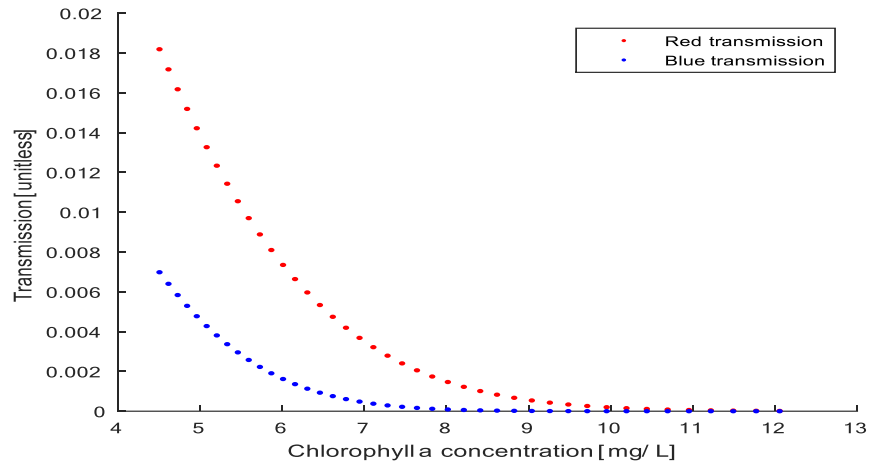


Figure 31 - Red and blue transmission as function of chlorophyll a concentration.

The results (Figure 31) reveal that the relation between the transmission and the chlorophyll a concentration is as expected; the transmission is decrease as the concentration level increases.

Figure 32, Figure 33 and Figure 34 shows the maximal (PAR<sub>imax</sub>) and current (PAR<sub>i</sub>) red and blue light intensities determined to be supplied in relation to the chlorophyll a concentration for each of the illuminations modes (continuous light, constant light-dark and sinusoid daylight) according to equations {53, 54, 55}, correspondingly.

Due to the limitation in the blue light intensity (1:6 ratio of blue:red LEDs), we cannot cover the full range of absolute light intensities for red and blue lights. Consequently, in our simulations, the specific blue light supply (SLS(blue) in equation 45) was not constrained; an effective calculated range between 0.032 to 0.045 [ $\mu\text{mol}\cdot\text{L}/\text{m}^2/\text{s}/\text{mg}$ ] was found for SLS(blue), while the maximum allowable value in our system is 0.028.

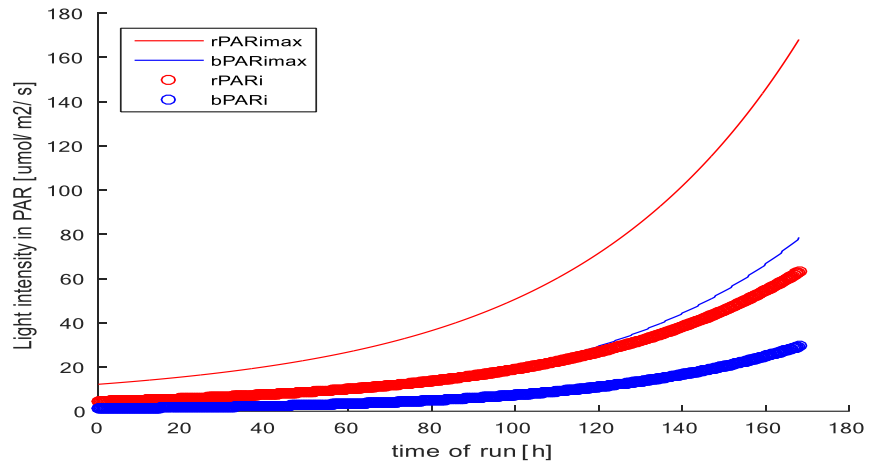


Figure 32 - Light intensity in PAR [ $\mu\text{mol}/\text{m}^2/\text{s}$ ] vs. growth period of seven days [days]. Results are plotted for each light color at continuous illumination mode. PARimax indicates the maximum light intensity to supply for each color according to the concentration level (shown in Figure 30), and PARi indicates the current light intensity to supply determined according to the illumination mode and the time in day. Results plotted at intervals of 15 minutes. Conditions:  $FrR=0.8$ ,  $SLS(\text{red})=SLS_{\text{max}}(\text{red})=0.096$ , effective  $SLS(\text{blue})=0.032-0.045$ .

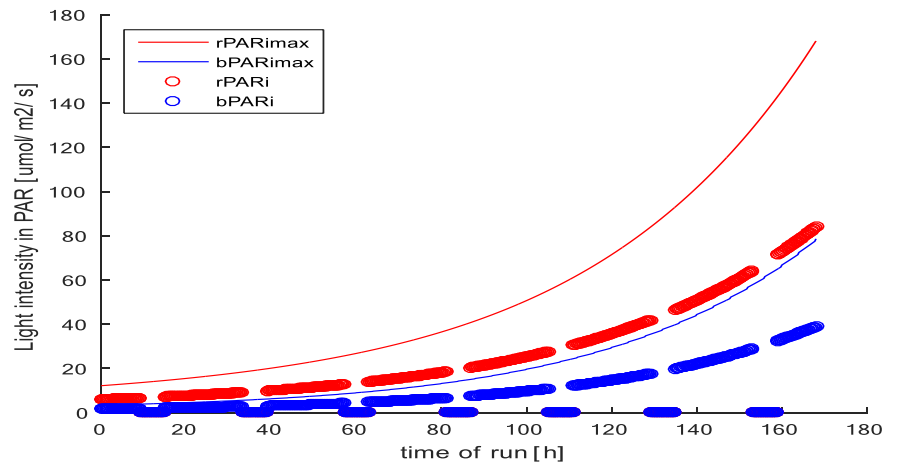


Figure 33 - Same as in Figure 32, for constant light-dark illumination mode.

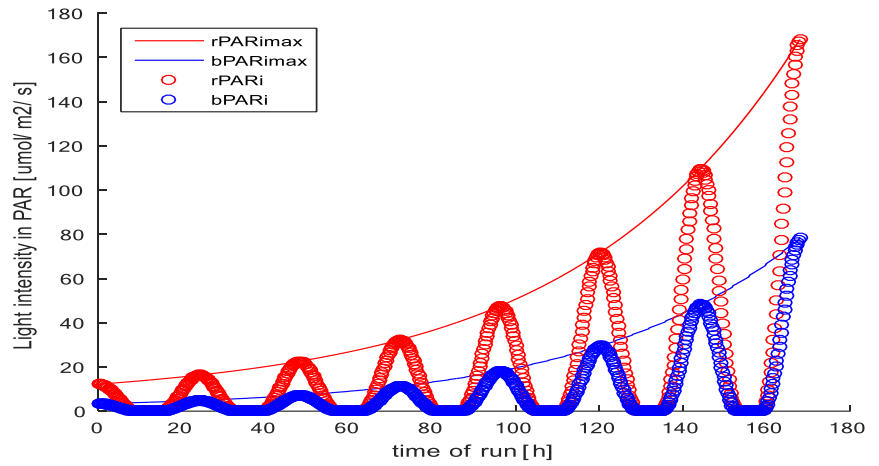


Figure 34 - Same as Figure 32, for sinusoid daylight illumination mode.

The results reveal (Figure 32, Figure 33 and Figure 34) that the maximum light to supply ( $PAR_{imax}$ ) is similar for all of the illumination modes, as opposed to  $PAR_i$ , which is determined according to  $PAR_{imax}$  and the time of day (as described in section 4.3.14.3.4). It is also shown, as expected and as described in Figure 9, that an increase in the concentration level leads to a power increase of the supplied light intensities.

The total light intensity supplied (equations {51,52} for red and blue lights), integrated over the growth period (2.96 [mmol/m<sup>2</sup>/7days]) and the total specific light available for absorption (equation 42) integrated over the growth period (0.118 [mmol·L<sup>2</sup>/m<sup>2</sup>/mg<sup>2</sup>/7days]) were similar for the three illuminations modes. This result is consistent with the basic calculation of light intensities according to the illumination modes; indeed, the latter is based on a constant light supply per day.

Figure 35, Figure 36 and Figure 37 show, for each illumination mode, the light available for absorption (<PAR>, calculated by equation 42) for each light color and their summation, and the calculated ratio between the lights ( $FrR$  parameter, calculated by equation 49) for growth period of seven days.



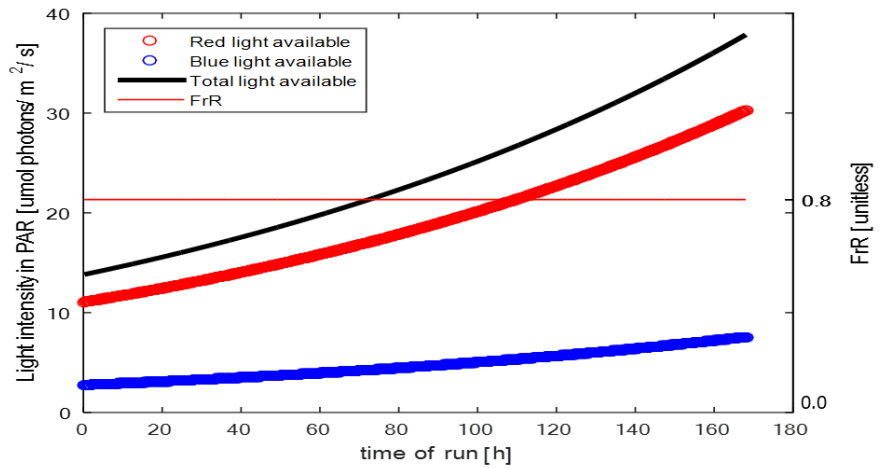


Figure 35 - Light available for absorbance ( $\langle \text{PAR} \rangle$ , calculated according to equation 42) for each light color and their summation and the fraction of the red light available for absorbance (calculated according to equation 49). Results obtained for continuous illumination mode. The light intensity used for the calculation of  $\langle \text{PAR} \rangle$  was the current light intensity ( $\text{PAR}_i$ ).

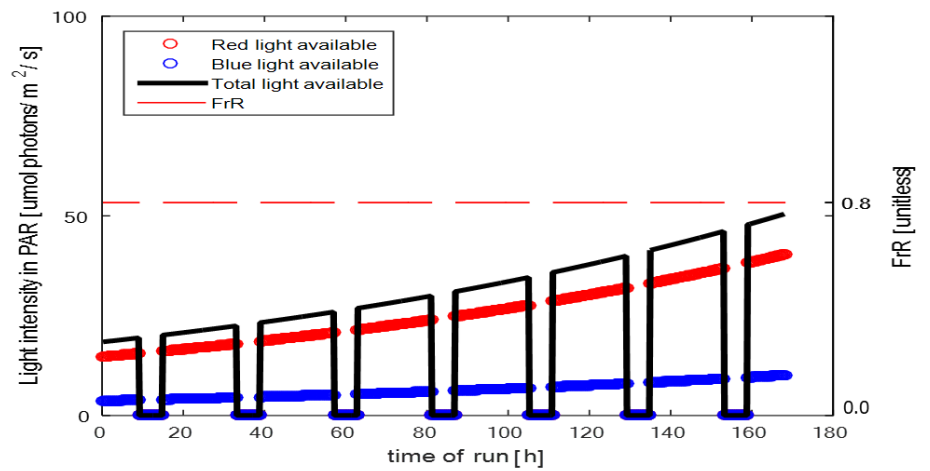


Figure 36 - Same as in Figure 35, for constant dark-light illumination mode. Light:dark cycle=18:6. The variable  $\text{FrR}$  is algebraically undetermined in the dark ( $=0/0$ ).

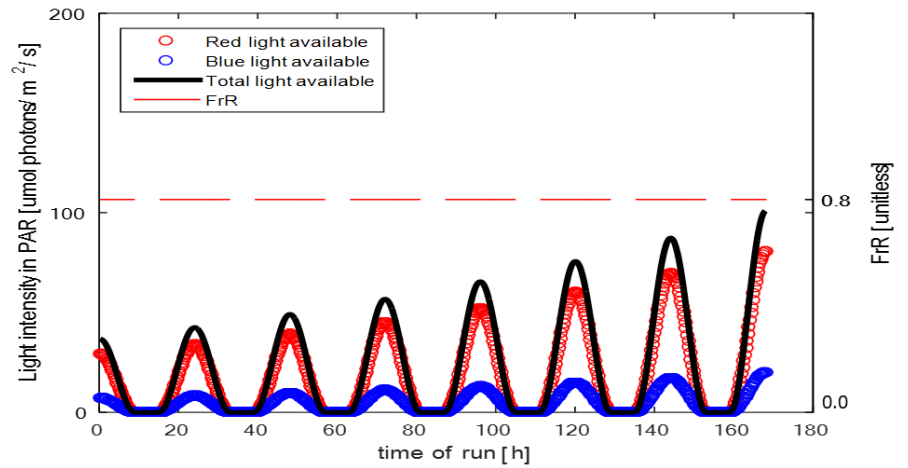


Figure 37 - Same as in Figure 36, for sinusoid daylight illumination mode.

It is shown that the fraction of red light available for absorption per biomass remains constant throughout the whole growth period. It is also shown, in compare to Figure 32, Figure 33 and Figure 34, that the light available for absorption is lower than the incident light, as expected.

In oppose to Figure 37, Figure 38 shows an example for lower  $FrR$ , in which the blue light available for absorption is higher than the red.

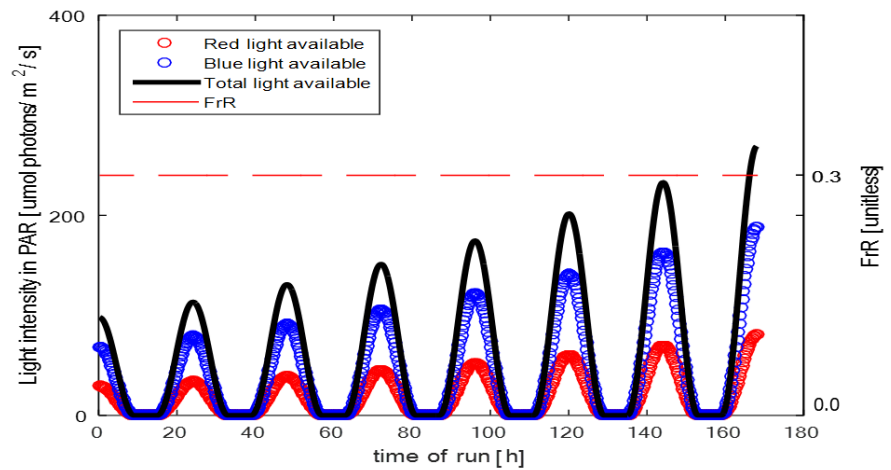


Figure 38 – Same as in Figure 37, for  $FrR=0.3$ .

Results (Figure 38) show that the blue light available for absorption is higher than the red light, as expected for  $FrR=0.3$ . However, the total light available for absorption is significantly higher in Figure 38, as compared to Figure 37. Since the blue light intensity is set in relation to the red light intensity, as

seen in equations {51,52}, the total light supplied is not constrained. That is, the red light is the first to be determined (according to the culture properties and system limitations) and only afterwards, the blue light is determined according to the desired  $FrR$ . This demonstrates a drawback of the algorithm. The  $FrR$  parameter, adjusted by the user, is not determining only the relation between the lights; it may also affect the total light intensity supplied.

## 6. Conclusions & Recommendations

As photo-bioreactors are usually used with relatively low concentration levels, the scattering effect could be neglected. However, as long as higher concentrations are measured, the scattering becomes more relevant and therefore it is reasonable to assume the simplified deterministic model would be less suitable, and the model we propose may become useful.

The phenomenon in which the scattering effect is significant at high concentrations levels was predicted by the stochastic model. It was shown by simulation that the total reflection (*i.e.*, scattering in a single dimension) was increased at high concentration levels (see the differences between Figure 26 and Figure 27).

Traditional use of Beer-Lambert could be extended using the findings of the stochastic model, such that the measured transmission was rectified accordingly (reduce the reflectance). Another sensor could be added for measuring and subtracting the reflectance.

In addition, the stochastic model could be adjusted to indicate the absorbance and reflection of a different PBR by re-setting the elementary probabilities for reflection and absorption of the PBR elements.

The curves describe the relation between the concentration (or in proportion, the number of layers of grouped cells) to the transmission shows similar behavior and order of magnitude for both the deterministic and stochastic models. The parameters in the deterministic model and the inputs for the stochastic model must be further adjusted in order to achieve matching curves, although it cannot be guaranteed that identical curves could be obtained.

The algorithm for controlling the environmental conditions was shown to achieve expected adjustment of the environmental light conditions, according to input by the user. However, the algorithm shows a drawback in the set of equations for defining a constant fraction between the lights (the parameter  $FrR$ ). The constant fraction is achieved throughout the growth period; however, changing the value of  $FrR$  affects the total light intensity supplied throughout the growth period. Moreover, tuning of the pH level was not tested by simulation.

The main limitation of this research is that continuous growth was not achieved by the control system. In addition, the Naïve model of Beer-Lambert (see equation A8) was not fitted to the heterogeneous dataset examined in section 5.35-3. Moreover, the assumptions of linearity was not tested for the approach used in the deterministic model.

Further research is necessary to validate the stochastic model against real measurements from the system. A calibration procedure should be conducted in order to evaluate the light scattered by the culture out of the photo-bioreactor. Indeed, this part of the incident light has not been taken into account in the currently operative model and the resultant Arduino sketch. The calibration should be conducted by adding a third light sensor at the incident face of the PBR, facing the culture, to assess the reflected light (in Hz) and convert it into PAR (in  $\mu\text{mol photons/m}^2/\text{s}$ ), by an additional calibration procedure.

In addition, the mixing rate of the culture was not considered and it may modulate the culture growth.

## 7. References

- Antoine D & Morel A (1996) Oceanic ~~p~~Primary ~~p~~Production: ~~1-~~~~a~~Adaptation ~~o~~f ~~a~~A ~~s~~Spectral ~~l~~Light-  
~~p~~Photosynthesis ~~m~~Model ~~i~~n ~~v~~View ~~o~~f ~~a~~Application ~~t~~o ~~s~~Satellite ~~c~~Chlorophyll ~~o~~Observations. *Global Biogeochemical Cycles* 10: 43-55.
- Barber J & Andersson B (1992) Too ~~m~~Much ~~o~~f ~~a~~A ~~g~~Good ~~t~~Thing: ~~l~~Light ~~c~~Can ~~b~~Be ~~b~~Bad ~~f~~For  
~~p~~Photosynthesis. *Trends in Biochemical Science* 17: 61-66.
- Barbosa MJ, Hoogakker J & Wijffels RH (2003) Optimisation of cultivation parameters in photobioreactors for microalgae cultivation using the A-stat technique. *Biomolecular Engineering* 20: 115-123.
- Bernard O & Rémond B (2012) Validation of a simple model accounting for light and temperature effect on microalgal growth. *Bioresource Technology* 123: 520-527.
- Beer (1852) Bestimmung der Absorption des rothen Lichts in farbigen Flüssigkeiten (Determination of the absorption of red light in colored liquids). *Annalen der Physik und Chemie* 86: 78-88.
- Bidigare R, Morrow J & Kiefer D (1989) Derivative analysis of spectral absorption by photosynthetic pigments in the western Sargasso Sea. *Journal of Marine Research*, 47: 323-341.
- Bidigare R, Ondrusek M, Morrow J & Kiefer D (1990) In vivo absorption properties of algal pigments. *Proceedings of SPIE, Ocean optics X*, 1302: 290-302.
- Bishop CM (1995) *Neural Networks for Pattern Recognition*. Oxford: Oxford University Press.
- Borowitzka MA (1996) Closed algal photobioreactors: design considerations for large-scale systems. *Journal of Marine Biotechnology* 4: 185-191.
- Borowitzka MA (1999) Commercial Production of Microalgae: Ponds, Tanks, and Fermenters. *Progress in Industrial Microbiology* 35: 313-321.
- Boussiba S & Aflalo C (2005) An insight into the future of Microalgal Biotechnology. *Innovations in Food Technology* 28: 37-39.
- Box GE & Cox DR (1964) An analysis of transformations. *Journal of the Royal Statistical Society, Series B (Methodological)* 26: 211-252.
- Bricaud A & Morel A (1986) Light attenuation and scattering by phytoplanktonic cells: a theoretical modeling. *Applied Optics* 25: 571-580.
- Carlsson AS, Beilen JB, Moller R & Clayton D (2007) Micro and macro algae: utility for industrial applications, outputs from the EPOBIO project. University of York, CPL Press, Newbury (UK) p. 86.
- Chen W, Sommerfeld M & Hu Q (2011) Microwave-~~a~~Assisted Nile ~~r~~Red ~~m~~Method ~~f~~For ~~i~~n ~~v~~ivo  
~~q~~Quantification ~~o~~f ~~n~~Neutral ~~l~~Lipids ~~i~~n ~~m~~Microalgae, *Bioresource Technology* 102: 135-141.
- Chisti Y (2007) Biodiesel from Microalgae. *Biotechnology Advances* 25: 294-306.
- Cnaan A, Laird NM & Slasor P (1997) Tutorial in biostatistics: Using the general linear mixed model to analyse unbalanced repeated measures and longitudinal data. *Statistics in Medicine* 16: 2349-2380.
- Cronquist A (1960) The Divisions and Classes of Plants. *Botanical Reviews* 26: 425-482.
- Doughman SD, Krupanidhi S & Sanjeevi CB (2007) Omega-3 fatty acids for nutrition and medicine: considering microalgae oil as a vegetarian source of EPA and DHA. *Current Diabetes Reviews* 3: 198-203.
- Durbin BP, Hardin JS, Hawkins DM & Rocke DM (2002) A variance-stabilizing transformation for gene-expression microarray data. *Bioinformatics* 18: 105-110.

- Duysens, LNM (1956) The flattering of the absorption spectrum of suspensions, as compared to that of solutions. *Biochimica et Biophysica Acta* 19: 1-12.
- Evers EG (1991) A model for light-limited continuous cultures – growth, shading, and maintenance. *Biotechnology and Bioengineering* 38: 254–259.
- Guiry MD (2012) How many species of algae are there? *Journal of Phycology* 48: 1057–1063.
- Gupta PL, Lee SM & Choi HJ (2015) A mini review: photobioreactors for large scale algal cultivation. *World Journal of Microbiology and Biotechnology* 31: 1409-17.
- Grinstead CM & Snell JL (2012) Introduction to probability. American Mathematical Soc.
- Harold H (1942) a spectrophotometric method for the analysis of chloroplast pigments. Biological Laboratories, Harvard University, Cambridge.
- Harrell F (2001) Regression Modeling Strategies with Applications to Linear Models, Logistic Regression, and Survival Analysis. Springer, ISBN: 978-1-4757-3462-1.
- Huesemann M, Crowe B, Waller P, Chavis A, Hobbs S, Edmundson S & Wigmosta M (2016) A validated model to predict microalgae growth in outdoor pond cultures subjected to fluctuating light intensities and water temperatures. *Algal Research* 13: 195-206.
- Kirrolia A, Bishnoi NR & Singh R (2013) Microalgae as a boon for sustainable energy production and its future research & development aspects. *Renewable and Sustainable Energy Reviews* 20: 642-656.
- Kok B (1956) On the inhibition of photosynthesis in intense light. *Biochimica et Biophysica Acta* 21: 234–244.
- Lee CG (1999) Calculation of light penetration depth in photobioreactors. *Biotechnology and Bioengineering* 4: 78–81.
- Li Y, Horsman M, Wu N, Lan CQ & Dubois-Calero N (2008) Biofuels from Microalgae. *Biotechnology Progress* 24: 815-820.
- Lichtenthaler HK & Buschmann C (2001) Chlorophylls and carotenoids: measurement and characterization by UV-VIS spectroscopy. in: *Current Protocols in Food Analytical Chemistry*, Vol. F.4.3, John Wiley & Sons, Inc. pp. 1-8.
- Loera-Quezada MM, Angeles G & Olguín EJ (2011) Effect of Irradiance on The Element Density, Size and Lipid Accumulation Of *Neochloris oleoabundans*, Review of Latinoamerican Ambient and Algal *Biotechnology* 2: 81–92.
- Ma X, Lu JQ, Brock RS, Jacobs KM, Yang P & Hu XH (2003) Determination of complex refractive index of polystyrene microspheres from 370 to 1610 nm. *Physics in Medicine and Biology*, 48: 4165-4172.
- Marcuse D (1972) Light transmission optics, second edition. Van Nostrand, New York.
- Mata TM, Martins AA & Caetano NS (2010) Microalgae for biodiesel production and other applications: A review. *Renewable and Sustainable Energy Reviews* 13: 217-323.
- McClure PJ, Baranyi J, Boogard E, Kelly TM & Roberts TA (1993) A predictive model for the combined effect of pH, sodium chloride and storage temperature on the growth of *Brochothrixthermosphacta*. *International Journal of Food Microbiology* 19: 161-178.
- Meireles LA, Guedes AC, Barbosa CR, Azevedo JL, Cunha JP & Malcata FX (2008) On-Line Control of Light Intensity in a Microalgal Bioreactor Using a Novel Automatic System, *Enzyme and Microbial Technology* 42: 554-559.
- Miron AS, Gomez AC, Camacho FG, Grima EM & Chisti Y (1999) Comparative Evaluation of Compact Photobioreactors for Large-Scale Monoculture of Microalgae, *Journal of Biotechnology* 70: 249-70.

- Moheimani NR (2005) The culture of Coccolithophorid Algae for carbon dioxide bioremediation. Murdoch University, PhD thesis.
- Ogbonna JC, Soejima T & Tanaka H (1999) An integrated solar and artificial light system for internal illumination of photobioreactors. *Journal of Biotechnology* 70: 289–297.
- Pottier L, Pruvost J, Deremetz J, Cornet JF, Legrand J & Dussap C G (2005) A fully predictive model for one-dimensional light attenuation by *Chlamydomonas reinhardtii* in a torus photobioreactor. *Biotechnology and Bioengineering* 91(5), 569-582.
- Rich PR (2003) The molecular machinery of Keilin's respiratory chain. *Biochemical Society Transactions* 1095-1105.
- Richmond A (2004) *Handbook of microalgal culture: Biotechnology and Applied Phycology*. Blackwell Science Ltd.
- Strid A, Wah SC & Jan MA (1994) UV-B ~~d~~Damage ~~a~~And ~~p~~Protection ~~a~~At ~~t~~The ~~m~~Molecular ~~l~~Level In ~~p~~Plants. *Photosynthesis Research* 39: 475-489.
- Tastan BE, Duygu E, Ilbaş M & Donmez G (2013) Utilization of LPG and gasoline engine exhaust emissions by microalgae. *Journal of Hazardous Materials* 246: 173-180.
- Thomas J & Kirk O (1994) *Light and Photosynthesis in Aquatic Ecosystems* (Second Edition). University Press: England Cambridge.
- Van der Meer F (2004) Analysis of spectral absorption features in hyperspectral imagery. *International Journal of Applied Earth Observation and Geoinformation*, 5: 55–68
- Ying K, Gilmour J & Zimmerman WB (2014) Effects of CO<sub>2</sub> and pH on growth of the microalga *Dunaliella salina*. *Journal of Microbial & Biochemical Technology* 6:167-173.
- Yuki I, Norio N, Fatimah MY, Satoru T & Tatsuki T (2014) Estimation ~~o~~Of ~~o~~Optimum ~~s~~Specific Light Intensity ~~p~~Per ~~c~~Cell ~~o~~On ~~a~~A ~~h~~High-~~c~~Cell-~~d~~Density ~~c~~Continuous ~~c~~Culture ~~o~~Of ~~c~~Chlorella zofingiensis not limited by nutrients or CO<sub>2</sub>, *Bioresource Technology* 162: 53–59.
- Zarmi Y, Bel G & Aflalo C (2013) Theoretical analysis of culture growth in flat-plate bioreactors: the essential role of timescales. In: *Handbook of Microalgal Culture* 2nd ed., Eds. A. Richmond, Q. Hu, Wiley-Blackwell pp. 205-224.

## 8. Appendices

### 8.1. Appendix A – Decomposition of light attenuation

Relations between light color, measurements, absorbance and scattering.

$$Att^{tot} = -\log\left(\frac{I_{out}^{tot}}{I_{in}^{tot}}\right) = -\log\left(\frac{I_{out}^{red} + I_{out}^{blue}}{I_{in}^{red} + I_{in}^{blue}}\right) \quad (A1)$$

Total light attenuation at any wavelength ( $\lambda$ ) is the sum of absorption by pigments and light scattering (Bricaud & Morel, 1986):

$$A_{\lambda}^{attn} = A_{\lambda}^{abs} + A_{\lambda}^{scat} \quad (A2)$$

When no absorption occurs (e.g., at 800 nm), the attenuation is due exclusively to scattering.

$$A_{800}^{abs} = 0 \Rightarrow A_{800}^{attn} = A_{800}^{scat}$$

Assuming that scattering is due exclusively to non absorbing (pigmentless) particles, the apparent attenuation by scattering depends on  $n$ , the ratio between the characteristic size of the particles to the wavelength ( $\lambda$ ) of the scattered light (Ma *et al.*, 2003). For instance, for small molecules (air, water, etc.),  $n \sim 4$ , while for micro particles (e.g., colorless cells),  $n$  is of the order of 0.1-0.6, depending on the size and shape of the particles. In this case, the contribution of scattering, depends also on the wavelength, and is given by:

$$A_{\lambda}^{scat} = A_{800}^{attn} \cdot \left(\frac{800}{\lambda}\right)^n \quad (A3)$$

Thus

$$A_{red}^{scat} = A_{blue}^{scat} \left(\frac{\lambda_{blue}}{\lambda_{red}}\right)^n \quad (A4)$$

Allowing the estimation of scattering-free absorbance by the algal pigments, at any wavelength.

$$A_{\lambda}^{abs} = A_{\lambda}^{attn} - A_{\lambda}^{scat} \quad (A5)$$

Finally, one can model the total absorbance by microalgal culture using Beer-Lambert law as a sum of individual contributions of each pigment (i: Chlorophyll and Carotenoid) at each wavelength.

$$Abs^{tot} = Abs^{red} + Abs^{blue} = \left[\sum_i \varepsilon_i^{red} \cdot C_i + \sum_i \varepsilon_i^{blue} \cdot C_i\right] \cdot width \quad (A6)$$

By normalizing concentrations to chlorophyll a concentration and assuming constant ratios of absorbing species to chlorophyll, we get:

$$Abs^{tot} = Abs^{red} + Abs^{blue} = \left[\sum_i \varepsilon_i^{red} \cdot \frac{C_i}{C_a} + \sum_i \varepsilon_i^{blue} \cdot \frac{C_i}{C_a}\right] \cdot C_a \cdot width \quad (A7)$$

The equation above generates a system of equations with coefficients of absorption ( $\varepsilon$ ) as parameters and concentrations ( $C_i$ ) as unknowns, resolvable in principle. Besides, all  $C_i$  are routinely measured independently by standard laboratory procedures for validation purposes.

Equation A7 could be extended using equation A2 to consider also the scattering by the cells, which assumed to be proportional to the algal density and depends on the particles size, shape, and density (Duysens, 1956).

$$Att^{tot} = Abs(\lambda) + Scat(\lambda) = \left[\sum_i \varepsilon_i(\lambda) \cdot \frac{C_i}{C_a} + scat(\lambda) \cdot \frac{C_d}{C_a}\right] \cdot C_a \cdot width, \quad (A8)$$



in which  $C_d$  and  $scat(\lambda)$  stands for the cell density and the effective dependency of the optical path at the particles shape and size.

## 8.2. Appendix B – System hardware specification

**Arduino board** – [Arduino-Mega 2560 R3](#)<sup>5</sup>.

**LEDs** – [Luxeon Rebel Star light-emitting diodes](#)<sup>6</sup> (LEDs) (Quadica Developments Inc., Canada).

**LEDs Panel** – 72 red LEDs; maximal wavelength: 665±5 nm. 12 blue LEDs; maximal wavelength: 452±5 nm. Power: ~3W/LED. The LEDs panel is assembled of 12 LEDs combos, where each LEDs combo includes 7 LEDs: 6 red and 1 blue. The six red LEDs in each LEDs combos is connected in series, and every two couples of LEDs combos is connected in parallel, under the control of a [Buck Block](#)<sup>7</sup> (constant current power supply) equipped with a 0-10 Volt dim circuit. The power supply provides a maximal current of 1.4 A. In addition, each set of six blue LEDs is connected in parallel and has maximal current of 1.4 A. Since the Arduino microprocessor may provide a maximal voltage output to the dim circuit of only 5V, the power supplies operate at half maximal power.

Figure 39 shows the electrical circuit (right) for the connection of six LEDs combos and a LEDs combo (left) of 6 red and 1 blue LEDs.

**Light sensors** – [TSL235R](#)<sup>8</sup>. Light intensity to frequency converter (Texas Advanced Optoelectronic Solutions Inc.).

**Digital temperature sensor** – [DS18B20](#)<sup>9</sup> (Maxim Integrated).

**pH sensor** – [pH\\_Circuit\\_5.0](#)<sup>10</sup> (Atlas Scientific).

**CO<sub>2</sub> Valve** – a solenoid valve, controlled by an electric current, for supplying CO<sub>2</sub>.

**Photo-bioreactor** – Polyethylene bag inside a metal cage (size 110x50x5 cm).

---

<sup>5</sup> <https://store.arduino.cc/usa/arduino-mega-2560-rev3>

<sup>6</sup> <http://www.luxeonstar.com/assets/downloads/DS68.pdf>

<sup>7</sup> [http://www.luxdrive.com/content/A009\\_BuckBlock\\_V1.pdf](http://www.luxdrive.com/content/A009_BuckBlock_V1.pdf)

<sup>8</sup> <https://www.sparkfun.com/datasheets/Sensors/Imaging/TSL235R-LF.pdf>

<sup>9</sup> <https://datasheets.maximintegrated.com/en/ds/DS18B20.pdf>

<sup>10</sup> [https://www.atlas-scientific.com/\\_files/\\_datasheets/\\_circuit/pH\\_Circuit\\_5.0.pdf](https://www.atlas-scientific.com/_files/_datasheets/_circuit/pH_Circuit_5.0.pdf)

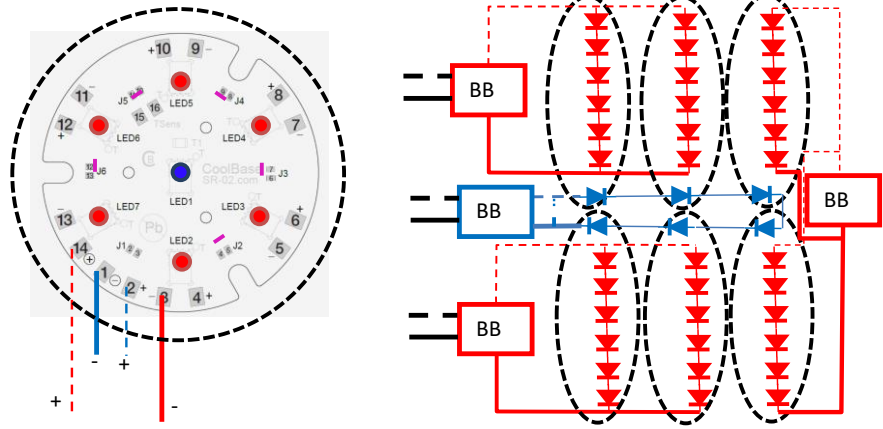


Figure 39 - electrical circuits at the LEDs panel. Left: LEDs combo of 6 red LEDs connect in series and 1 blue LED. Right: Buck Block (BB) power supply of 1400 mA.

### 8.3. Appendix C – Calculated incident light at the surface of the PBR

The local red and blue light intensities (in Watt/cm<sup>2</sup>) is calculated for each squared cm element of the incident face of the PBR. The contribution from each LED to such a surface element was calculated as follows:

$$light\ power_i \cdot \frac{1}{d_i^2}, \quad (C1)$$

where  $light\ power_i$  is the total power in Watt emitted by a specific LED  $i$  at zero distance, and  $d_i$  is the distance between the LED and the local surface element.

The total light intensity (in Watt/cm<sup>2</sup>) at each surface element on the PBR surface is the sum of contributions from all LEDs as follows:

$$local\ light\ intensity_k = \sum_i light\ intensity_i \cdot \frac{1}{d_i^2}, \quad (C2)$$

where  $k$  is the index of surface elements (total of  $92 \times 48$  elements) on the PBR surface.

The  $local\ light\ intensity_k$  was calculated for each squared cm composing the PBR surface, for each of the twelve LEDs combos. The results for the red and blue lights are presented in Figure 40 and Figure respectively.

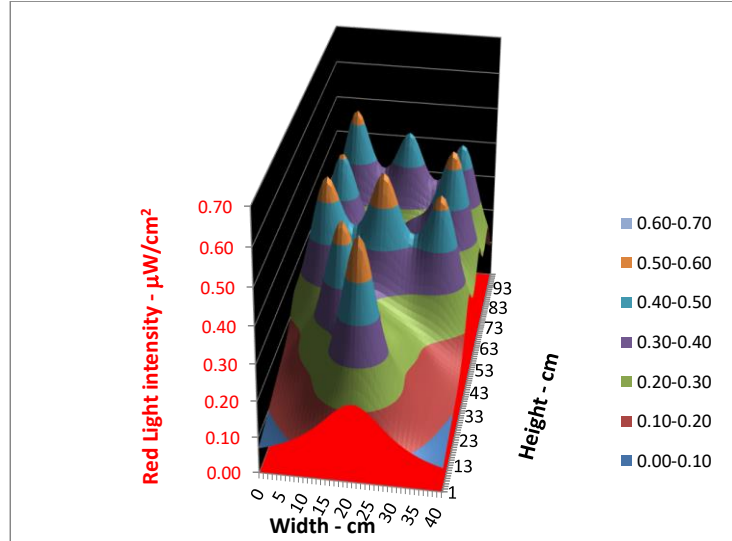


Figure 40 - Total red incident light at the face of the PBR. Calculated for red PWM = 240.

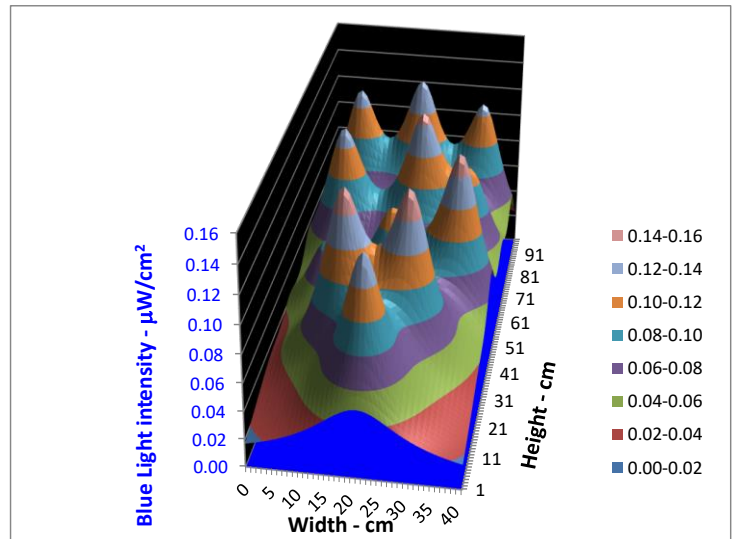


Figure 41 - Total blue incident light at the face of the PBR. Calculated for blue PWM = 240.

#### 8.4. Appendix D – Analysis of the heterogeneous dataset

The model to formulate shall lean on the theoretical model described in section 4.2.14.2.1, given by 19. The dependent variable,  $C_a$ , is denoted as  $Y$ ; the variable  $Abs(red)$ , thereby considered as independent, is denoted as  $X$ ; The effective scattering coefficient,  $K(\lambda)$ , is denoted as  $\beta_{K(\lambda)}$ , and shall be determined empirically by minimizing the sum of squared errors of observed (see Table 14 for the observations) and predicted  $Y$  values.

Table 14 - Observations gathered within one year, composing the heterogeneous dataset.

Chl a [mg/L]	Chl b [mg/L]	Car [mg/L]	DW [mg/L]	$L_{in,ref}(red)$ [Hz]	$L_{out,ref}(red)$ [Hz]	$L_{in,ref}(blue)$ [Hz]	$L_{out,ref}(blue)$ [Hz]
11.51	6.073	10.87	760.0	15516	3.100	7482	0.30
10.71	4.130	15.12	596.0	16438.9	31.30	8925	1.20
10.48	3.711	5.936	725.0	15170	29.90	7998	0.950
9.063	3.248	5.069	586.6	14588	46.51	7629	1.150
6.060	2.71	5.406	540.0	14985	52.90	7997	0.60
7.833	2.504	3.894	333.3	16302	70.61	8930	1.550
11.85	5.193	7.697	620.0	15794	13.05	8412	0.425
9.577	4.204	5.968	506.6	15625	23.30	8402	0.50
6.877	3.116	4.695	380.0	16549	65.90	9141	1.050
5.009	2.440	3.142	313.3	15736	150.2	8404	1.775
1.386	1.079	1.171	63.33	15802	1176	7605	73.33
12.48	4.864	9.432	440.0	15342	24.74	7335	0.490
13.59	5.027	7.182	543.3	16647	15.25	8190	0.493
12.47	4.576	7.236	415.0	15641	6.440	7595	0.513
16.09	5.699	10.63	616.7	15133	8.433	7244	0.683
18.44	6.598	15.11	680.0	15084	8.834	7195	0.583
4.810	1.786	2.859	366.2	16000	254.4	8400	7.790

For simplification, the constants in equation 19 are combined into new constants,  $A_1$  and  $A_2$ .  $A_1$  represents the inverse of transmission in the absence of algae, and is calculated as follows:

$$A_1 = \frac{PAR_{in,blank}(red)}{PAR_{out,blank}(red)} = \frac{Hz_{in,ref,blank}(red) \cdot Hz2PAR_{in}^{red}}{Hz_{out,ref,blank}(red) \cdot Hz2PAR_{out}^{red}} = 17.18 \quad (D1)$$

where  $PAR_{in/out,blank}(red)$  represents the light intensity at 140 PWM for the incident and exiting sides of the PBR and  $Hz2PAR_{in/out}(red)$  is the conversion factor from local Hz measurements by the sensor to global PAR intensity on the PBR surface, formulated by the calibrations (see chapter 5.25.2), the latter are presented in Table 15.

Table 15 - Values for conversion factors from local Hz measured by the sensors to global PAR at the PBR surfaces and reference values for blank, used for the definition of  $A_1$ .

$Hz_{in,ref,blank}^{red}$	$Hz_{out,ref,blank}^{red}$	$Hz2PAR_{in}^{red}$	$Hz2PAR_{out}^{red}$
14755.95	3027.91	0.05311	0.01488

On the other hand,  $A_2$ , representing the denominator in equation 19, is calculated as follows:

$$A_2 = (\varepsilon_a(\lambda) + \varepsilon_b(\lambda) \cdot C_b^* + \varepsilon_c(\lambda) \cdot C_c^*) \cdot C_d^* \cdot width =$$

$$(\varepsilon_a(red) + \varepsilon_b(red) \cdot \overline{C_b^*} + \varepsilon_c(red) \cdot \overline{C_c^*}) \cdot \overline{C_d^*} \cdot 4 = 22.70, \quad (D2)$$

where the effective absorption coefficients ( $\varepsilon_i^\lambda$ ) were determined according to published *in vivo* measurements (Pottier *et al.*, 2005) and were averaged over the wavelength range (see Figure 2 and equation 14), see first row of Table 16.

Table 16 – Values for the definition of  $A_2$ . Dry weight was calculated in relations to chlorophyll a since the former assumes to be proportional to the algal concentration in the suspension.

	Chlorophyll a	Chlorophyll b	Carotenoid	Dry weight
$\varepsilon^{red} [m^2 \cdot mg^{-1}]$	0.07523	0.07815	0.0	NA*
$\overline{C^*}$	1	0.40146	0.6616	53.2383

\* Dry weight has no color, thus no epsilon.

For the purpose of further analysis,  $C_x^*$ , the concentrations relative to  $C_a$ , were arbitrarily taken as the average of the observations measured in the laboratory (see Table 14); they are calculated as follows:

$$\overline{C_x^*} = \frac{\sum_{i=1}^n \frac{C_{x,i}}{C_{a,i}}}{n} \quad (D3)$$

Note that using the average as estimators assumes the dataset is homogenous, which is conceptually wrong since each observation reflects a unique physiological state of the culture (*i.e.*, different pigments composition) (see section 5.35-3 for further explanation).

Follows equation 19 with the above notations:

$$Y = \left( \frac{-\log(X \cdot A_1)}{A_2 \cdot \beta_{K(\lambda)}} \right)^{0.5} + \text{epsilon} \quad (D4)$$

Where *epsilon* represents the noise that could accumulate in each estimation of the model. *epsilon* is assumed to have constant variance and its mean, over all measurements, is assumed to vanish.

Accordingly,  $Y_{pred}$  is defined as:

$$Y_{pred} = \left( \frac{-\log(X \cdot A_1)}{A_2 \cdot \hat{\beta}_{K(\lambda)}} \right)^{0.5} \quad (D5)$$

The estimation is done similarly to linear regression, using least square method. Since the function is non-linear, the equation does not have an analytic solution, therefore it is solved numerically (using optimization).

The error in each measurement  $i$  is thereby defined as:

$$\text{error}_i = Y_i - Y_{i,pred} = Y_i - \left( -\frac{\log(X \cdot A_1)}{A_2 \cdot \hat{\beta}_{K(\lambda)}} \right)^{0.5} \quad (D6)$$

Where  $\hat{\beta}_{K(\lambda)}$  is the estimate for  $\beta_{K(\lambda)}$ .

The non-linear least square problem is solved by minimizing the *SSE*, which is defined as:

$$SSE(Y, X, A_1, A_2 / \beta_{K(\lambda)}) = \sum_{i=1}^n (\text{error}_i)^2 = \sum_{i=1}^n \left( Y_i - \left( -\frac{\log(X \cdot A_1)}{A_2 \cdot \hat{\beta}_{K(\lambda)}} \right)^{0.5} \right)^2 \quad (D7)$$

Note that the *SSE* varies according to  $\beta_{K(\lambda)}$ , while  $Y, X, A_1, A_2$  are considered as knowns.

An optimization function ("optimize" R package) were used to minimize the *SSE* (see [github link](#)<sup>11</sup> for the R script). Follows is a formal definition of the optimization problem.

$$Z = \text{minimize } SSE(Y, x, A_1, A_2 | \beta_{K(\lambda)})$$

Subject to

$$\begin{aligned}\beta_{K(\lambda)} &\leq 10^{-1} \\ \beta_{K(\lambda)} &\geq 10^{-7}\end{aligned}$$

The limits for  $\beta_{K(\lambda)}$  were defined after manually place values for  $\hat{\beta}_{K(\lambda)}$  indicated that it target value has an order of magnitude of  $\sim 10^{-3}$ .

The optimal  $\hat{\beta}_{K(\lambda)}$  for which the *SSE* has been minimized and the results for the prediction are summarized in the first line of Table 17. [Figure 42](#) shows the observations (red pluses) and the Chlorophyll a concentration (green line) as a function of the red transmission measured by the system in Hz and converted to PAR.

The low  $R^2$  in the first row of Table 17 and the green line of predictions presented in [Figure 42](#) indicates that the obtained model does not go through "the mean" of  $Y$  values. Furthermore, for red transmission ( $X$ ) values above  $\sim 0.0005$ , the model overestimate the chlorophyll a concentration ( $Y$ ). Therefore, we conclude that the model is not suitable for that problem.

Hence, the model in equation D4 is extended in a speculative way, by adding a parameter,  $\beta_{pow}$ , replacing the constant 0.5 power.

$$Y = \left( -\frac{\log(X \cdot A_1)}{A_2 \cdot \beta_{K(\lambda)}} \right)^{\beta_{pow}} + \text{epsilon} \quad (D8)$$

The new equation could alter it shape to fit  $Y$  values. This equation includes our suggestion (given by equation 19), and the commonly used model (see section [8.18.4](#)) as special cases for which  $\beta_{pow} = 0.5$  1, respectively. Therefore, equation D8 gives more flexibility to fit the data by estimating also the power coefficient.

Note that this equation also includes the scattering coefficient multiplying, which does not included in the commonly used model.

The *error* is defined as:

$$\text{error2}_i = Y_i - Y_{2i, \text{pred}} = Y_i - \left( -\frac{\log(X \cdot A_1)}{A_2 \cdot \hat{\beta}_{K(\lambda)}} \right)^{\hat{\beta}_{pow}} \quad (D9)$$

The *SSE* to be minimized is defined as:

$$SSE2 = \sum_{i=1}^n (\text{error2}_i)^2 = \sum_{i=1}^n \left( Y_i - \left( -\frac{\log(X \cdot A_1)}{A_2 \cdot \hat{\beta}_{K(\lambda)}} \right)^{\hat{\beta}_{pow}} \right)^2 \quad (D10)$$

That is, the optimization will be conducted in recursion of two steps (a) minimization of *SSE2* over  $\beta_{pow}$  (between -2 to 2), in which (b) *SSE* is minimized over  $\beta_{K(\lambda)}$ .

<sup>11</sup> [https://github.com/EladDan/EladThesis\\_Model1](https://github.com/EladDan/EladThesis_Model1)

$$Z = \text{minimize } SSE2(SSE(Y, x, A_1, A_2/\beta_{K(\lambda)})|\beta_{pow})$$

Subject to

$$\begin{aligned}\beta_{pow} &\leq 2 \\ \beta_{pow} &\geq -2 \\ \beta_{K(\lambda)} &\leq 0.1 \\ \beta_{K(\lambda)} &\geq 0.0000001\end{aligned}$$

The results are shown in the second row of Table 17 and in the blue line (y\_pred2) indicating the predictions in [Figure 42](#).

A different equation is used in order to make sure that the curve of the models tried earlier are not constrained by a particular form of  $Y$ . Note that the following model does not consider the theoretical models described earlier.

$$Y3 = 10^{-(\beta_0 + x \cdot \beta_1)} \quad (D11)$$

For formulating the suggested model in equation *D11*, the target variable ( $Y3$ ) is log transformed (on 10 basis), and a linear regression model is build to predict it.

$$Y3_{transform} = -\log_{10} Y3 = \beta_0 + x \cdot \beta_1 \quad (D12)$$

The results are shown in the third row of Table 17 and in the black line of predictions in [Figure 42](#).

To conclude, this section shows that all of the models tried did not succeed in predicting the chlorophyll a concentration based on the heterogeneous dataset. However, the best results is shown for the model in which the estimate power ( $\hat{\beta}_{pow}$ ) was close to 1.0, in oppose to the power in our model (0.5).



Table 17 - Results for fitting the parameters in the deterministic model to raw experimental results as visually presented in Figure 42. The first row shows the results for fitting  $Y_{pred}$  to  $Y$  in equation D4 by changing  $\beta_{K(red)}$ . The second row shows the results for fitting  $Y_{pred}$  to  $Y$  in equation D8 by changing  $\beta_{pow}$  and  $\beta_{K(red)}$ . The third row shows the results for fitting  $Y_{pred}$  to  $Y$  in equation D11.

	$\hat{\beta}_{K(\lambda)}$	$\hat{\beta}_{pow}$	SSE	SST	$R^2$
Fit $Y_{pred}$ to $Y$ in equation D4 by changing $\beta_{K(red)}$	0.0007844	0.5	105.8	199.5	0.470
Fit $Y_{pred}$ to $Y$ in equation D8 by changing $\beta_{pow}$ and $\beta_{K(\lambda=665)}$	0.01075	1.0891	69.87	199.5	0.650
	$\hat{\beta}_0$	$\hat{\beta}_1$	SSE	SST	$R^2$
Fit $Y_{pred}$ to $Y$ in equation D11 by changing $\beta_0$ and $\beta_1$	-2.553	276.98	73.204	199.5	0.633

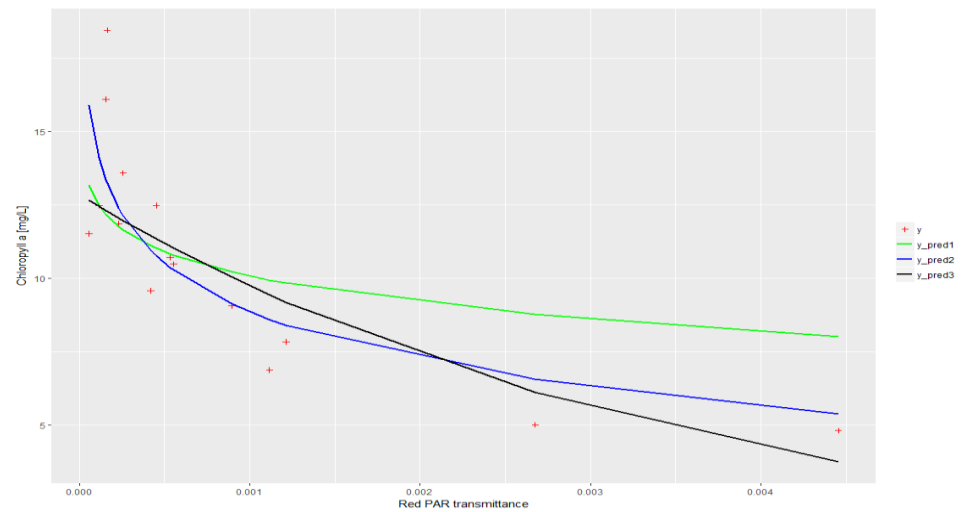


Figure 42 - Chlorophyll a: real observations vs. predictions as function of red PAR transmission. Prediction made by fitting the parameters in equations D4 ( $y_{pred1}$ ), D8 ( $y_{pred2}$ ) and D11 ( $y_{pred3}$ ) to real observations.

## תקציר

בשנים האחרונות גדל ומתפתח תחום המחקר העוסק במיקרו-אצות, זאת עקב הערך הרב הטמון בחומרים שונים אשר מייצרות אצות אלו, תחת לחצים סביבתיים שונים. בהתאם לכך, מגדלים כיום זנים שונים של מיקרו-אצות לצורכי הפקת חומרים אלו ונחקרים התנאים הסביבתיים המאפשרים ייצור מוגבר שלהם.

מטרת מחקר זה הייתה יצירת מערכת בקרה אשר תשמש ככלי ייעודי לגידול מיקרו-אצות ובחינתו דרך שליטה במשתני הסביבה, אשר מכוונים על ידי המשתמש. פלט המערכת הינו מידע אודות תנאי הסביבה והגידול וערכי הפרמטרים הפיזיולוגיים אשר מאפשרים גידול אופטימלי. המערכת הינה שימושית במחקר פיזיולוגי של זני מיקרו-אצות שונים. בנוסף פותחו שני מודלים: מודל דטרמיניסטי לחיזוי ריכוז האצות במתקן הגידול אשר הורחב בעזרת כלים סטטיסטיים ומודל סטוכסטי לתיאור מעבר האור במתקן הגידול בממד אחד.

הפיתוחים הספציפיים שנעשו במסגרת המחקר הינם:

1. תוכנת מערכת הבקרה.
2. פרוצדורת כיול אור אשר מתרגמת את קריאות חיישני האור למונחי קרינה פוטו-סינטטית (-photosynthetically active radiation).
3. אלגוריתם לגידול מיקרו-אצות במתקן גידול ייעודי (photo-bioreactor).
4. מודל דטרמיניסטי לחיזוי ריכוז האצות במתקן הגידול.
5. מודל סטוכסטי המתאר את מעבר האור בתוך מתקן הגודל והתרבית, בממד אחד.

המערכת פותחה באמצעות בקר מסוג Arduino Mega 2560, הקולט מידע משני חיישני אור (נכנס ויוצא), חיישן טמפרטורה וחיישן חומציות (pH). כמו כן, הבקר שולט על ברז לאספקת CO<sub>2</sub> ומערך של נורות LED בצבעים שונים. התכנות לבקר נעשה בתוכנת Arduino והמידע המוצג וממשק השליטה תוכנתו בתוכנת Megunolink Pro. המידע שנאסף על ידי המערכת נותח בעזרת R, Matlab ו-Excel.

מערכת הבקרה ושליטה כוללת שני מודולים עיקריים; הראשון הינו שליטה באור הכולל הקרנת אור בהתאם לקלט המשתמש (מצב הארה, יחס צבע אור אדום: כחול, יחס כמות אור לתא), מדידת האור משני צדי מתקן הגידול, חישוב ריכוז האצות בהתאם למודל הדטרמיניסטי שפותח והתאמת עוצמת האור לריכוז האצות המחושב. המודול השני אחראי על מדידה רציפה של הטמפרטורה והחומציות בתרבית. כמו כן, מתבצע איזון של רמת החומציות באמצעות פתיחה וסגירה של ברז CO<sub>2</sub> אשר מספק מקור פחמן התומך בגידול ומעלה את רמת החומציות בתרבית, אשר משתנה בזמן תהליך הפוטו-סינתזה. לשם כך, נקבע ערך מטרה לרמת החומציות, אשר מתעדכן באופן שוטף בהתאם לרמת האור המסופקת וריכוז האצות בתרבית. אלגוריתם הבקרה נבחן ותוצאותיו נבחנו להיות כעקביות והגיביות.

ניתוח של המידע שנאסף נעשה בכמה חלקים של המחקר: (א) אימות של הנחות המחקר, (ב) פיתוח פרוצדורת כיול המתרגמת את קריאות חיישני האור למונחי קרינה פוטו סינטטית ובנוסף מעריכה את בליעת האור על ידי מתקן הגידול (בהעדר מיקרו-אצות) ו- (ג) התאמת הפרמטרים במודל הדטרמיניסטי לתצפיות שנאספו באמצעות המערכת ונמדדו במעבדה בהתאמה.

**מילות מפתח:** מיקרו-אצות, מערכת שליטה, מערכת בקרה, אלגוריתם שליטה, שיטות סטטיסטיות, שרשראות מרקוב, ארדואינו, בליעת אור, מעבר אור, פיזור אור.




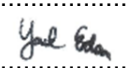

אוניברסיטת בן-גוריון בנגב  
הפקולטה למדעי ההנדסה  
המחלקה להנדסת תעשייה וניהול

## מודלים דטרמיניסטיים וסטוכסטיים להפחתת אור ואלגוריתם בקרה לגידול מיקרו-אצות

חיבור זה מהווה חלק מהדרישות לקבלת תואר מגיסטר בהנדסה

מאת: אלעד דן

מנחים: דר' קלוד אפללו, פרופ' ישראל פרמט ופרופ' יעל אידן

26/10/17	תאריך		חתימת המחבר
25/10/17	תאריך		אישור המנחה/ים
26/10/17	תאריך		אישור המנחה/ים
26/10/17	תאריך		אישור המנחה/ים
26/10/17	תאריך		אישור יו"ר ועדת תואר שני מחלקתית

25/10/2017

ה' חשון ה'תשע"ח

אוניברסיטת בן-גוריון בנגב  
הפקולטה למדעי ההנדסה  
המחלקה להנדסת תעשייה וניהול

## **מודלים דטרמיניסטיים וסטוכסטיים להפחתת אור ואלגוריתם בקרה לגידול מיקרו-אצות**

חיבור זה מהווה חלק מהדרישות לקבלת תואר מגיסטר בהנדסה

מאת: אלעד דן

25/10/2017

ה' חשון ה'תשע"ח